2014

Characterization of the Biological Role of a Putative Porphyromonas gingivalis RNA-binding Protein

Ramana Cvitkovic
Virginia Commonwealth University

Characterization of the biological role of a putative *Porphyromonas gingivalis* RNA-binding protein

A thesis submitted in partial fulfillment of the requirements for the degree of Masters of Science in Physiology and Biophysics at Virginia Commonwealth University.

By

ROMANA CVITKOVIC
B.S. in Biology, Brigham Young University, 2010
Masters in Physiology and Biophysics, Virginia Commonwealth University, 2014

Director: JANINA P. LEWIS, PH.D
ASSOCIATE PROFESSOR, PHILIPS INSTITUTE OF ORAL HEALTH RESEARCH
SCHOOL OF DENTISTRY

Virginia Commonwealth University
Richmond, Virginia
July 2014

Acknowledgements

First, I would like to express my deepest appreciation and thanks to my faculty advisor, Dr. Janina Lewis. Thank you for your support, patience and encouragement, and for the active and collaborative learning environment you have built in your lab. I am especially grateful for your continuous mentorship both within research and beyond, and for allowing me to keep my long-term goals in sight.

I would also like to thank my committee members Dr. Todd Kitten and Dr. Liya Qiao for their insight, guidance, and direction on this project. Additional thanks go to Dr. Harvey Schenkein, Dr. Iain Morgan, Dr. Andrew Yeudall, Dr. Myrna Serrano, Dr. Joseph Turner, and Rennie Berry for the use of their facilities and equipment.

A tremendous thank you goes to my fellow colleagues for their invaluable time, support and shared laughter, especially Ross Belvin, Nicai Zollar, Soheil Rostami, Chris Wunsch, David Smith, Kat Sinclair, and Holly Dwyer.

Last, but certainly not least, I would like to thank my wonderful mother, Vesna Mirjacic, whose faith and support has always been the foundation to my successes. I am truly grateful each and every day to have such a valiant supporter in my corner; you are an irreplaceable best friend.

Table of Contents

List of Tables

Page

List of Figures

Page

List of Abbreviations

P. gingivalis	*Porphyromonas gingivalis*
PG	*Porphyromonas gingivalis*
PG0893	hybrid cluster protein, *hcp*, gene
PG1421	ferrodoxin gene
PG1820	cytochrome c nitrite reductase, catalytic subunit NrfA
PG1821	cytochrome c nitrite reductase, small subunit NrfH
PG0627	putative *P. gingivalis* RNA-binding protein (RBP)
°C	Degree Celsius
µg	microgram
µl	microliter
mM	millimolar
min(s)	Minute(s)
BHI	Brain Heart Infusion
LB	Luria-Bertani
E. coli	*Escherichia coli*
PBS	Phosphate-buffered Saline
OD	Optical density
SDS	Sodium dodecyl sulfate
MOI	Multiplicity of Infection
FITC	Fluorescein isothiocyanate

Abstract

Characterization of the biological role of a putative *Porphyromonas gingivalis*

RNA-binding protein

By Romana Cvitkovic, MS

A thesis submitted in partial fulfillment of the requirements for the degree of Masters of Science in Physiology at Virginia Commonwealth University.

Virginia Commonwealth University, 2014

Major Director: Dr. Janina P. Lewis
Associate Professor, The Philips Institute of Oral Health Research
School of Dentistry

Porphyromonas gingivalis, a gram-negative anaerobic bacterium, is a major etiological agent in the initiation and progression of severe forms of periodontal disease. Oral bacteria like *P. gingivalis* are subject to continually changing conditions as a consequence of host eating, oral hygiene patterns and subgingival temperatures. As such survival requires an adaptive response to environmental cues, but little is known about the mechanism by which *P. gingivalis* controls co- and post-transcriptional regulation of RNA levels and potentially protein expression. RNA-binding proteins (RBPs) are evolutionarily conserved across species and are involved in such regulatory mechanisms. However, *P. gingivalis* currently has no identified RBP. Recently, PG0627 has become an ideal candidate for a putative RBP due to its sequence homology to RBPs across various species. By characterizing PG0627, we can gain better insight into the function of

this hypothetical protein and determine if it indeed behaves like an RNA-binding protein. A host of studies were done on a PG0627-deficient *P. gingivalis* mutant, V3139, in order to determine the biological role of the protein encoded by the gene. Our bioinformatics analysis indicated that PG0627 had sequence homology to several RNA recognition motifs or RBPs. Furthermore, our PG0627-deficient mutant, when compared to W83, exhibited decreased cell-associated iron content, decreased total interactions and invasions with eukaryotic cells, and decreased protease activity. Conversely, our PG0627-deficient mutant displayed slightly increased growth in the presence of nitrosative stress, and in hemin-depleted conditions. In conclusion, our results support that PG0627 is a valid candidate for an RNA-binding protein in *P. gingivalis*.

Chapter 1: INTRODUCTION

1.1 Periodontal Disease

1.1.1 General

Periodontal diseases are chronic inflammatory diseases affecting the well-vascularized connective tissues that comprise the supporting tissues of the teeth (Chapple et al., 2000). These diseases range in severity from mild and reversible inflammation of the gingiva to progressive destruction of periodontal ligament and alveolar bone, eventually leading to tooth loss (Lamont and Jenkinson, 1998). Periodontal diseases are very prevalent with an estimated 50% of adults in the US that have experienced some form of the disease, though less than 10% have the severe forms (Lamont and Jenkinson, 2010). Of the worldwide population, an estimated 300 million are believed to be affected by the disease (Pihlstrom et al., 2005; Wayakanon et al., 2013).

1.1.2 Initiation and Progression

The initiation of periodontitis begins with an accumulation of dental plaque below the gum line in the gingival crevice and on teeth (Figure 1). Dental plaque is made up of a microbial biofilm of over 700 different bacterial species, ranging from commensal to potentially virulent organisms (Rylev and Kilian, 2008). These organisms are highly-evolved and highly-specialized, having adapted survival strategies favoring growth in the oral cavity (Darveau and Page, 2000). A dynamic equilibrium exists between normal bacterial oral flora and the innate host defense system, and a diseased state is likely due

to an imbalance of the two (Darveau, 2010). The ability of a pathogen to colonize and proliferate within a particular environmental niche in the host is essential for the initiation of an infection. Growth depends, in part, on the ability of a pathogen to scavenge essential nutrients.

Microbiological analyses have shown that the composition of commensal oral bacteria isolated from healthy sites is significantly different from those isolated from diseased sites. The microbial load was found to be low in healthy sites (10^2-10^3 isolates from individual sulcus), consisting mostly of gram-positive bacteria with about 15% gram-negative rod species (Darveau and Page, 2000). Conversely, characterization of the periopathogenic microbial flora revealed a higher microbial load (10^5-10^8 isolates from individual pockets), with 15-50% of isolates being gram-negative (Darveau and Page, 2000; Tanner et al., 1996). Severe forms of periodontal disease in adults are known to be associated with an increased number of gram-negative anaerobic bacteria (Lamont and Jenkinson, 1998). These findings are all in line with the temporally distinct patterns of microbial colonization within the oral cavity (Aas et al., 2005). The initial colonizers of the dental plaque biofilm are principally oral streptococci and actinomyces (Hasegawa et al., 2007). Establishment of these organisms facilitates the subsequent colonization of additional actinomyces and related gram-positive rods along with gram-negative bacteria. Further maturation is characterized by colonization by gram-negative anaerobes, such as *Porphyromonas gingivalis* (Kolenbrander et al., 2000; Rosan and Lamont, 2000). Once colonization of the subgingival area has occurred, organisms that shed from the plaque biofilm can interact with host epithelial cells that both have a barrier function and act as sensors of microbial infection (Ismail and Hooper, 2005). While many common oral

organisms can adhere to gingival epithelial cells, only a subset of these organisms, particularly *P. gingivalis*, can invade host cells (Lamont and Jenkinson, 1998; Tribble et al., 2006) and possess a remarkable array of virulence factors (Lamont and Yilmaz, 2000), including immune response suppressors, proteolytic enzymes that degrade host tissues and adherence factors that promote bacterial survival (Jandik, 2008).

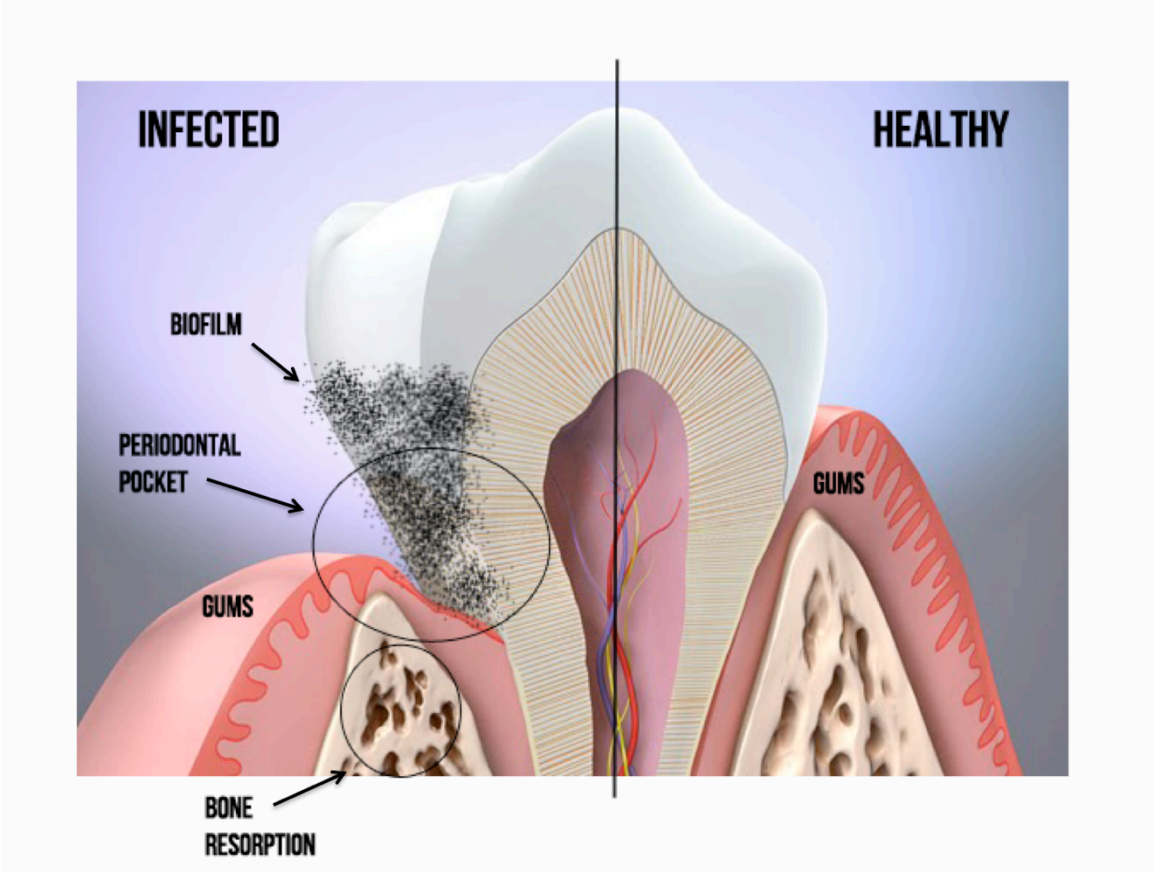

Figure 1. Pathogens involved in the progression of periodontitis shed from biofilm aggregated on tooth enamel and proceed to invade host cells. Adapted from http://drjerrypaz.files.wordpress.com/2011/03/tooth_anatomy_overview.jpg.

1.1.3 Prevention and Treatment

Prevention of periodontal diseases is based on controlling the causal or risk factors, with the most widely accepted risk factor being the biofilm that forms on the teeth in the absence of effective oral hygiene (Pihlstrom et al., 2005). However, various other host factors have also been shown to play a role in the initiation and progression of periodontal diseases and are important considerations in the prevention and treatment of periodontitis, including smoking, tobacco use, pregnancy, puberty, genetics, obesity, poor nutrition, psychosocial stress, depression and systemic diseases such as diabetes (Lamont and Jenkinson, 2000; LeResche and Dworkin, 2002; Pihlstrom et al., 1980).

Oral hygiene procedures such as tooth brushing and flossing are the primary form of prevention of biofilm buildup. Use of mouthwashes and dentrifices containing antibacterial drugs can reduce biofilm and are generally not associated with the emergence of a resistant microbiota (Sreenivasa and Gaffar, 2002). However, once all healthy oral hygiene procedures are ceased, the biofilm begins to develop on the teeth within 24 hours and causes gingivitis in 10-21 days (Loe et al., 1965). When this occurs, the primary treatment of periodontal disease is then through anti-infective non-surgical treatment aimed at controlling the biofilm. Dental plaque and calculus can be removed from tooth-crown and root surfaces through scaling and root planning. Supplemental use of local antibiotics, local antiseptic drugs, systemic antibiotics and systemic use of sub-antimicrobial low-dose doxycycline have been shown to provide some additional benefit compared to debridement alone (Haffajee et al., 2003; Hanes and Purvis, 2003; Hung and Douglass, 2002; Preshaw et al., 2004). Furthermore, nitro-imidazoles, tetracyclines and azithromycin are used most often for antibiotic therapy for anaerobic bacteria like *P.*

gingivalis (Mombelli and Samaranayake, 2004). However, this therapy poses a problem. Though antibiotics can penetrate human tissue, they transverse the plasma membrane of human cells very poorly. Thus, the bacteria that reside intracellularly such as *P. gingivalis* are protected from antimicrobial activity and can subsequently escape from their host cell to re-establish infection and disease (Wayakanon et al., 2013).

Given this escape mechanism of *P. gingivalis*, much is being done to study the various virulence factors of the bacteria as an alternative target for therapy.

1.2 *Porphyromonas gingivalis*

Porphyromonas gingivalis, a gram-negative anaerobe, is a major etiological agent in the initiation and progression of severe forms of periodontal disease (Lamont and Jenkinson, 1998). This bacterium is non-motile, asaccharolytic and rod-shaped with over 2000 known genes and exhibits smooth, raised colonies. When grown on blood agar plates, the colonies progress from an initially creamy-white color to black after 7-10 days, which correlates with the concentration of protoheme (Murakami et al., 2004).

In addition to being a major culprit in periodontal disease, *P. gingivalis* is also implicated as an accessory factor in certain systemic conditions, including increased risk of atherosclerotic heart disease and aspiration pneumonia (Seymour et al., 2007), pre-term delivery, stroke, and diabetes (Boston University Medical Center, 2011). Despite these epidemiological associations, the mechanisms for the various relationships remain unknown, but current hypotheses postulate an interplay between common susceptibility, systemic inflammation with increased circulating cytokines and mediators, direct infection and cross-reactivity or molecular mimicry (Seymour et al., 2007).

This pathogen is perhaps the most intensively studied oral organism at the molecular level and its pathogenicity is attributed to a panel of potential virulence factors.

1.2.1 Virulence Factors

Virulence is defined as the relative capacity of a microbe to cause disease or interfere with a metabolic or physiological function of a host, and virulence factors are thus molecules or components of a microbe that are capable of harming the host (Holt and Ebersole, 2005; Poulin and Combes, 1999; Slots, 1999). *Porphyromonas gingivalis* produces a large number of these enzymes, proteins and end-products of their metabolism that are active against a broad spectrum of host proteins and provide mechanisms not only for host invasion but also for evasion of host defenses (Holt et al., 1999). These latter compounds include proteinase inhibitors, immunoglobulins, iron-containing proteins, bactericidal proteins, extracellular matrix proteins, and proteins involved in phagocytic functions, such as complement fixation and coagulation (Potempa et al., 1995). Conversely, virulence factors considered to be of importance in host invasion include the capsule, lipopolysaccharides (LPS), extracellular/surface cysteine proteases, and fimbriae (Hajishengallis, 2009; Lamont and Jenkinson, 1998).

The capsule of *P. gingivalis* forms the outermost layer of the bacteria, thereby protecting it from the host immune response and promoting its survival (Singh et al., 2011). Separate studies have revealed that encapsulated *P. gingivalis* strains exhibit increased virulence as well as decreased phagocytosis when compared to non-encapsulated strains (Grenier and Mayrand, 1987; Singh et al., 2011; Van Steenbergen et

al., 1987). The capsule has also been implicated in down-regulation of pro-inflammatory cytokine production (Brunner et al., 2010).

The outer membrane of most gram-negative bacteria contains a major surface component called lipopolysaccharides or LPS. *P. gingivalis* can release copious amounts of outer membrane vesicles containing LPS, which can then penetrate periodontal tissue and participate in the destructive innate host response associated with disease (Grenier and Mayrand, 1987; Grenier et al., 1995; McCoy et al., 1987; Moore et al., 1986; Schwartz et al., 1972). LPS plays a critical role in mediating inflammation and inducing cells to secrete pro-inflammatory cytokines, particularly interleukin-1β (IL-1β), tumor necrosis factor-α (TNF-α) and IL-6. Most gram-negative LPS are known to stimulate the production of pro-inflammatory cytokines mainly through toll-like receptor (TLR) 4 and nuclear factor-κB (NF-κB) while most gram-positive peptidoglycan and lipopeptides use the TLR2 receptor (Darveau et al., 2004). However, *P. gingivalis* LPS-induced cytokine production has been elucidated to signal through both TLR4 and the TLR2 (Zhang et al., 2008).

Fimbriae are adhesive hair-like appendages emanating from the bacterial cell surface. They are involved in cellular attachment, and mediate adhesion and invasion into host epithelial cells (Holt et al., 1999). Fimbriae have also been reported to induce the expression of inflammatory cytokines in human gingival fibroblasts and mouse peritoneal macrophages, strongly suggesting that fimbriae play a crucial role in bacterial interactions with host gingival tissues (Hanazawa et al., 1991; Murakami et al., 1994; Ogawa et al., 1994).

1.2.1.1 Cysteine Proteases

One of the potentially significant virulence characteristics of *P. gingivalis* is the large number of hydrolytic enzymes that are produced, specifically the gingipains. Gingipains are major cysteine proteases found in *P. gingivalis* and consist of lysine (Lys-X) and arginine (Arg-X) specific proteases. They cleave after lysine and arginine residues and are encoded for by three genes: *kgp* for Lys-X, and *rgpA* and *rgpB* both coding for Arg-X (Okamoto et al., 1995; Okamoto et al., 1996). These extracellular proteases are believed to play a major role in the pathogenesis of periodontal disease as they are able to degrade a variety of host proteins which can serve as a source of nutrients, as well as have the potential to deregulate host defense (Travis et al., 1997). Specifically, these proteases can directly degrade host tissue, activate host pro-enzymes, neutralize the host immune response, degrade immunoglobulins, inactivate cytokines and their receptors, increase vascular permeability and promote bleeding (Kuramitsu et al., 1995). Moreover, the hemagglutinin/adhesion domain of these enzymes, which is similar to the *P. gingivalis* HagA hemagglutinin, has been shown to possess hemagglutinin activities and thus aid in hemin acquisition from hemoglobin molecules in erythrocytes (Curtis et al., 1996; Han et al., 1996; Pike et al., 1996; Sroka et al., 2001).

1.2.2 Predicted Mechanism of Invasion

Entry of *P. gingivalis* into gingival epithelial cells, which are nonprofessional phagocytic cells, is rapid and requires the bacteria and host cells to be metabolically active (Yilmaz et al., 2006). *P. gingivalis'* adherence to and invasion of epithelial cells are triggered primarily by the binding of major fimbriae to β1 integrin receptors (Yilmaz

et al., 2002). The invasion strategy is accompanied by the phosphorylation and activation of putative integrin-signaling and structural proteins as well as by significant remodeling of the actin cytoskeleton, suggesting that rearrangements of the host cell signaling proteins permit bacterial entry into epithelial cells (Yilmaz et al., 2002; Yilmaz et al., 2003). *P. gingivalis* is nonmotile in the extracellular space, invades epithelial cells in high numbers and is then localized to the cytoplasm (Belton et al., 1999). *In vitro*, the bacterium is capable of intracellular replication and remains viable for extended periods in epithelial cells. Likewise, invaded epithelial cells do not die and are anti-apoptotic and thus further contribute to the survival of *P. gingivalis* in the host (Yilmaz et al., 2006).

1.2.3 Host Response

Once the pathogen has invaded the host, the body's immune system fights the bacteria, releasing cytokines and chemokines thereby initiating the immune response as seen in Figure 2 (Bainbridge et al., 2010). However, this results in inflammation and bone resorption as the immune response actively combats the bacteria. If the condition is not treated, bones, gums and connective tissue are destroyed and teeth may have to be removed (Rylev and Kilian, 2008).

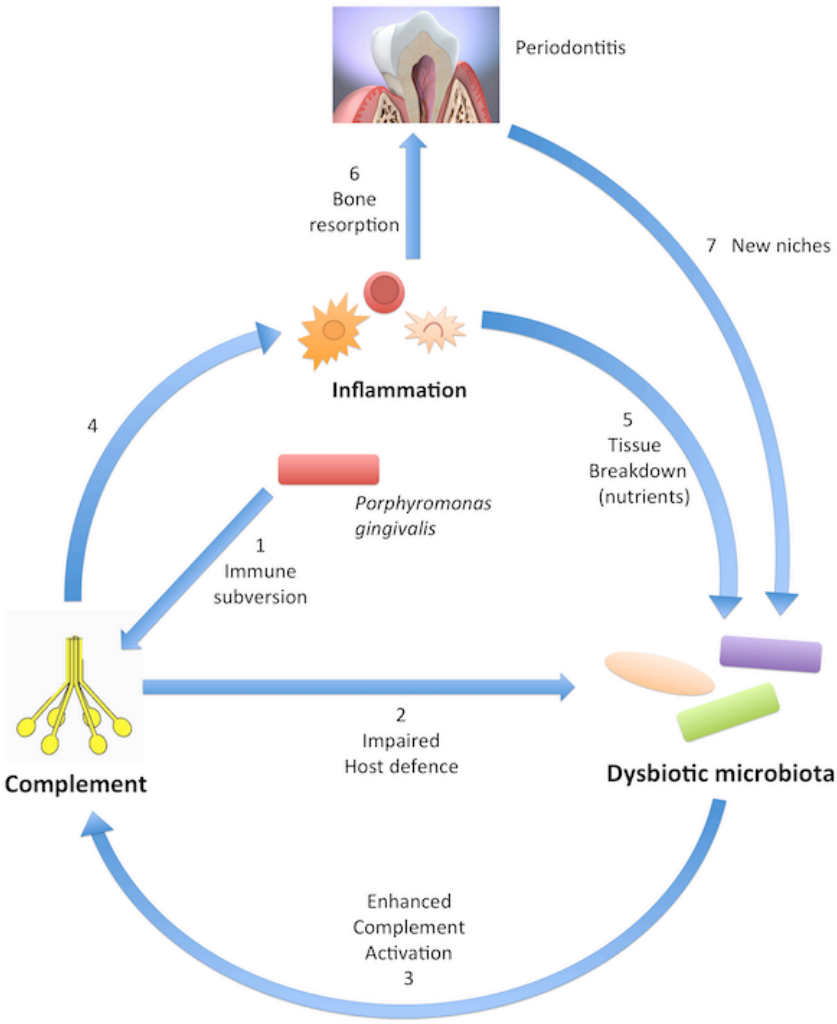

Figure 2. *Porphyromonas gingivalis*-induced dysbiosis and periodontal disease. *Porphyromonas gingivalis* subverts complement and impairs host defense, leading to overgrowth of oral commensal bacteria, which causes complement-dependent inflammation. Adapted from "The Keystone-Pathogen Hypothesis" by Hajishengallis et. al. 2012, http://www.nature.com/nrmicro/journal/v10/n10/fig_tab/nrmicro2873_F2.html

1.2.4 Role of Iron

P. gingivalis, like most living organisms, has an obligate iron requirement for growth and survival, yet the bacterium does not produce the essential nutrient itself (Lamont and Jenkinson, 1998). While many microorganisms have developed diverse and elaborate systems to obtain this element, including the production of siderophores which chelate environmental iron, *P. gingivalis* employs no such mechanism in iron-limited host environments (Bramanti and Holt, 1991; Genco, 1995; Schifferle et al., 1996). Instead, it scavenges iron from the host organism in the form of hemoglobin (Genco and Dixon, 2001). Heme is preferentially obtained from hemoglobin and is acquired through the activity of the cell surface Arg- and Lys-specific proteinase-adhesin complexes (Dashper et al., 2004; Shi et al., 1999; Shizukuishi et al., 1995). Hemoglobin released by lysis of erythrocytes is rapidly bound by haptoglobin and similarly, hemin is complexed to hemopexin (Lewis et al., 1999). As both of these compounds can be used as iron sources by *P. gingivalis*, this indicates that this bacterium has a mechanism for removing the hemin from these host iron-binding proteins (Bramanti and Holt, 1991). Although *P. gingivalis* is capable of utilizing various hemin-containing compounds, Shizukuishi et al. have shown that this organism utilizes hemoglobin more efficiently than other iron-containing compounds (Bramanti and Holt, 1991; Genco, 1995; Shizukuishi et al., 1995).

On *P. gingivalis*, acquired hemin is stored on the cell surface, a feature considered to give rise to the characteristic black-pigmented appearance of its colonies (Genco, 1995). The intact hemin molecule (Figure 3) can be transported into the bacterium in an energy-dependent process regulated by the levels of available hemin, and specific

interactions between the protoporphyrin IX ring and outer membrane proteins appear to initiate the uptake process (Bramanti and Holt, 1991; Genco et al., 1994).

In the oral cavity itself, the levels of hemin are likely to show variance based on genetics, nutrient intake and other factors. Bleeding as a result of gingival inflammation can elevate subgingival hemin concentrations and may be one factor that predisposes a site to *P. gingivalis* accumulation (Lamont and Jenkinson, 1998). *P. gingivalis* has also developed mechanisms that will increase the availability of hemin such as the proteolytic activity of the cysteine proteases discussed previously.

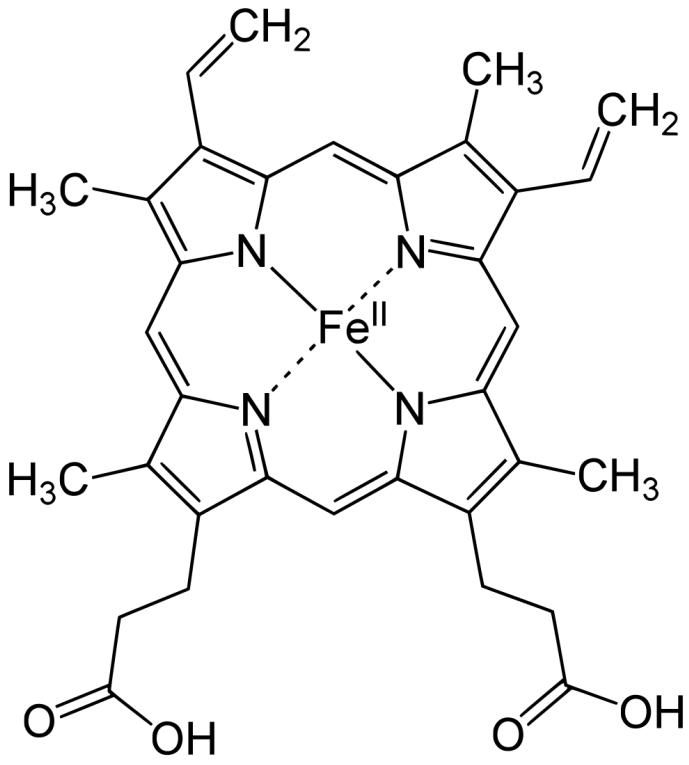

Figure 3. Schematic of heme molecule utilized by *P. gingivalis*, iron-protoporphyrin IX. Abstracted from Wikipedia Commons. (http://upload.wikimedia.org/wikipedia/commons/thumb/b/be/Heme_b.svg/1000px-Heme_b.svg.png)

1.2.5 Oxygen

Although *P. gingivalis* is an anaerobic bacterium, it does possess a low tolerance to oxygen and could thus be classified as an aerotolerant anaerobe (Diaz et al., 2002). That is, while it is incapable of colony formation on plates incubated aerobically, it can tolerate, for a limited time, the presence of atmospheric oxygen and it will grow in the presence of oxygen concentrations lower than that in air (Diaz and Rogers, 2004). During colonization of the oral tissues, *P. gingivalis* is exposed to various oxidative stress conditions, including saliva, the tongue, and the buccal mucosa (Dahlen et al., 1992; Lamont and Jenkinson, 2000; Van Steenbergen et al., 1993). This exposure leads to the presence of an unfavorable redox potential, and the damaging effects of reactive oxygen species (ROS) might challenge the bacterium's survival before finding the appropriate anaerobic microenvironment in which to establish itself and proliferate (Diaz and Rogers, 2004). The growth of *P. gingivalis* under oxygenated environments is also accompanied by changes in fermentation end-products, cell morphology, anti-oxidant enzymes and proteinase activity (Diaz and Rogers, 2004). Given these factors, it is essential for *P. gingivalis* to develop efficient oxidative stress protection mechanisms in order to survive oxygen exposure, but the mechanism is not currently well established.

1.2.6 Nitrogen

Although *P. gingivalis* is dependent on nitrogenous substrates for energy, it must also be able to withstand the high concentrations of nitrite/nitric oxide that are particularly high in the oral cavity, thanks in part to high dietary nitrate intake (Shah and Gharbia, 1989). Nitric oxide is a highly reactive and cytotoxic free radical that can react

with oxygen and other molecules to result in the formation of toxic reactive nitrogen species (Hochgrafe, 2008).

Following intake of foods rich in sucrose, the pH in the oral cavity drops drastically due to metabolic conversions of the sugar to acid, thus creating conditions that are favorable for the chemical generation of nitric oxide from nitrite (Lewis et al., 2012; Palmerini et al., 2003). Nitric oxide may also be generated from nitrite during metabolism through the respiratory nitrite reductase system, NrfHA (Spiro, 2006). However, a third source may come from host eukaryotic cells that respond to microbial infection by producing nitric oxide and 0_2-related species in the innate immune response (Fang, 1997).

Despite these high concentrations of nitrite/nitric oxide in the oral cavity, little is known about the mechanism by which *P. gingivalis* tolerates nitrosative stress and detoxifies nitrite/nitric oxide.

1.2.7 Regulation by RBPs

Oral bacteria, including *P. gingivalis*, are subject to continually changing conditions as a consequence of host eating, oral hygiene patterns and subgingival temperatures (Lamont and Jenkinson, 1998). As such survival requires an adaptive response to environmental cues, but little is known about the mechanism by which *P. gingivalis* controls co- and post-transcriptional regulation of RNA levels and potentially protein expression. RNA-binding proteins (RBPs) are evolutionarily conserved across species and are involved in such regulatory mechanisms. However, *P. gingivalis* currently has no identified RBP. Recently, PG0627 has become an ideal candidate for a putative RBP due to its sequence homology to RBPs across various species.

One such RBP is Hfq which is common to diverse bacterial lineages and has key roles in the control of gene expression. This protein is active co- and post-transcriptionally, and serves several purposes in the cell. First, Hfq can suppress protein synthesis by aiding a sRNA to bind the 5' region of its target mRNA, thus rendering the 5' region inaccessible for translation initiation (Vogel and Luisi, 2011). Conversely, it can boost translation by guiding an sRNA to the 5' region of its target mRNA in order to disrupt a secondary structure that otherwise inhibits ribosome binding (Vogel and Luisi, 2011). Additionally, Hfq can protect sRNAs from ribonuclease cleavage or present some RNAs in such a way as to promote RNA turnover by rendering the 3' ends accessible for polyadenylation and subsequent 3'-to-5' exonucleolytic degradation (Vogel and Luisi, 2011).

A second protein which seems to share a great deal of protein sequence homology is a *H. sapiens* Cleavage stimulation factor 64kDA, particularly the N-terminal RRM recognition motif (for short, CstF-64). CstF-64 directly interacts with single-stranded RNAs via its RNA recognition motif (RRM) and plays important roles in mRNA 3' processing (Chan et al., 2011; Takagaki et al., 1996). This protein binds a wide range of G/U-rich sequences on ssRNA with comparable affinity, yet is not highly specific for any one target sequence (Canadillas and Varani, 2003). Thus, much like that of RBPs, it displays slow kinetics and has the ability to bind tightly to a class of sequences without strong preference for any particular sequence, yet it can discriminate effectively against other RNAs. RBPs are known to bind to various motifs and ribosomal binding sites in order to instill their effect in degrading or stabilizing RNA, as well as inhibiting or stabilizing translation as stated previously.

1.2.8 PG0627

Due to its strong protein sequence homology to cross-species RBPs, and in particular, the N-terminal RRM of CstF-64, PG0627 was chosen as a candidate gene for a putative RNA-binding protein in *P. gingivalis* (Tables 1 and 2). If this is confirmed, it would be the first RBP elucidated in this oral bacterium.

PG0627 is defined as a putative RBP according to the Los Alamos National Laboratory *P. gingivalis* database (Los Alamos National Security, LLC, 2010). It is located in the cytoplasm, has a molecular weight of 11.5kDa, a gene length of 291bp and is composed of 96 amino acids (Figure 4).

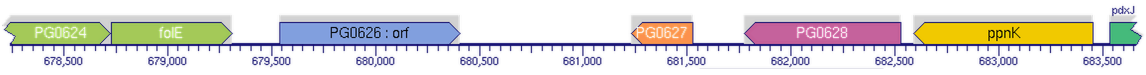

Figure 4. Locus of PG0627 in the *P. gingivalis* genome. As is seen here, the gene comprises a single transcriptional unit, color-coded in orange.

Table 1. Nucleotide sequence similarities of PG0627 to RBP sequences in other genes.

Nucleotide Sequence			
Organism	**PG0627 Residues**	**Protein**	**Similarity**
Treponema pallidum	1-76	Putative RBP (gbAAC65342.1)	53%
Synechocystis sp.	3-76	RBP (gbAAA85379.1)	54%
Brugia malayi	1-76	Putative RBP (gbAAC47624.1)	50%

Table 2. Protein sequence similarity of PG0627 to proteins present in other proteins.

Protein Sequence			
Organism	**Protein**	**E-value**	**Similarity**
Homo sapiens	N-terminal RRM domain of Cleavage stimulation factor 64KDa subunit (PDB: 1P1T)	6.3E12	62%

1.2.9 Other Genes of Interest

Four other genes of interest that are thought to help *P. gingivalis* adapt to environmental cues include, PG0893, PG1421, PG1820, and PG1821.

PG0893 is a hybrid cluster protein (Hcp) that is thought to protect *P. gingivalis* from exposure to nitric oxide by converting NO to other forms. PG1421 is a ferredoxin, which is an iron-sulfur protein that can change the oxidation state of iron by mediating electron transfer in redox reactions. PG1820 (NrfA) and PG1821 (NrfH) are both part of the cytochrome c nitrite reductase system. This subunit spans the periplasm (NrfA) and inner membrane (NrfH) and is thought to convert nitrite into ammonia thus playing a role in detoxification of nitrosative stress. Taken together, these four genes are thought to be part of the nitrosative stress protection mechanism network in *P. gingivalis*.

1.3 Research Objectives

Hypothesis:

We believe that *P. gingivalis* candidate proteins RBP (PG0627), NrfA (PG1820), NrfH (PG1821), Hcp (PG0893) and ferrodoxin (PG1421), may be involved in adaptation of *P. gingivalis* to environmental conditions.

Aim 1: As *P. gingivalis* has been known to respond to environmental cues, we believe that PG0627, a putative RNA-binding protein, may play a role in altering RNA levels by degrading or stabilizing the RNA itself, or altering protein levels. Thus, it is significant to characterize the biological role of the putative RBP-deficient mutant, via:

I. Bioinformatics
II. Metal Content Assays
III. Growth Studies
    a. Hemin Depletion
    b. Nitrosative Stress
IV. Oxidative Stress
V. Protease Activity Assays
VI. Total Interactions and Invasions in Eukaryotic Cells
VII. Gene Expression
VIII. Proteomics

Aim 2: Although *P. gingivalis* is dependent on nitrogenous substrates for energy, it must also be able to withstand the high levels of nitrosative stress that are particularly high in

the oral cavity. Homologous sequences and products across other species of the four genes listed below were shown to be readily involved in nitrosative stress protection mechanisms, and for that reason have been studied here. Thus, the aim is to create mutant knockout strains deficient in the following genes in order to investigate their role in protection from nitrosative stress: PG0893, PG1421, PG1820, PG1821. This is being studied via:

I. Generation of PCR Fusion Products

II. Ligation, Cloning into pCR 2.1 TA Vector

III. Electroporation

IV. Mutant Confirmation

V. Phenotypic Assessment of Mutant's Ability to Survive Under Nitrosative Stress

Chapter 2: MATERIALS AND METHODS

2.1 Bacterial Strains and Plasmids

The bacterial strains and plasmids used in this study are listed in Table 3.

Table 3. Strains and plasmids used in this study

Bacterial Species	Strain	Plasmid	Description	Reference
P. gingivalis	W83	Parental Strain		Lewis and Macrina, 1999
	V3139	PG0627 (RBP-deficient mutant)		Lewis et al. (unpublished)
E. coli	One Shot® Top 10 cells	Chemically competent cells		Invitrogen (Catalog Number: C404003)
E. coli		pCR®2.1	PCR TA cloning vector	Invitrogen

2.2 Media Growth Conditions

2.2.1 *Porphyromonas gingivalis*

Porphyromonas gingivalis strains were grown in brain heart infusion broth (BHI; Difco Laboratories, Detroit, MI) supplemented with hemin (5μg/ml; Sigma-Aldrich, St. Louis, MO), yeast extract (5mg/ml; Sigma-Aldrich, St. Louis, MO), vitamin K (0.5μg/ml; Sigma-Aldrich, St. Louis, MO), and L-cysteine (1mg/mL; Sigma-Aldrich, St. Louis, MO). The *P. gingivalis* strains were grown anaerobically in a chamber at an atmosphere of 10% CO_2, 10% $H_{2,,}$ 80% N_2 at 37°C.

2.2.2 *Escherichia coli*

Escherichia coli was grown aerobically at 37 °C in Luria-Bertani broth (LB; Invitrogen; Cat. No. 12780029) or on LB agar. Kanamycin (50 μg/mL) was added to select for recombinant strains.

2.3 *Porphyromonas gingivalis* Cell Culture Preparation

P. gingivalis parental and mutant strains were spread onto blood agar plates (TSA II, 5% sheep blood; BBL, Cockeysville, MD) with clindamycin (0.5 μg/ml) and grown anaerobically at 37°C. Once colonies were observed on the plates (3-7 days), a sterile inoculating loop was used to scoop the colonies, inoculate into BHI medium and grow at 37°C. The cultures were diluted nearly daily to ensure that bacteria stayed in the log phase of growth until ready for harvesting. Once the cultures reached an optical density (OD_{660}) of 0.5-0.7, they were ready for further use.

2.4 Generation of *P. gingivalis* Mutant Strains

Four potential mutant strains, ΔPG0893, ΔPG1421, ΔPG1820 and ΔPG1821, were generated for the purpose of characterization in *P. gingivalis*. A fusion PCR technique was used to generate these mutants where the upstream and downstream gene fragments and the selective cassette were first amplified separately by PCR using primers that produced overlapping ends (Cha-aim et al., 2012; Ho et al., 1989; Szewczyk et al., 2006). A second PCR round then used primers to fuse the fragments together in the desired order, essentially replacing the gene with the selective cassette without the use of any restriction enzymes, and creating a knockout. All genes were amplified using Platinum® Taq DNA Polymerase High Fidelity kit (Invitrogen; Carlsbad, CA). All PCR purifications of the PCR products were done using the MiniElute PCR Purification kit (Qiagen; Valencia, CA).

2.4.1 Isolation of *ermF* cassette

The *ermF* cassette is an 800 bp gene and was used as a selection factor for the mutant strains. It encodes resistance to erythromycin, and in anaerobic conditions, to clindamycin. It was isolated from the pVA2198 plasmid containing the 2 kb *ermF-ermAM* antibiotic resistant gene cassette (Fletcher et al., 1995). It was thus used as the template DNA to amplify the *ermF* cassette using primers ermFF and ermFR, and then purified (Table 4).

2.4.2 Generation of PCR Products

Fusion PCR techniques were used to generate linear PCR products without the use of restriction enzymes, creating a knockout of each gene (Cha-aim et al., 2012; Ho et

al., 1989; Szewczyk et al., 2006). 250-300 bp upstream and downstream homologous flanking regions of the target genes were amplified using *P. gingivalis* W83 genomic DNA as a template and then purified. In the first PCR round, the flanking regions of the target region were amplified using the primers in Table 4, e.g. 1820F1-1820R1 primers and 1820F2-1820R2 primers (Integrated DNA Technologies; Coralville, IA). The primers 1820F2 and 1820R2 were designed so that the amplification products generated had sequences homologous to the ends of the *ermF* cassette (also Table 4). The fragments generated from the first round of PCR as well as the *ermF* fragment were then used as templates for the second round of PCR, in which, for example, 1820F1 and 1820R2 primers were used to create a linear product suitable for transformation (Figure 5). This was done using the Gibson Assembly Master Mix per manufacturer's instructions (NEB, Cat. No. E2611L). Gibson Assembly efficiently joins multiple overlapping DNA fragments in a single-tube isothermal reaction, regardless of fragment length or end compatibility. The same two-step PCR process was done for genes PG0893, PG1421 and PG1821. The conditions used in the PCR reactions were: 1) one cycle of denaturing at 94°C for 5 minutes, 2) 35 cycles of denaturing at 94°C for 2 minutes and annealing at 53°C for 30 seconds, 3) elongation at 68°C for 3 minutes, and 4) final extension at 68°C for 7 minutes. The fused products were then confirmed via gel electrophoresis.

Table 4. Primers used for fusion PCR for PG0893, PG1421, PG1820, PG1821 and *ermF*.

Name	Description	Sequence (5' → 3')
PG0893F1	PG0893 Forward Upstream	TACCGAAGTTTTCGATCAGC
PG0893R1	PG0893 Reverse Upstream	CCCCCGGGGGCCCCCCCTTCCGATACGGTTATCCT
PG0893F2	PG Forward Downstream	GGGGGGGGGGGGGGGCTGAGAGCCAACCGATCATA
PG0893R2	PG Reverse Downstream	GGGTATGCGGTAAGGACTTT
PG1421F1	PG1421 Forward Upstream	CGAGCTATACCGAAGGATGA
PG1421R1	PG1421 Reverse Upstream	CCCCCGGGGGCCCCCAATTAACCGCCCCTGACTAC
PG1421F2	PG1421 Forward Downstream	GGGGGGGGGGGGGGGCGACTTAAACGCGAATGAAT
PG1421R2	PG1421 Reverse Downstream	GAGGCATACCTCAAGAGTGG
PG1820F1	PG1820 Forward Upstream	TTGGCTGCTATCAAAAGACC
PG1820R1	PG1820 Reverse Upstream	CCCCCGGGGGCCCCCAAAAGGAAATGACCCCCATA
PG1820F2	PG1820 Forward Downstream	GGGGGGGGGGGGGGGGACCGCGAGGAGATGTATAA
PG1820R2	PG1820 Reverse Downstream	GCTCTATGGTGGTGGTGTTC
PG1821F1	PG1821 Forward Upstream	GACCGCGAGGAGATGTATAA
PG1821R1	PG1821 Reverse Upstream	CCCCCGGGGGCCCCCGCTCTATGGTGGTGGTGTTC
PG1821F2	PG1821 Forward Downstream	GGGGGGGGGGGGGGGGTACCTGCTGAGCTAGCGATT
PG1821R2	PG1821 Reverse Downstream	CAGGACGACTCTGAGCATTT
ermEF	ermE Forward	GGGGGCCCCCGGGGGCGATAGCTTCCGCTATTGCT
ermER	ermE Reverse	CCCCCCCCCCCCCCCCTTTTACGTTTCCGCTCCATCGCC

* Tails, in blue, were added to create homologous flanking regions to the gene, in black.

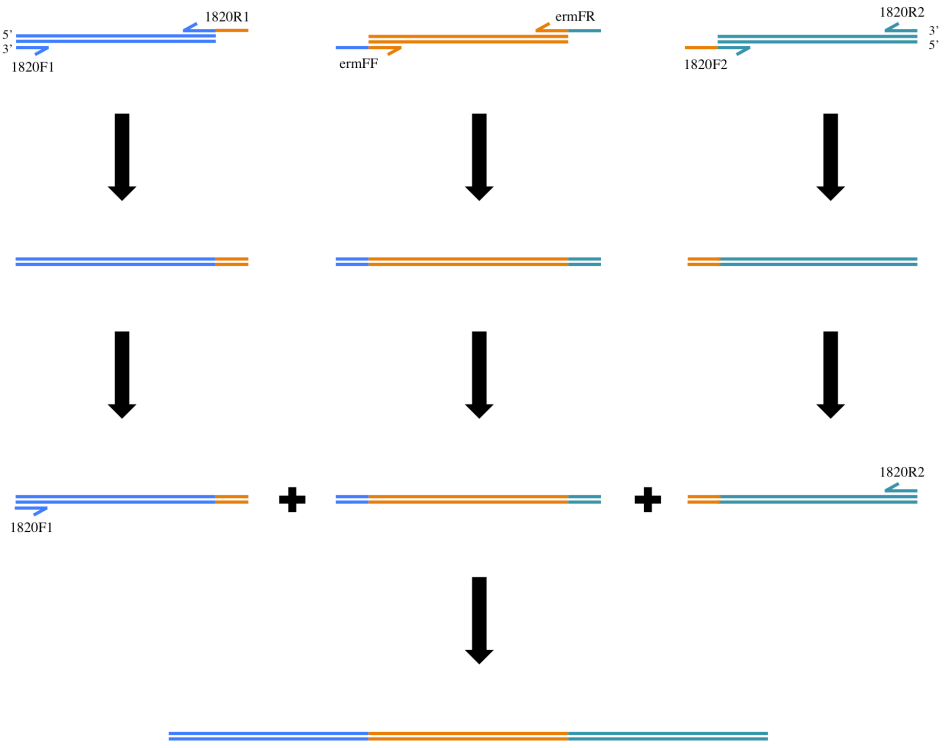

Figure 5. Schematic diagram of two rounds of fusion PCR used to generate linear fused gene products of PG0893, PG1421, PG1820 and PG1821. PG1820 and *ermF* were used as a specific example.

2.4.3 PCR Purification

After gel confirmations, PCR products were purified using the MiniElute PCR Purfication Kit using manufacturer's instructions (Qiagen; Cat. No. 28006).

2.5 Cloning and Transformation

Once the desired PCR fragments were produced, the products were individually cloned into the pCR® 2.1 vector (Figure 6) and transformed into One Shot® TOP10 Chemically Competent *E. coli* cells using manufacturer's instructions (TA Cloning® Kit; Invitrogen, Cat No. KNM2040-01).

The *E. coli* cells with the plasmid vector with the desired insert were then plated on LB agar plates supplemented with clindamycin for antibiotic resistance (0.5ug/ul) and with X-gal for blue-white screening (16µl), and incubated overnight at 37°C. When at least one white colony with the desired insert appeared, the colony was swiped with a sterile inoculating loop and inoculated with 3mls of LB (Luria-Broth; Affymetrix, Cleveland, OH) and allowed to grow overnight in shaking incubator at 37°C. The next day, the plasmid DNA vector was isolated from *E. coli* using the QIAprep Spin MiniPrep Kit (Qiagen, Cat. No. 27104). In order to confirm that the plasmid indeed carries the desired insert, it was verified via *Eco*RI digestion for 15 minutes at 37°C (10µl plasmid, 1ul *Eco*RI, 3µl 10X Buffer and 16µl distilled water; *Eco*RI restriction enzyme, NEB, Cat No. R0101S). The digested colonies were then run on a gel to confirm size.

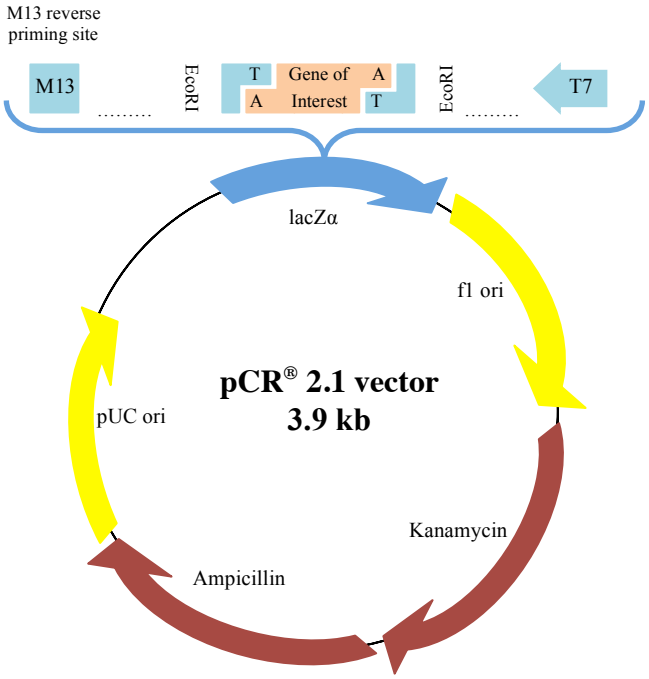

Figure 6. Schematic diagram of the pCR® 2.1 TA vector with inserted PCR products and *Eco*RI restriction digest sites.

2.6 Electroporation and Plating

From an actively growing blood agar plate with culture, one streak of *P. gingivalis* colonies were swiped with a sterile inoculating loop and inoculated into 3mls of BHI media (Bovine Heart Infusion, pH 7.2; Recipe: 37g BHI, 5g yeast extract, 1g cysteine HCl, 5ml hemin, 4ml 1M NaOH, 200µl vitamin K). Cultures were grown overnight in an anaerobic chamber at 37°C, inoculated in a 1:10 dilution with BHI media the next day, and grown overnight in the same conditions again. The following morning, 1-150 ml bottle of fresh pre-warmed BHI media was inoculated with 500-650µl of overnight culture. These cultures were then grown overnight once more in the same conditions until the OD_{660} was between 0.4 and 0.7. Cells were harvested and washed twice with electroporation buffer (recipe: distilled water with 10% glycerol, 1mM magnesium chloride; filter sterilized).

To electroporate and allow homologous recombination (Figure 7), 100µl of cells were placed in sterile 0.2cm gap electrode cuvette, 10µg of PCR product were added to cells, and cells were pulsed with the BIO-RAD gene pulser set at 2500V (Gene Pulser® II Electroporation System; Hercules, CA). In the chamber, 500µl of BHI media were added to each cuvette, incubated at 37°C and grown overnight.

The next day, cells were plated on blood agar plates supplemented with clindamycin (0.5µg/ml) and the plates incubated 3-10 days at 37°C until colonies grew. Upon colony appearance, colonies were re-streaked on a fresh blood agar plate with clindamycin, checked for contamination, and the insert was confirmed via one round of PCR followed by gel confirmation. Daily 1:10 culture dilutions were also started for quick availability as needed, with OD_{660} maintained between 0.5 and 1.

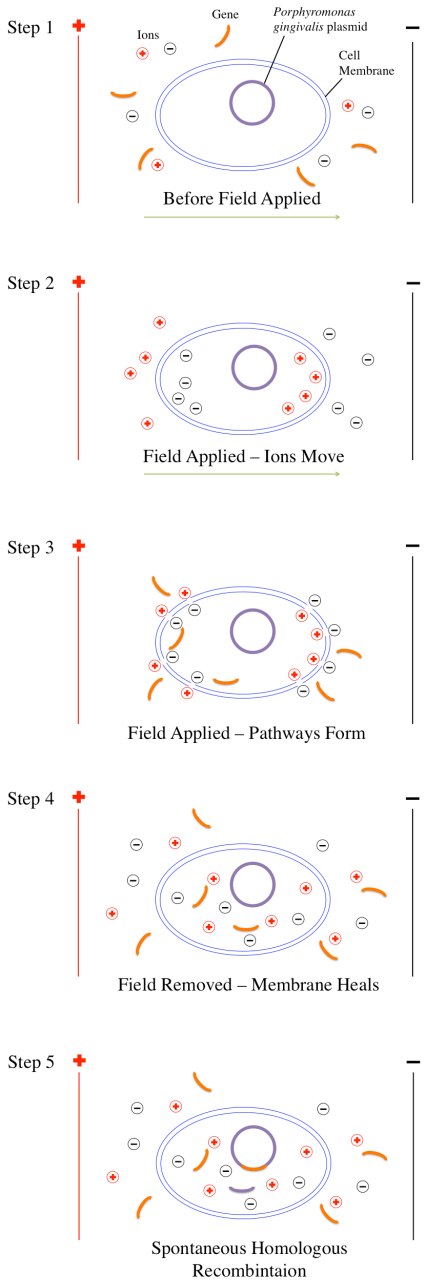

Figure 7. Electroporation

Figure 7. Electroporation is a mechanical transfection method that uses an electrical pulse to create temporary pores in cell membranes through which DNA can pass into cells. Steps: 1) Electroporation exposes a cell to a high-intensity electric field that temporarily destabilizes the membrane; 2) During this time, the membrane is highly permeable to exogenous molecules present in the surrounding media; 3) DNA then moves into the cell through these holes; 4) When the field is turned off, the pores in the membrane reseal, enclosing the DNA inside and 5) allowing homologous recombination to occur spontaneously.

2.7 Bioinformatics

Basic bioinformatics information was generated querying several databases and modeling websites for a best-fit homology model of PG0627. Research was also conducted to determine if PG0627 is indeed a good candidate gene to code for an RNA-binding protein in *P. gingivalis*. First, the Los Alamos National Laboratory *P. gingivalis* database (Los Alamos National Security, LLC, 2010) was used to determine a protein database (PDB) structure with high sequence similarity that could be used as a reference model for PG0627 protein structure. Next, one-to-one threading by Phyre2 was conducted using this reference protein model and PG0627 to generate a homology model (Kelley and Sternberg, 2009), and the models and overlays were generated via UCSF's Chimera software. A separate modeling inquiry was also conducted (to confirm validity of the generated model) via the Swiss Institute of Bioinformatics (SIB) ExPASy website utilizing SWISS-MODEL (Arnold et al., 2006), which is a fully automated protein structure homology-modeling server that "models protein tertiary and quaternary structure using evolutionary information" (Biasini et al., 2014). As model quality estimation is an essential component of protein structure predictions since the accuracy of a model determines its usefulness for practical applications, the SWISS-MODEL provides model quality estimates based on a QMEAN (quality model energy analysis) potential (University of Basel, 2014) specifically re-parameterized for models built by SWISS-MODEL (Benkert et al., 2009; Benkert et al., 2011). Further confirmation that PG0627 is indeed an RBP was resolved via InterPro (https://www.ebi.ac.uk/interpro/), a repository of databases for protein sequence analysis and classification.

2.8 Determination of Metal Content

From overnight cultures of 6ml grown in BHI, pellets were harvested and washed twice with chelex treated buffer (50mM HEPES, 50mM NaCl). This eliminated the extracellular metal content present. Next, added to the pellets was 3ml of the same chelex treated buffer but supplemented with 8M urea, in order to denature and unfold the DNA. Samples were sonicated for three minutes at 20% duty cycle on ice, and centrifuged at 8500 rpm for 30 minutes. Subsequently, the supernatant was removed from each sample for analysis via either ICP-MS or colorimetric ferrozine assay.

2.8.1 ICP-MS

Inductively coupled plasma mass spectrometry, or ICP-MS, is an analytical technique used for elemental determinations. Using argon gas, elements in the liquid samples are converted to ions, and then separated and detected by a mass spectrometer (Wolf, March 2005). Results were given as relative abundance of individual metal ions (Mg, Fe, Co, Ni, Cu, Zn) in parts per trillion and compared to standards.

2.8.2 Colorimetric Ferrozine Assay

Fe(II) ions form a magenta colored solution with ferrozine, and this reaction is used to quantitatively analyze Fe^{2+}(aq) in solution using a UV-Vis spectrophotometer. 500µl of sample was incubated with 0.01M ferrozine and 5M ammonium acetate (buffer) for five hours anaerobically, and a deep purple color developed. Optical density readings were taken at 562nm, the absorbance of the colored reaction, and then relative abundance was quantified in parts per million from a standard curve.

2.9 Protease Assays

N-alpha-Benzoyl-D,L-arginine 4-nitroanilide hydrochloride (DL-BAPNA; Sigma, Catalog No. B4875) and D-Phe-Pro-Lys-pNA (Sigma, Catalog No. SCP0126) are chromogenic substrates for proteolytic enzymes such as trypsin, amidase, and balterobin. Hydrolysis of these substrates at the bond between the arginine and the p-nitroaniline moieties (DL-BAPNA) or the lysine and p-nitroaniline moieties (D-Phe-Pro-Lyz-pNA) releases the chromophore p-nitroaniline, which can be detected by colorimetric analysis.

The remaining 15µl of cells from the transcriptome preparation below was resuspended in 200-400µl of PBS, and diluted sufficiently so that when approximately 4-10µl of sample are combined with 500µl of 1M Tris-HCl pH 8.0 in VIS cuvettes, the OD_{405} reading was near 0.050.

2.9.1 Arg-X Activity

For the Arg-X activity assay, 5µl of sample was aliquoted out into a VIS cuvette, in triplicates. 500µl of 1M Tris-HCl pH 8.0 with 4mM TCEP were added into each cuvette, and a blank was also created. TCEP is a reducing agent used to break disulfide bonds. Baseline absorbance values were recorded to ensure all samples were roughly around an OD_{405} of 0.050. 50µl of DL-BAPNA at a concentration of 4.3mg/ml of DMSO was quickly added to each cuvette including the blank. After 5 minutes, absorbance values were once again taken at 405nm. This was repeated again as needed every 15-30 minutes until an activity plateau was reached.

2.9.2 Lys-X Activity

For the Lys-X activity assay, 5µl of sample was aliquoted out into a VIS cuvette, in triplicates. 500µl of 1M Tris-HCl pH 8.0 with 4mM TCEP was added into each cuvette, and a blank was created. Baseline absorbance values were recorded to ensure all samples were roughly around an OD_{405} of 0.050. 25µl of D-Phe-Pro-Lys-pNA at a concentration of 4.9mg/ml of DMSO was quickly added to each cuvette, including the blank. After 5 minutes, absorbance values were once again taken at 405nm. This was repeated again as needed every 15-30 minutes until an activity plateau was reached.

2.10 Total Interactions and Invasions

Total interactions and invasions of *P. gingivalis* strains with eukaryotic human umbilical vein endothelial cells (HUVEC) was determined through fluorescent tagging with Fluorescein Isothiocyanate (FITC; Sigma, St. Louis, MO), quenching via trypan blue and analyzed via flow cytometry (BD FACS Canto II, Becton Dickinson, Franklin Lakes, New Jersey).

Fresh HUVEC cells were prepared the day before analysis, as well as 3ml of bacterial cultures with OD_{660} readings between 0.4 and 0.7. The bacteria were washed twice with PBS anaerobically, resuspended in 1ml PBS and 2µl of FITC was added to samples. Samples were mixed for one hour at $4^{o}C$ in the dark. After incubation, samples were returned to the anaerobic chamber, washed twice more with PBS and resuspended in 2ml of HUVEC media. Absorbance was once again taken and an MOI of 100 bacterial cells to 1 HUVEC (100:1) was made and allowed to incubate for 30 minutes at $37^{o}C$ before reading.

Fluorescence was measured using the BD FACS Canto II flow cytometer equipped with an argon ion laser having a single excitation wavelength of 488nm, with computer-assisted data analysis. FITC fluorescence was captured (emission wavelength of 518nm) and plotted against the number of cells for a calculation of total interaction. Total invasion readings were done immediately after interaction readings, by adding 25µl of 100ug/ml trypan blue to samples. Trypan blue acted as an extracellular quencher thereby only counting invasions. Samples were incubated with trypan blue for no more than 2 minutes, as time longer than that will begin to completely rupture the cells. At least 10,000 cells were captured and analyzed for each sample for each of the interaction and invasion readings. Healthy populations were gated and analyzed using the FCS Express software, and gates were set to eliminate any unstained material or debris. Median was used as a measurement of relative absorbance of FITC for analysis and plotted in a graph.

2.11 Hemin Depletion

On day -2, a fresh culture of bacteria in BHI media supplemented with vitamin K was grown. The following day, absorbance readings at OD(660) were recorded, and a 1:10 dilution in BHI media was created and grown until an OD(660) of 1.0. On day 0, a 1:10 dilution in mycoplasma media supplemented with vitamin K but without hemin was made, and OD(660) readings were taken two days later just prior to the next passage. To make mycoplasma media, 20 grams of the BBL Mycoplasma Broth Base (BD, St. Louis, MO) was suspended in 1 liter of purified water, and mixed thoroughly. The solution was then warmed gently until the solution was complete, and autoclaved at 121^{o}C for 15

minutes to sterilize. It was finally cooled to 50^{o}C and 200µl of vitamin K enrichment was added.

Passaging of bacterial samples was done every other day in 1:10 dilutions of mycoplasma media without hemin until absorbance readings were less than 0.1.

2.12 Nitrosative Stress

Bacterial cultures (10ml) were prepared using mycoplasma media with and without 5µg/ml hemin supplemented, and passaged twice before being grown to an optical density at 660nm of 0.05 anaerobically. Various concentrations of nitrosative stress-generating species were then added to the cultures: nitrate ($NaNO_3$; 40mM, 20mM) or nitrite ($NaNO_2$; 8mM, 4mM, and 1mM).

Aliquots of 1ml were removed at various time points (0 h, 4 h, 8 h, and 16 h), and growth was monitored by measuring the OD(660). Three sets of biological triplicates were conducted on different days to ensure significance of the results.

2.13 Oxidative Stress

BHI-agar plates were prepared (20g/L agar, 37g/L brain-heart infusion, 5µg/ml hemin, 5mg/ml yeast extract, 0.5µg/ml vitamin K, 1mg/ml L-cysteine) and allowed to equilibrate in the anaerobic chamber. Overnight cultures of W83 and V3139 bacterial cells were allowed to grow to a final OD_{660} of 0.7, and 200µl of 7 x 10^8 cells/ml cell suspension were plated on the BHI-agar plates. After 30 minutes, sterile filter discs were placed in the center of each plate, and 90µl of one of the following concentrations of H_2O_2 (used as an oxidizing agent) was added to each filter disc: 1% or 5%.

Plates were wrapped with parafilm and incubated in an anaerobic chamber at 37^{o}C for 5-7 days or until the diameter of growth inhibition zones created around the discs could be measured.

2.14 RNA Sequencing and Library Generation

2.14.1 Transcriptome

From an overnight culture of a mutant strain, a DP positive (2,2-dipyridyl, a high-affinity iron chelator) and DP negative sample was created. For DP negative samples, 4.5ml of BHI media was combined with 500ul of bacterial culture. For DP positive samples, 20µl of DP, 4.5ml of BHI media, and 500ul of bacterial culture were combined. The cultures were then grown anaerobically for 4-6 hours or until the OD_{660} reached 0.5. The cells were harvested, and the pellets resuspended in 50µl of PBS, pH 7.4. Samples were frozen at -80^{o}C for long-term storage.

2.14.2 RNA Isolation

From the transcriptome preparation above, 35µl wer aliquoted out to use for RNA isolation (RNeasy Mini Kit, Qiagen, Catalog No. 74104). Benchtop, pipettors, and tube holders were cleaned with 70% ethanol followed by RNase Zap (Life Technologies, Catalog No. AM9780) prior to starting. Everything was set up next to an open flame and a new box of pipette tips was opened. 500ul of Buffer RLT with beta-merceptoethanol was added to the samples, vortexed and transferred to the Lysing Matrix B 2ml tubes with 0.1mm silica spheres. To this, 500ul of acid phenol: chloroform was added to samples in the fume hood, and samples were bead beated at 6.0 M/S for 45 seconds. They

were then immediately placed on ice for 5 minutes, and centrifuged at 4^{o}C for 10 minutes at 13000rpm. To fresh microcentrifuge tubes, 400µl of 100% ethanol was added. Then, in the fume hood, the supernatant was pipetted out into these new tubes with ethanol added. Mixtures were transferred to the RNeasy spin columns, spun down and the flow-through was discarded. 600µl of RW1 buffer was then added, spun down and the flow-through was discarded once more. 70ul of Buffer RDD was pre-mixed with 10µl of DNase enzyme (RNase-Free DNase Set, Qiagen, Catalog No. 79254) per sample. The 80ul mixture was added onto each column, and incubated at room temperature for 30-40 minutes. During this time, a denaturing RNA gel was prepared (below).

After incubation, 250µl Buffer RW1 was added to the above spin columns with RNA, spun down and the flow-through was discarded. 500µl Buffer RPE was added, spun down and the flow-through was discarded again. This last step was repeated once more for a total of two times. The nearly empty columns were spun down for 2 additional minutes to get rid of any residual wash buffer, and columns were transferred to clean microcentrifuge tubes. 50ul of RNase- and DNase-free water was added to the columns, incubated for 1 minute, and spun down for 3 minutes at 13000rpm. Concentration of RNA were measured using the NanoDrop spectrophotometer, a denaturing RNA gel was run for confirmation of RNA isolation, and samples were then stored at -20^{o}C for short-term or -80^{o}C for long-term storage.

2.14.3 Denaturing RNA Gel

Gel apparatus, tray and comb, as well as glassware were all treated with RNase Zap and rinsed with nuclease-free water. For the large apparatus, 1gram agarose was

melted in 72ml nuclease-free water for about 2 minutes. After cooling, 10ml of 10X nuclease-free MOPS buffer was added as well as 1µl Gel Star. In the fume hood, 18ml formamide was also added and the gel poured. Combs were then inserted and the gel was allowed to solidify in the hood. Samples were prepared using 3µg of sample and 2µl of formaldehyde loading dye, bringing samples up to 12-13µl total using nuclease-free water. Samples were heated to 55^{o}C for 15 minutes in a water bath. 12µl samples were loaded into the gel and 1X nuclease-free MOPS buffer was added. Samples were run at 35 volts for one hour, and visualized via a UV transilluminator. Intact total RNA run on the denaturing gel should exhibit sharp 23S and 16S rRNA bands.

2.14.4 Library Generation

RNA isolates were treated with the DNA-free DNase Kit (Life Technologies, Catalog No. AM1906) before proceeding.

Using NuGEN Technologies Ovation Complete Prokaryotic RNA-Seq DR Multiplex Systems Kit (NuGEN Technologies, Catalog Nos. 0326, 0327), cDNA libraries were created without the additional step to reduce rRNA levels (Figure 8). This kit is designed for strand-specific expression analysis by incorporation of a nucleotide analog during the second strand cDNA synthesis and subsequent ligation to a pair of double-stranded adaptors also containing the same analog in one strand. After ligation, the cDNA strand and adaptor containing the analog were selectively removed, leaving only one cDNA strand, with both adaptor sequences attached. Unique barcoded adaptors were also utilized for up to 16-plex sequencing. Samples were submitted to the Nucleic Acid Center for quality check and Illumina Sequencing.

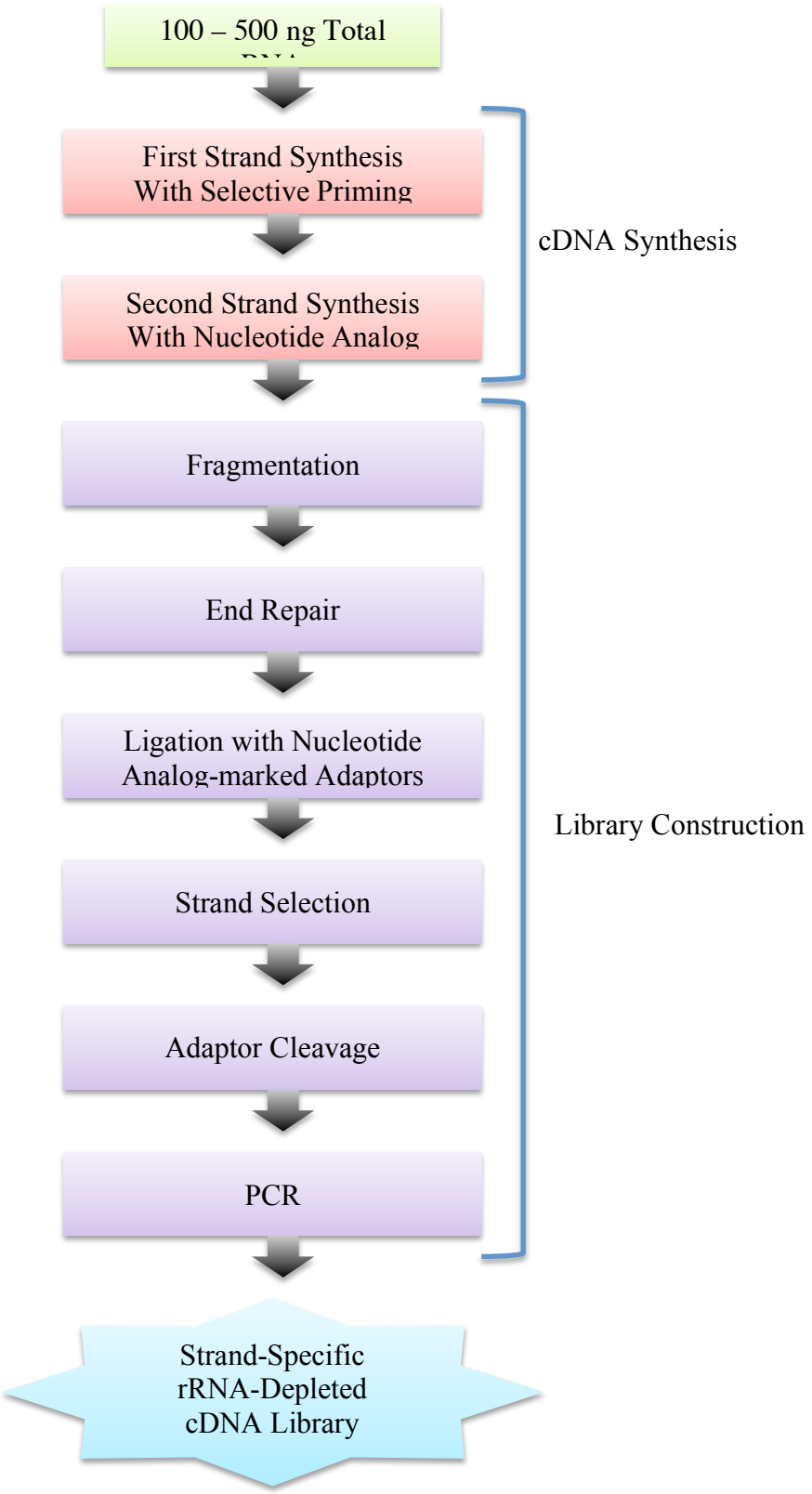

Figure 8. cDNA Library Generation Workflow.

Figure 8. cDNA Library Generation Workflow. The streamlined workflow consists of a double-stranded cDNA generation using selective priming, fragmentation of double-stranded cDNA, end repair to generate blunt ends, adaptor ligation, strand selection via nucleotide analog-targeted degradation and PCR amplification to produce the final library. The entire workflow takes approximately 9 hours. Adapted from NuGEN Ovation Complete Prokaryotic RNA-Seq DR Multiplex Systems Kit.

2.15 Proteomics

From an overnight culture of a mutant strain, DP positive and DP negative samples were created. For DP negative samples, 27.5ml of BHI media was combined with 2.5ml of bacterial culture. For DP positive samples, the following was combined in order: 120µl of DP with 27.5ml of BHI media and 2.5ml of bacterial culture. Cultures were grown overnight in an anaerobic chamber at 37°C. The next day, cultures were grown to an OD_{660} of between 0.5 and 1. Next, the cells were harvested and washed with 100mM Tris-HCl, pH8 and resuspended in 1ml of the same buffer. Samples were transferred to microcentrifuge tubes and lysed using the ultrasonicator at 50% duty cycle, three times for 2 minutes each. Samples were then spun down, and to the cell lysate, 1µl of benzonase was added to degrade all DNA and RNA. After 5 minutes of incubation, 1M guanidine HCl was added to denature proteins. Samples were then spun down for 10 minutes at 14000rpm, and the supernatant saved. Acetone precipitation of proteins was then done to remove any remaining small soluble substances, and repeated twice. It was then resuspended in 100µl of 10mM ammonium bicarbonate, run on a protein gel for confirmation, and absorbance at A280nm was taken and noted using the NanoDrop Spectrophotometer. Samples were then submitted to the Chemical and Proteomic Mass Spectrometry Core Facility (VCU Oliver Hall, 4^{th} Floor) for protein ID with spectral counting analysis. This process was repeated for a total of three times, not done concurrently to ensure sample integrity.

Chapter 3: RESULTS

3.1 Bioinformatics

Basic bioinformatics was conducted in order to resolve a best-fit homology model of the *P. gingivalis* gene PG0627. Analysis was also done to determine whether PG0627 is indeed a good candidate for a putative RNA-binding protein.

Utilizing Los Alamos Laboratory's Oralgen server, a protein structure model was sought in order to serve as a reference model for homology for PG0627. The top protein database hit from PDB was a *Homo sapiens* gene, N-terminal RRM domain of Cleavage stimulation factor 64 KDa subunit (CstF-64), which has a sequence similarity of 62% to PG0627 (Figure 9). One chain of this monomer served as a reference model for which PG0627 was fitted to using one-to-one threading on Phyre2. The model returned from the database had a confidence of 99.79% where 84 of PG0627's 97 amino acid residues perfectly matched to the CstF-64 chain. Models were created using UCSF's Chimera software and the overlay was generated via the MatchMaker structure comparison tool (Figure 10).

Figure 9. Amino acid sequence alignment of PG0627 and CstF-64. Generated using Phyre2. "Predicted Secondary structure" and "Query Sequence" are for PG0627, while the remaining three lines are for the N-terminal RRM domain of CstF-64. Adapted from: http://www.sbg.bio.ic.ac.uk/phyre2/phyre2_output/b1249fb70001e324/summary.htm

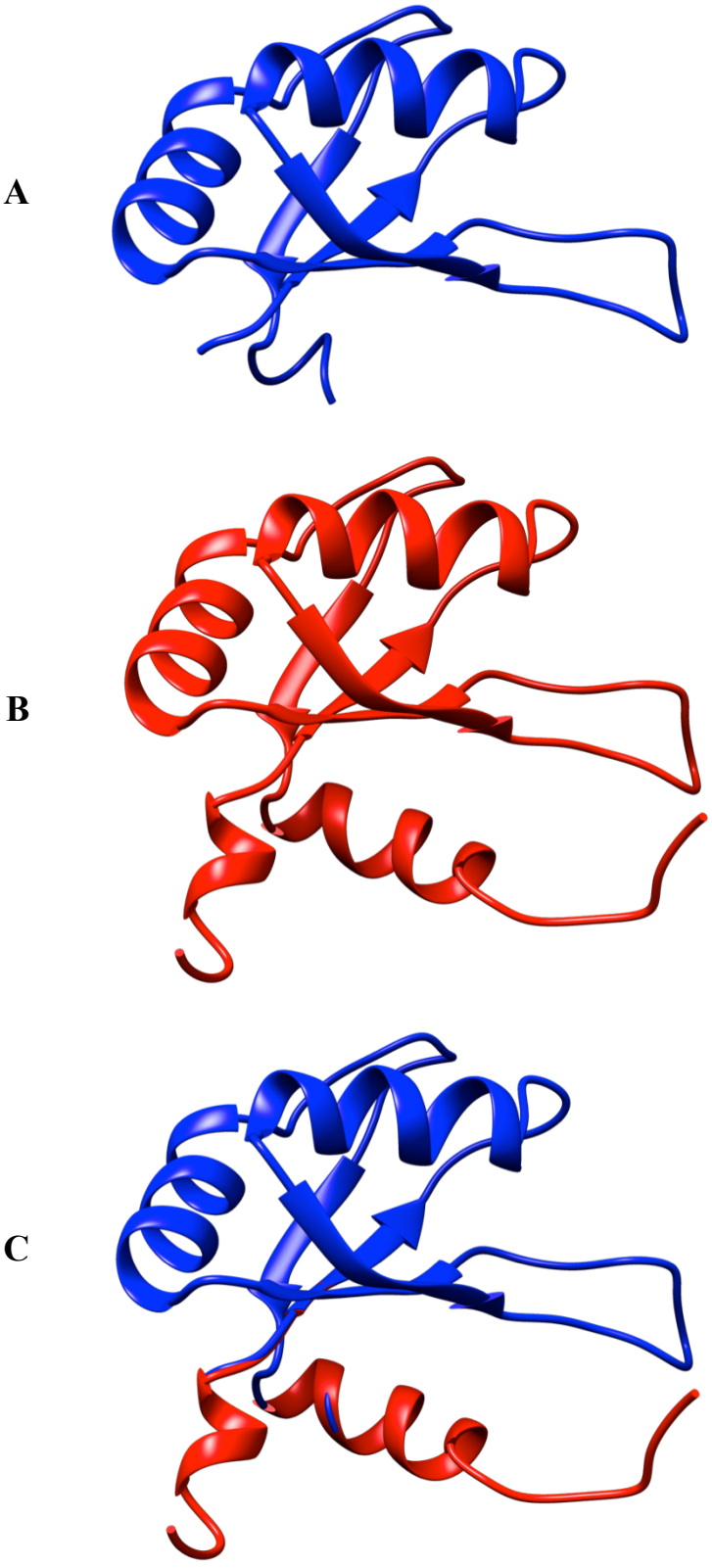

Figure 10. Homology model of putative RNA-binding protein, PG0627.

Figure 10. Homology model of putative RNA-binding protein, PG0627, A, in blue. Modeled on N-terminal RRM domain of Cleavage stimulation factor 64 KDa subunit in *H. sapiens*, chain A (PDB ID: 1P1T), B, in red. Overlay of the two structures is depicted in C with same color scheme. Generated using UCSF's Chimera software.

To confirm validity of the generated homology model of PG0627, a second modeling database inquiry using differing algorithms was done via the Swiss Institute of Bioinformatics (SIB) ExPASy website utilizing SWISS-MODEL as well as QMEAN for measuring model quality. ExPASy's SWISS-MODEL tool returned three models, with the top hit once again being PDB ID: 1P1T Chain A, the N-terminal RRM domain of CstF-64. The total QMEAN score (Table 5), which is a composite score of energetics of the model and reflects the predicted global model reliability ranging from 0 to 1, was 0.814. This indicates the model is a low-energy one and with a significant QMEAN score (Benkert et al., 2009; Benkert et al., 2011). The secondary structure agreement was also significant at 86.9%. This reaffirmed that the homology model generated both via Phyre2 and SWISS-MODEL was significant.

Table 5. Energetics and QMEAN score of RBP homology model.

Model Name	RBP Homology Model
C-beta interaction energy:	-59.56
All-atom pairwise energy:	-3100.55
Solvation energy:	-15.48
Torsion angle energy:	-24.51
Secondary structure agreement:	86.9%
Solvent accessibility agreement:	81.0%
Total QMEAN score:	0.814

* Adapted from:

http://swissmodel.expasy.org/qmean/cgi/index.cgi?job_id=3bf31efaf8e38667688422fc683f3c86

Next, to determine whether PG0627 is indeed a good candidate for a putative RNA-binding protein, InterPro was used. InterPro is a repository of databases for protein sequence analysis and classification, and can quickly give information about motifs within a protein structure (Figure 11). First, the GENE3D database indicated that residues 4-92 of PG0627 represent a nucleotide-binding domain with an alpha-beta plait structure, which is consistent with that of a ferredoxin-like (beta-alpha-beta)$_2$ fold, such as that found in RNA-binding domains of various ribonucleoproteins (Bochkarev et al., 1995; Kielkopf et al., 2004). Second, three separate databases indicated that the PG0627 protein sequence is indeed an RNA recognition motif domain: 1) Pfam, residues 5-74; 2) SMART, residues 4-77; and 3) PROSITE, residues 3-81.

A

B

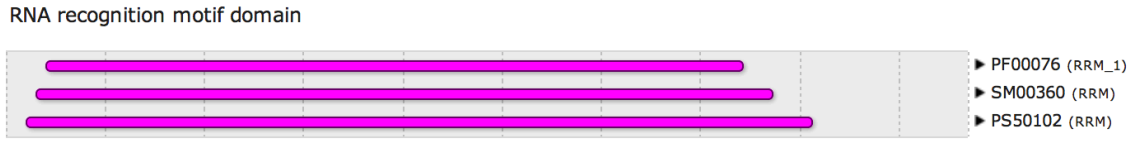

Figure 11. InterPro database results indicating PG0627 contains a nucleotide-binding domain (A) as well as an RNA recognition motif domain (B). Adapted from: https://www.ebi.ac.uk/interpro/sequencesearch/iprscan5-S20140618-190020-0897-20706388-pg

3.2 Metal Content

The graphs in figures 12 and 13 below illustrate the intracellular metal content of W83 versus V3139. Overnight cultures were washed with chelex treated buffer and then lysed releasing the cells' intracellular content. Finally, one biological set was analyzed via inductively coupled plasma mass spectrometry (ICP-MS) while three biological sets of triplicates was analyzed via a colorimetric ferrozine assay.

According to figure 12, a decrease in content of the following metals was seen in V3139 compared to W83: a 1.57-fold decrease in magnesium, a 1.23-fold decrease in iron, a 10.62-fold decrease in cobalt, and a 3.66-fold decrease in nickel. Meanwhile, a 1.21-fold increase and 2.35-fold increase was seen with copper and zinc, respectively, in V3139 compared to W83.

According to figure 13, V3139 in iron excess conditions had a1.22-fold decrease in intracellular iron compared to W83. In iron-depleted conditions (through the addition of 2,2-dipyridyl, or DP), V3139 saw a similar 1.18-fold decrease compared to W83.

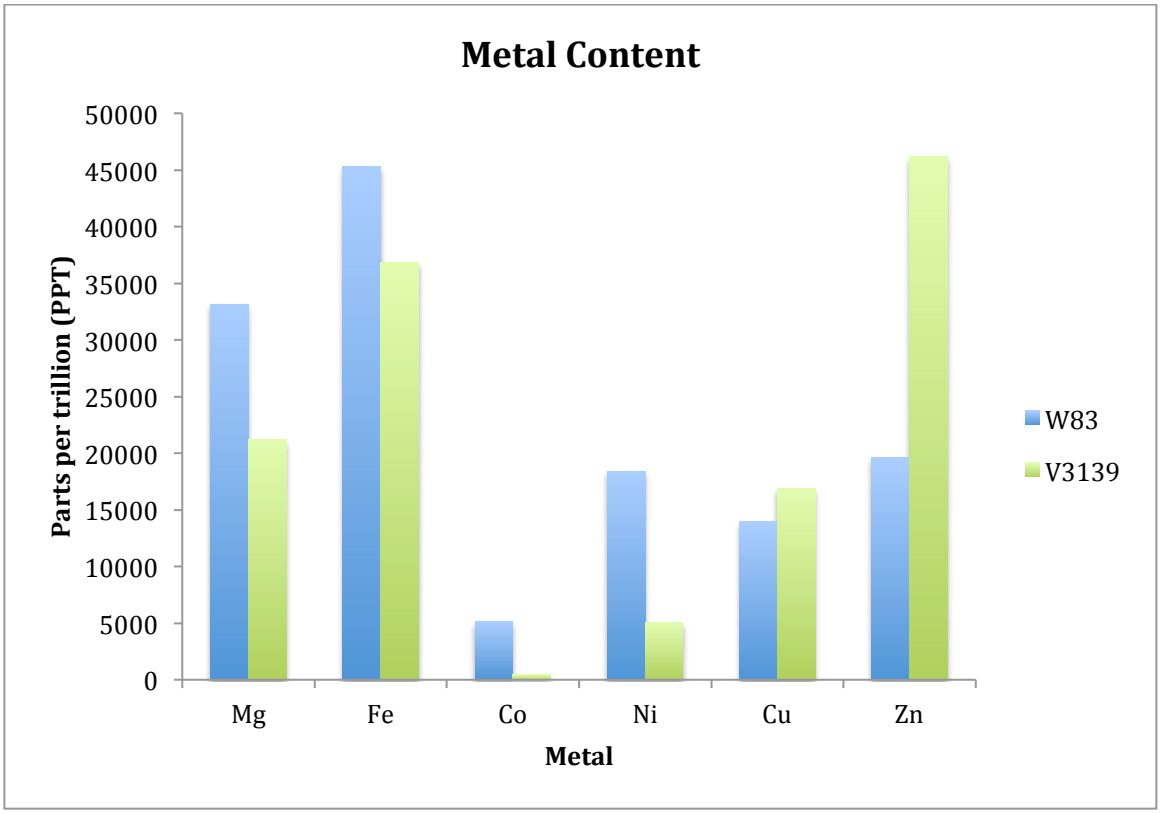

Figure 12. Intracellular metal content via ICP-MS of W83 and V3139. Values are displayed in parts per trillion. Graph shows only one biological set of data.

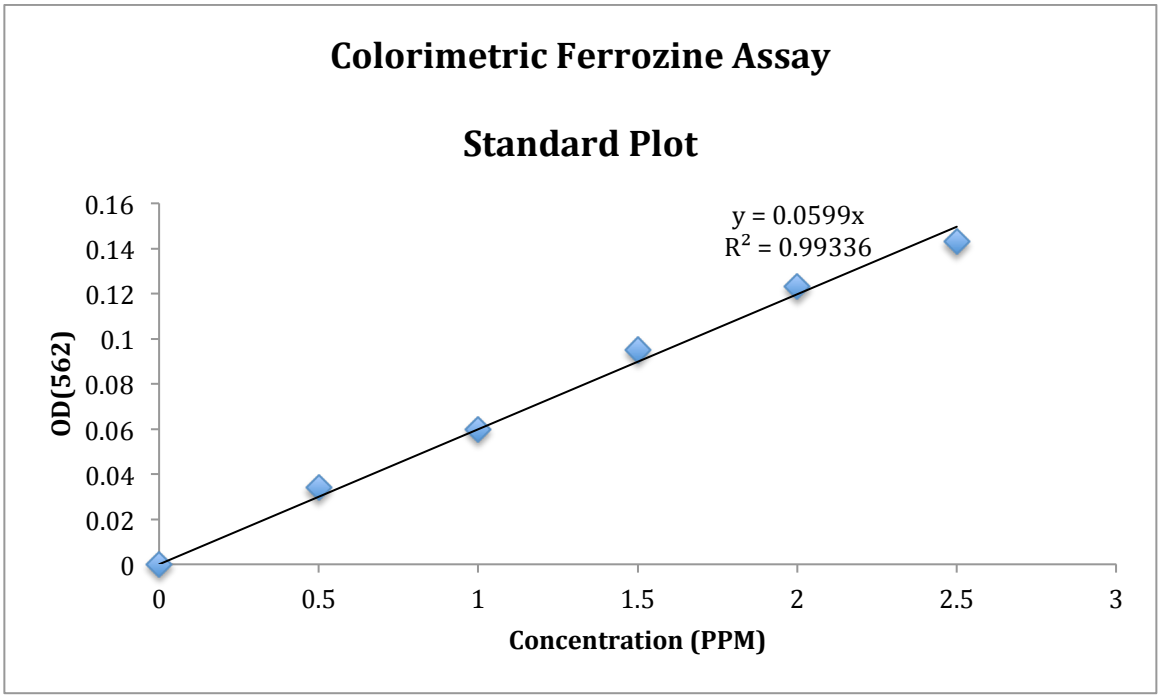

Samples	OD(562)	Concentration (Parts per million)
W83	0.1566	2.6136
V3139	0.1284	2.1443
W83+DP	0.0982	1.6398
V3139+DP	0.0831	1.3875

Figure 13. Intracellular iron content via ferrozine assay of W83 and V3139. Graph depicts three biological sets of triplicates. Optical densities were converted to concentrations using an iron standard curve with concentrations of 0.5 ppm, 1.0 ppm, 1.5 ppm, 2.0 ppm and 2.5 ppm from a 100ppm iron stock solution.

3.3 Arg-X and Lys-X Protease Activity

The graphs in figures 14 and 15 depict the protease activity of Arg-X and Lys-X in V3139 versus W83 strains in both iron-excess and iron-limited conditions.

In figure 14, the chromophore p-nitroaniline was released upon the hydrolysis of the substrate DL-BAPNA and is reflective of relative arginine protease activity. In iron excess conditions, V3139 displays a 1.79-fold decrease in arginine protease activity compared to W83. Similarly in iron limited conditions, V3139 shows a 1.59-fold decrease in protease activity compared to W83. Overall for both strains, arginine protease activity was greater in iron limited conditions than in iron excess conditions.

In figure 15, the chromophore p-nitroaniline was released upon the hydrolysis of the substrate D-Phe-Pro-Lyz-pNA and is reflective of relative lysine protease activity. Similar to that seen above, W83 showed a greater lysine protease activity in iron limited than in iron excess conditions. However, V3139 saw a significant decrease in lysine protease activity in iron limited conditions compared to that in iron excess conditions. Additionally, in iron excess conditions, V3139 showed a 1.10-fold decrease in activity compared to W83. However, in iron limited conditions, V3139 saw a 2.04-fold decrease in lysine protease activity compared to W83.

Overall for all graphs, the paired student t-test p-values were below 0.05 indicating that the data is in fact significant and not simply due to chance.

Lastly, arginine protease activity is significantly higher than lysine protease activity across all strains grown in either iron excess or iron limited conditions.

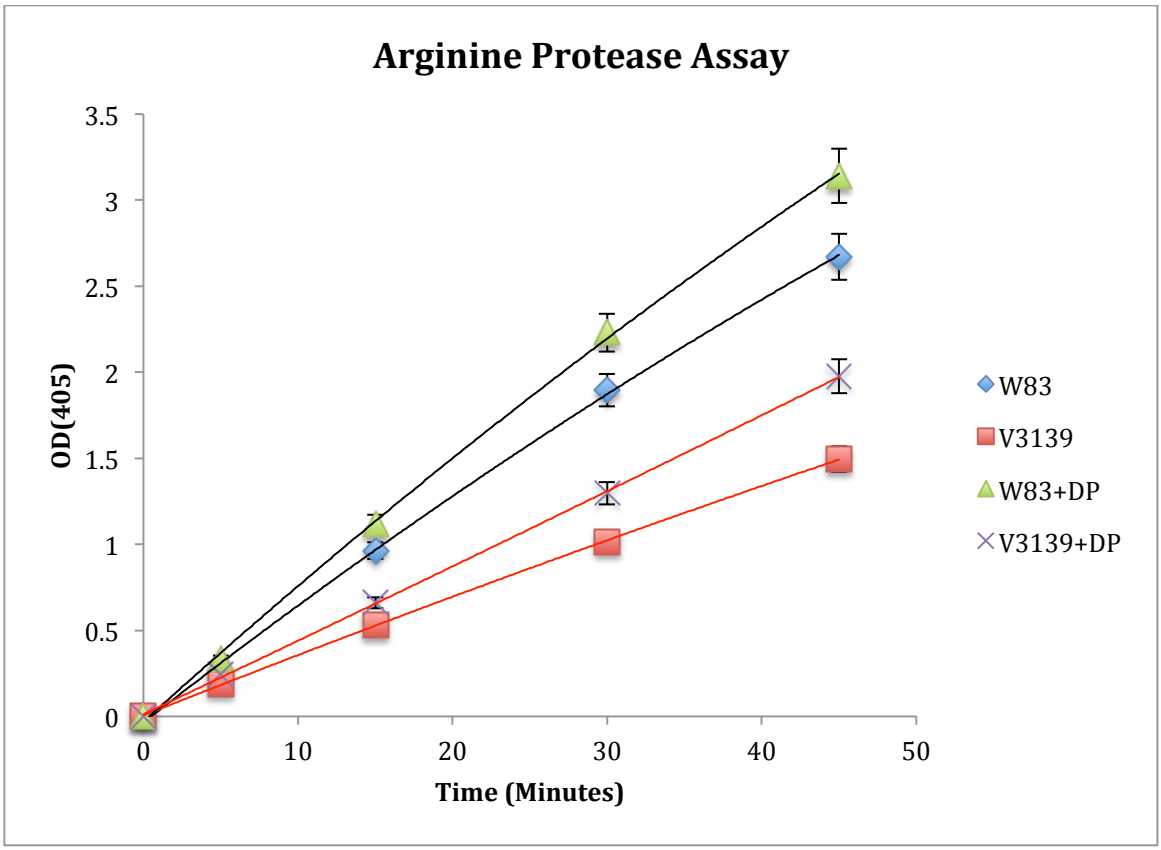

Figure 14. Arginine protease assay. The chromophore pNA is detected at a wavelength of 405nm and is thus relative to arginine protease activity when the substrate DL-BAPNA is used. For ease of viewing, red lines highlight the trends for V3139, while the black lines highlight the trends for W83. Three sets of biological replicates were done.

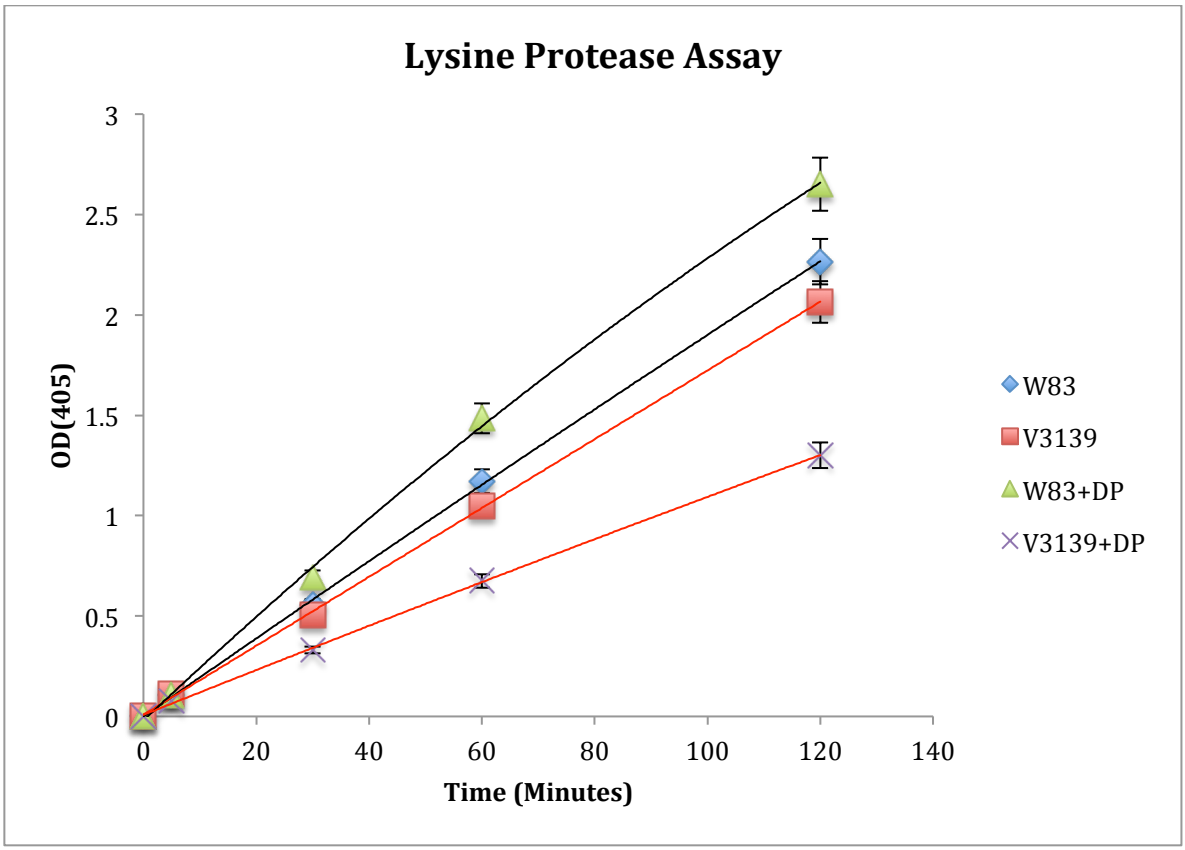

Figure 15. Lysine protease assay. The chromophore pNA is detected at a wavelength of 405nm and is thus relative to lysine protease activity when the substrate D-Phe-Pro-Lyz-pNA is used. For ease of viewing, red lines highlight the trends for V3139, while the black lines highlight the trends for W83. Four sets of biological replicates were done.

3.4 Interactions of *P.gingivalis* Strains with Host

The graphs in figure 16 depict the total extracellular interactions and total intracellular invasions of V3139 and W83 strains into eukaryotic HUVEC. HUVEC were grown to confluency while V3139 and W83 were grown from overnight cultures, washed, incubated with FITC and washed again before introduction to HUVEC at an MOI of 100:1. Analysis via flow cytometry showed that total extracellular interactions had a 1.15-fold decrease between V3139 cells and HUVEC compared to W83 and HUVEC. Similarly, total intracellular invasions had a 1.13-fold decrease between V3139 cells and HUVEC compared to W83 and HUVEC.

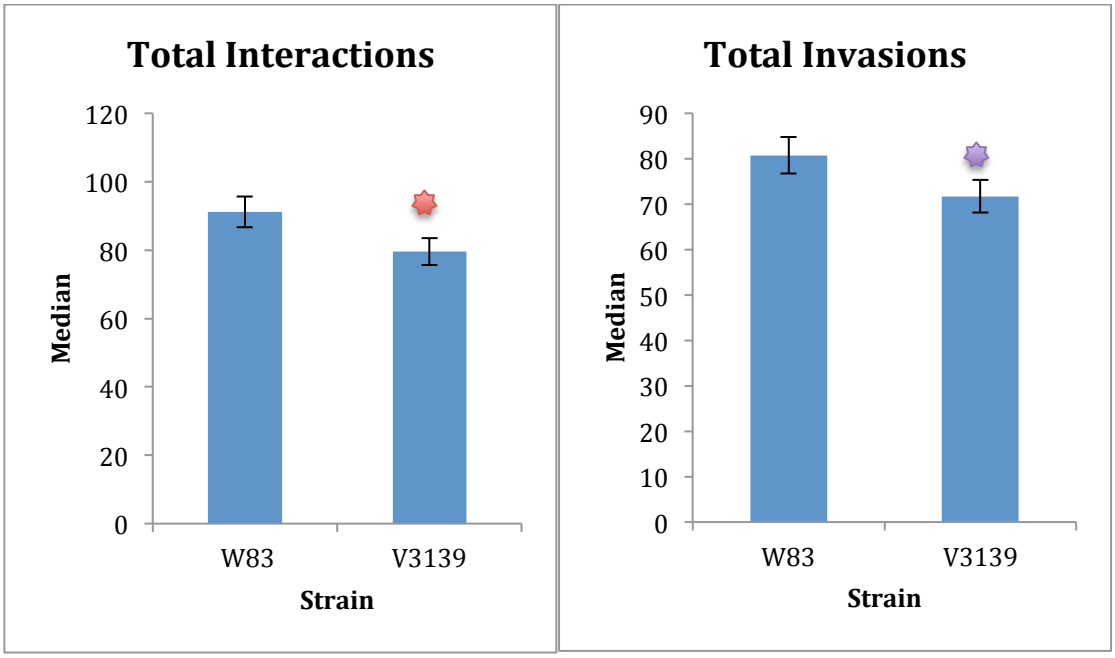

Figure 16. Total interactions and total invasions of *P. gingivalis* strains into eukaryotic cells. Fluorescent tagging with FITC was used to quantify total extracellular interactions between the bacterial strains, either V3139 or W83, and eukaryotic HUVEC. Quenching of extracellular FITC by trypan blue was then used to quantify total invasions between the bacterial strains and eukaryotic HUVEC. Red asterisk indicates a student paired t-test value of $p = 0.087$; purple asterisk indicates a $p = 0.159$. Five biological replicates were done for each condition.

3.5 Growth Studies

Two differing growth studies were performed in order to elucidate whether V3139 grows differentially compared to W83 in various conditions.

3.5.1 Hemin Depletion

The graph in figure 17 illustrates growth of V3139 versus W83 strain in hemin-depleted conditions. A decrease in growth was expected in W83 as hemin, the iron-containing protoporphyrin, is an essential nutrient for growth of *P. gingivalis*. However, an unexpected occurrence was the high growth of V3139 under conditions of low hemin. At day 0, all samples were grown to an OD(660) of 1.0 in BHI supplemented with vitamin K. The first 1:10 passage in mycoplasma without hemin was conducted, and an OD(660) taken two days later just prior to the second passage. This continued through day 8 when the optical density fell below 0.1 for both strains (not pictured). Data from day 6, or the third passage, showed statistically useable and valid data and is depicted in figure 17. This graph illustrates that V3139 grew better in a hemin-depleted state compared to W83, as the OD(660) reading measure at 0.890 for V3139 compared to W83 which was at 0.673. This translates to a 33% decrease in growth of W83 and an 11% decrease in growth in V3139.

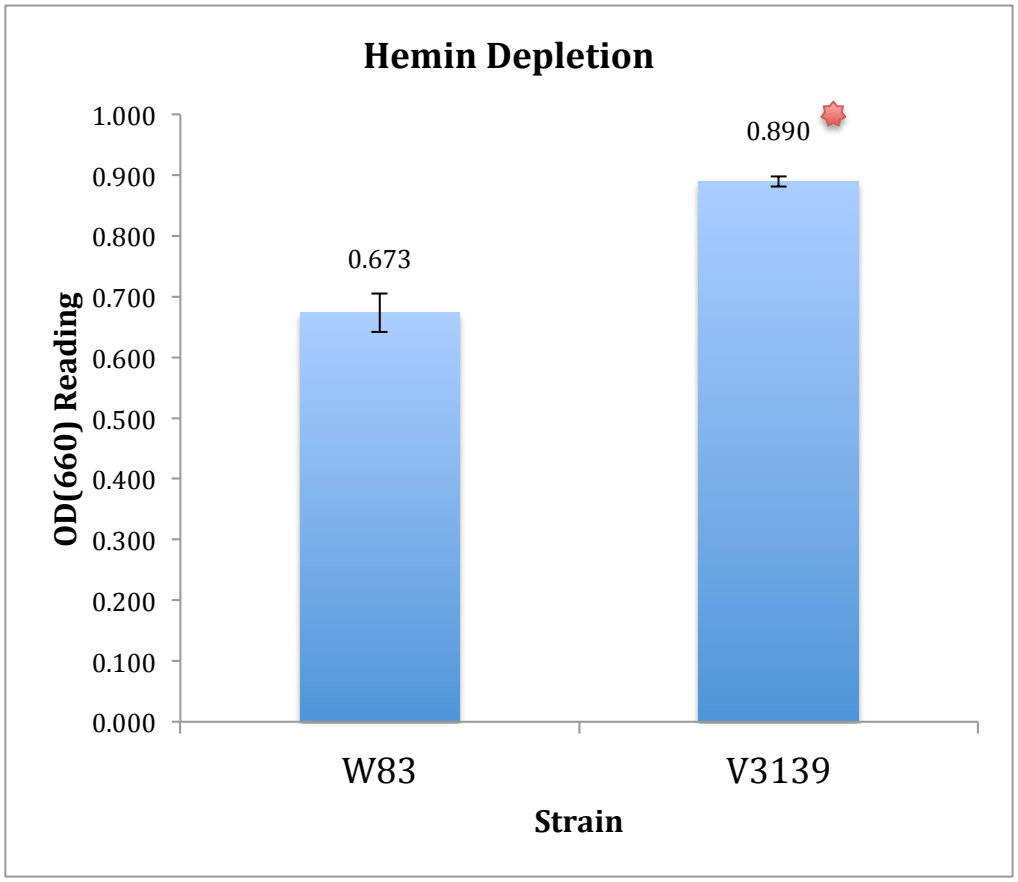

Figure 17. Growth in a hemin-depleted conditions. Samples were passaged in mycoplasma media without hemin added. Data is taken from the third passage of each strain. Red asterisk indicates paired student t-test value of p = 0.000325. Number displayed above respective bar shows OD(660) value.

3.5.2 Nitrosative Stress

The graphs in figures 18 and 19 illustrate the susceptibility of W83 and V3139 strains to nitrosative stress. This study utilized various concentrations of nitrosative-stress generating compounds added after the first optical density reading, including: $NaNO_3$: 40mM, 20mM and $NaNO_2$: 8mM, 4mM, and 1mM. Samples were grown in mycoplasma buffer supplemented with hemin or without, and OD(660) taken at 0, 4, 8 and 16 hours.

In both figures 18 and 19, a similar trend is apparent. Under growth with various concentrations of nitrate, V3139 grows better than W83 in both hemin-excess and hemin-limited conditions, with a marked further increase in growth differences in the hemin-limited conditions. In both strains, there wasn't a considerable difference in growth inhibition between 40mM $NaNO_3$ and 20mM $NaNO_3$. Under growth with various concentrations of nitrite, V3139 once again grows better than W83 in both hemin-excess and hemin-limited conditions, with a marked further increase in growth differences in the hemin-limited conditions. Markedly, V3139 displays a small growth inhibition difference between 1mM $NaNO_2$ and 4mM $NaNO_2$, while the wild-type shows a slightly larger effect between the two in terms of growth inhibition. Also of note is the decrease in overall growth in the hemin-limited condition compared to hemin excess for both W83 and V3139 strains.

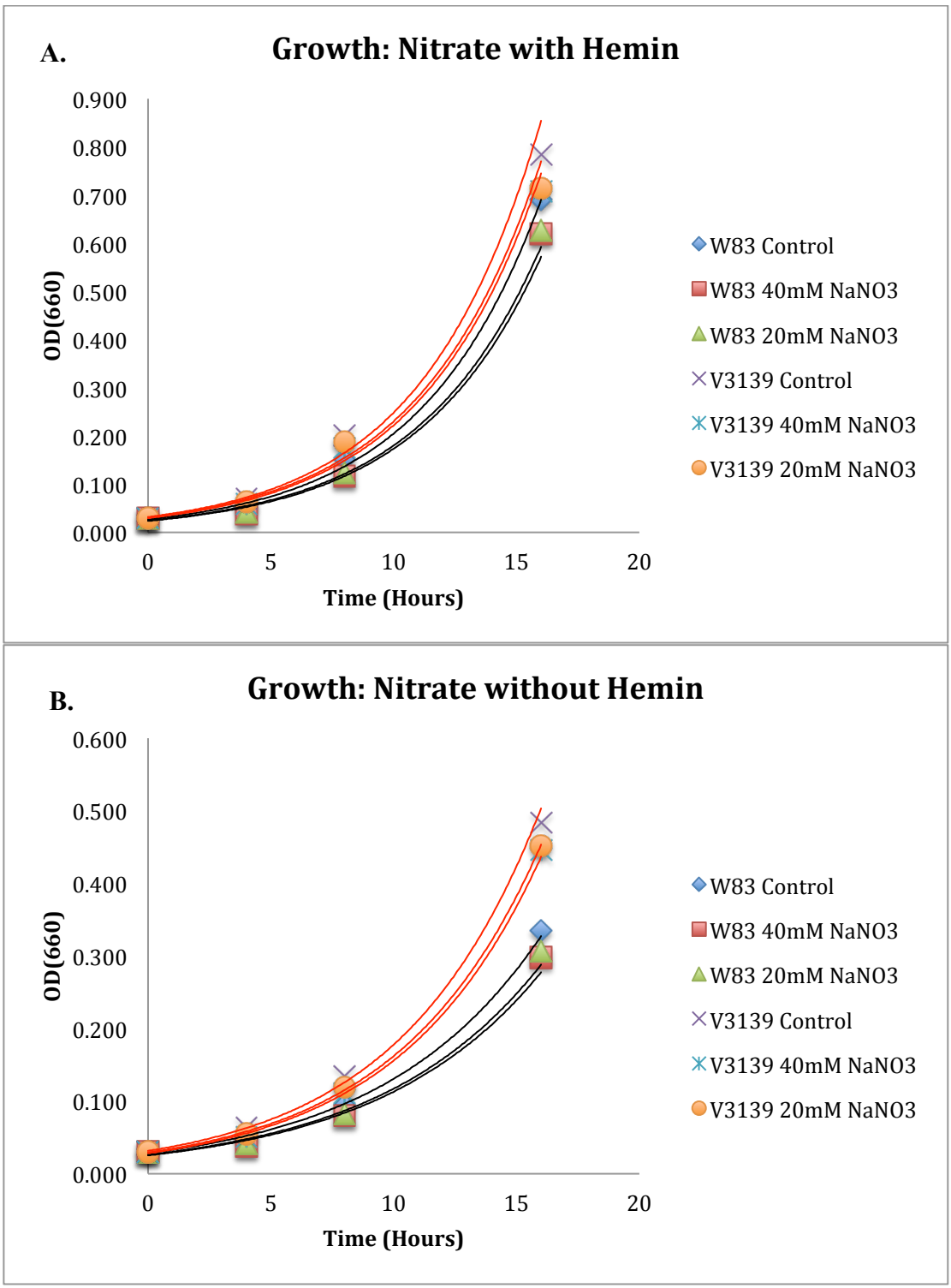

Figure 18. Growth study under various sodium nitrate concentrations, with hemin (A) and without hemin (B). For ease of viewing, red lines highlight the trends for V3139, while the black lines highlight the trends for W83.

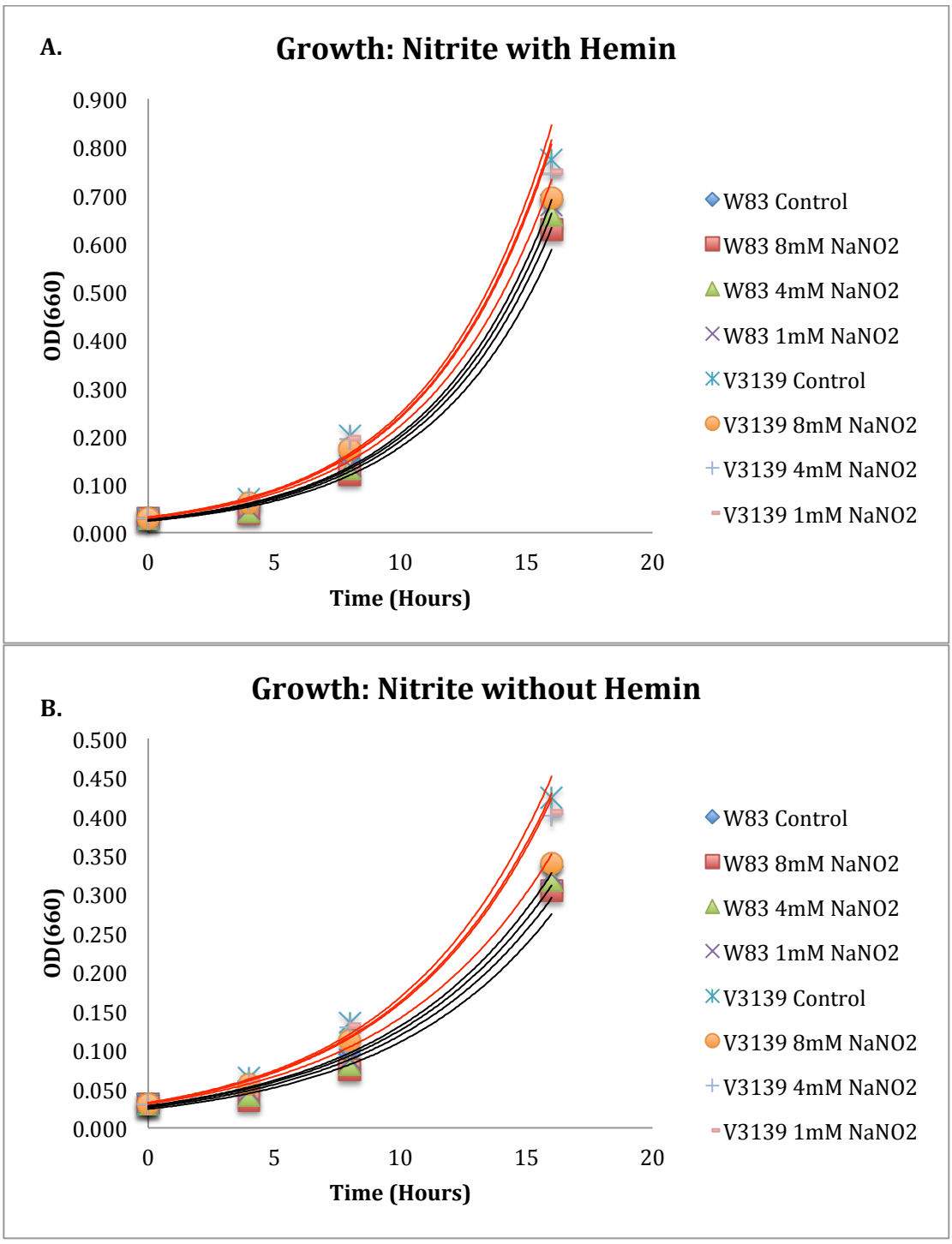

Figure 19. Growth study under various sodium nitrite concentrations, with hemin (A) and without hemin (B). For ease of viewing, red lines highlight the trends for V3139, while the black lines highlight the trends for W83.

3.6 Oxidative Stress

The graph in figure 20 illustrates the susceptibility of W83 and V3139 strains to oxidative stress. This disc diffusion study utilized cultures grown overnight and plated on BHI-agar plates, with two concentrations of hydrogen peroxide added, 1% and 5%. Strains were allowed to grow for 5-7 days or until diameters of the zones of growth inhibition could be measured for each plate (Figure 21).

According to figure 20, there is a slight decrease, i.e. 0.03cm, in the diameter of the zone of growth inhibition in V3139 strain compared to W83 in 1% H_2O_2. However, for 5% H_2O_2, there is a marked decrease of 0.16cm in diameter seen with V3139 compared to W83. The paired student t-test p-value is less than 0.0001 for both studies and reflects that although the margins are rather small, the data is significant.

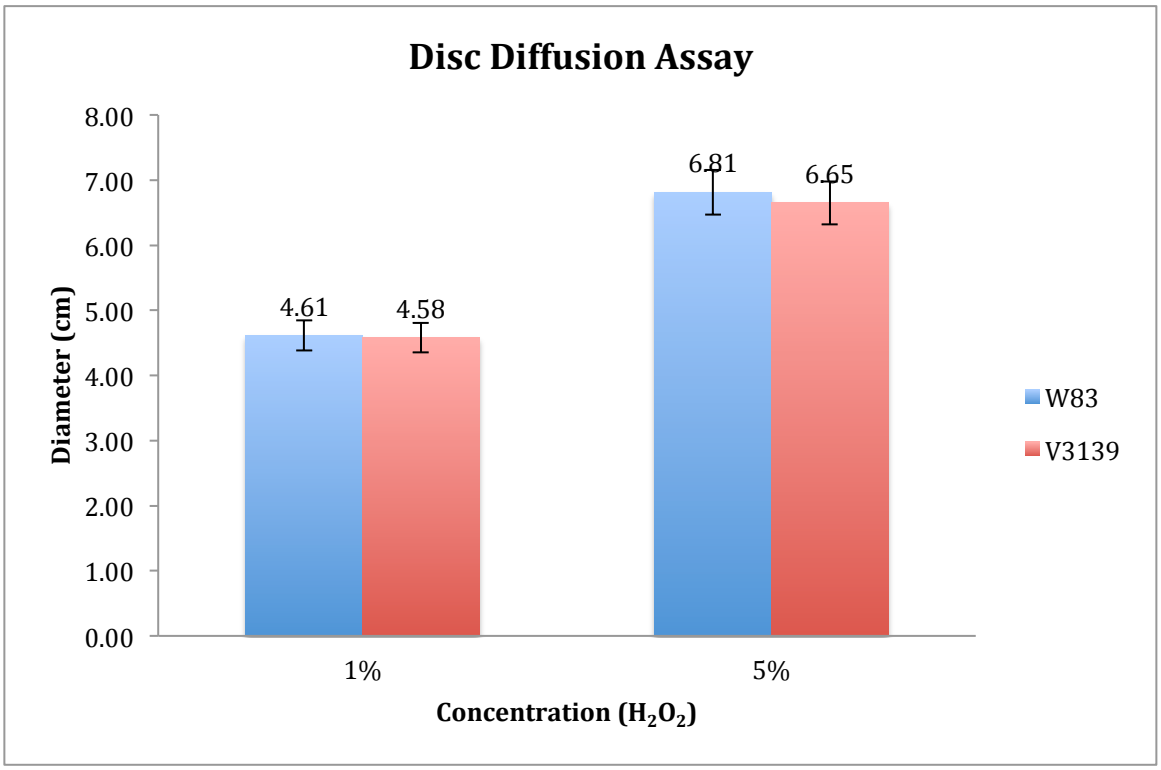

Figure 20. Disc diffusion assay with various concentrations of hydrogen peroxide. Numbers above bars indicate respective average diameter, in cm, of the zones of inhibition for each strain in triplicates. Four biological sets were done. P-value < 0.0001.

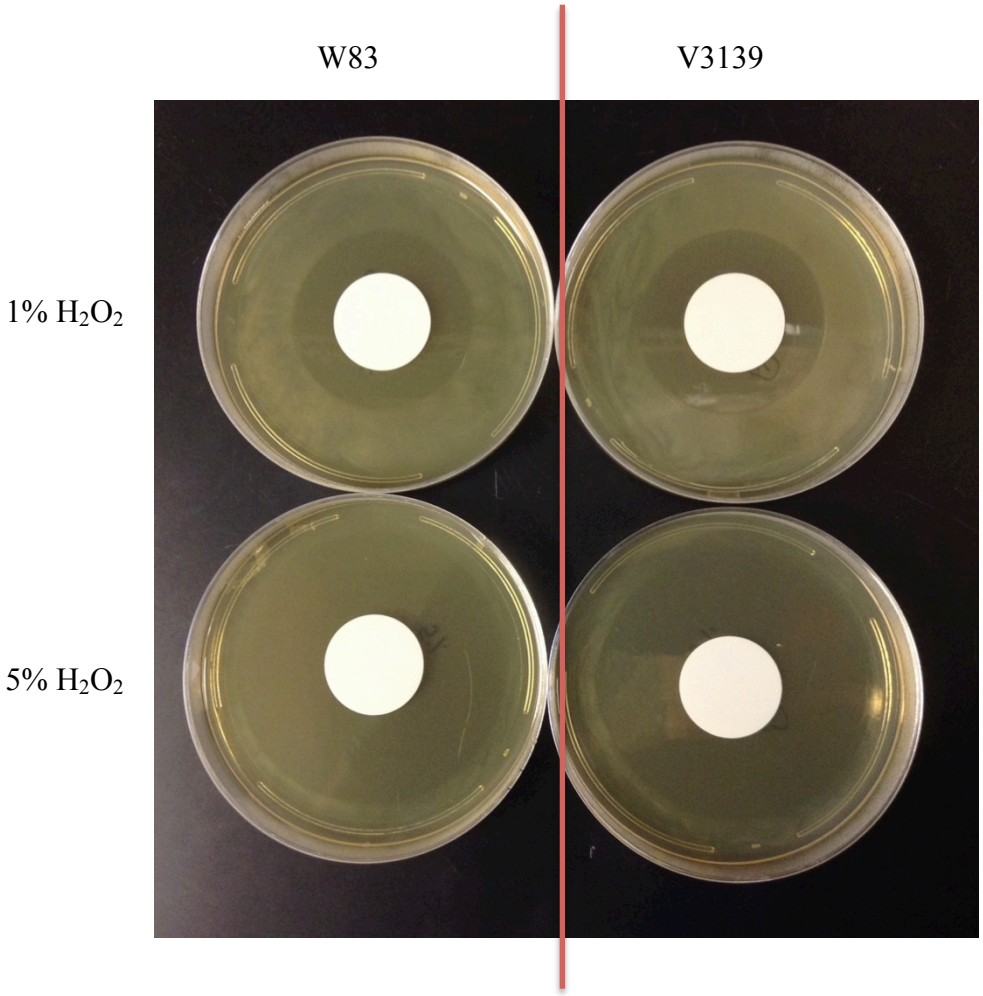

Samples	1% H_2O_2	5% H_2O_2
W83	4.61 (± 0.02)	6.81 (± 0.02)
V3139	4.58 (± 0.02)	6.65 (± 0.0001)

Figure 21. Image of the disc diffusion assay for oxidative stress. White-colored cloudiness indicates growth zones of respective strain, W83 or V3139. Clear area encircling the white filter disks are the measure zones of growth inhibition, diagramed in the table as means. Standard deviation are given in parentheses. Four biological sets were done. P-value < 0.0001.

3.7 RNA Sequencing

3.7.1 RNA Isolation

From the transcriptome preparation, RNA isolation was conducted on W83 and V3139 cells in order to prepare samples for further RNA library preparation. A denaturing RNA gel was run to confirm that the RNA did not degrade and could be further utilized. The sharp double bands in figure 22 correspond to 23S and 16S rRNA and indicate intact RNA samples. Furthermore, there is no apparent streaking also confirming good quality samples.

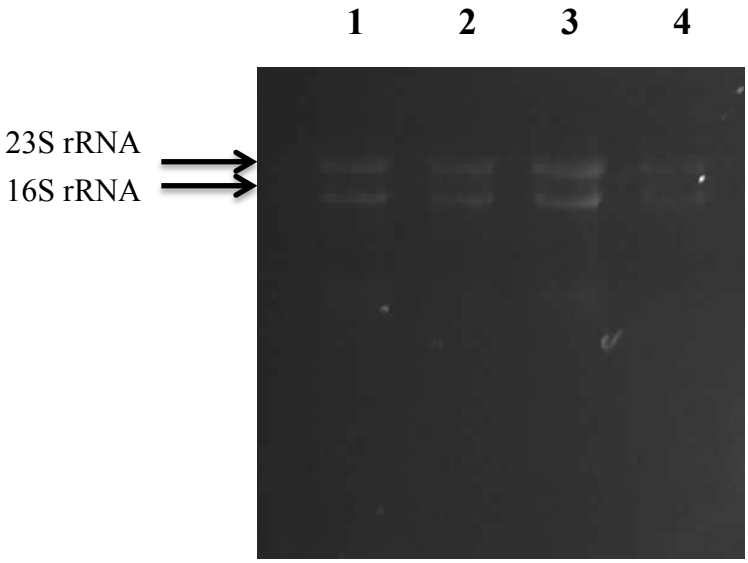

Figure 22. Denaturing RNA gel to confirm intact RNA. Gel apparatus, tray and comb, and glassware were all treated with RNase Zap and rinsed with nuclease-free water. 1g agarose was melted in 72ml nuclease-free water; 10ml of 10X nuclease-free MOPS buffer was added, followed by 1µl Gel Star. In the fume hood, 18ml formamide was also added. Samples were prepared using 3µg of sample and 2µl of formaldehyde loading dye, bringing samples up to 12-13µl total using nuclease-free water. Samples were heated to 55^{o}C for 15 minutes in a water bath. 12µl samples were loaded into the gel and 1X nuclease-free MOPS buffer was added. Samples were run at 35 volts for one hour, and visualized via a UV transilluminator. Lane 1: W83; lane 2: V3139; lane 3: W83 with 2,2-dipyridyl; lane 4: V3139 with 2,2-dipyridyl. Sharp double bands corresponding to 23S and 16S rRNA indicate intact samples.

3.7.2 RNA Library Generation

RNA isolated from W83 and V3139 was then used to generate RNA libraries as described in the materials and methods section. Two biological sets of libraries were generated on different dates, and samples were submitted to the VCU Nucleic Acid Research Facility in Sanger Hall to be validated and sequenced.

3.7.2.1 Validation of RNA Library

The graphs in figures 23-30 depict the bioanalyzer validation results for our samples. The results indicate that the RNA libraries I generated were ready for sequencing as all samples not only had peaks at less than 1000bp, but also had the largest peak at around 800bp indicating good fragment size quality.

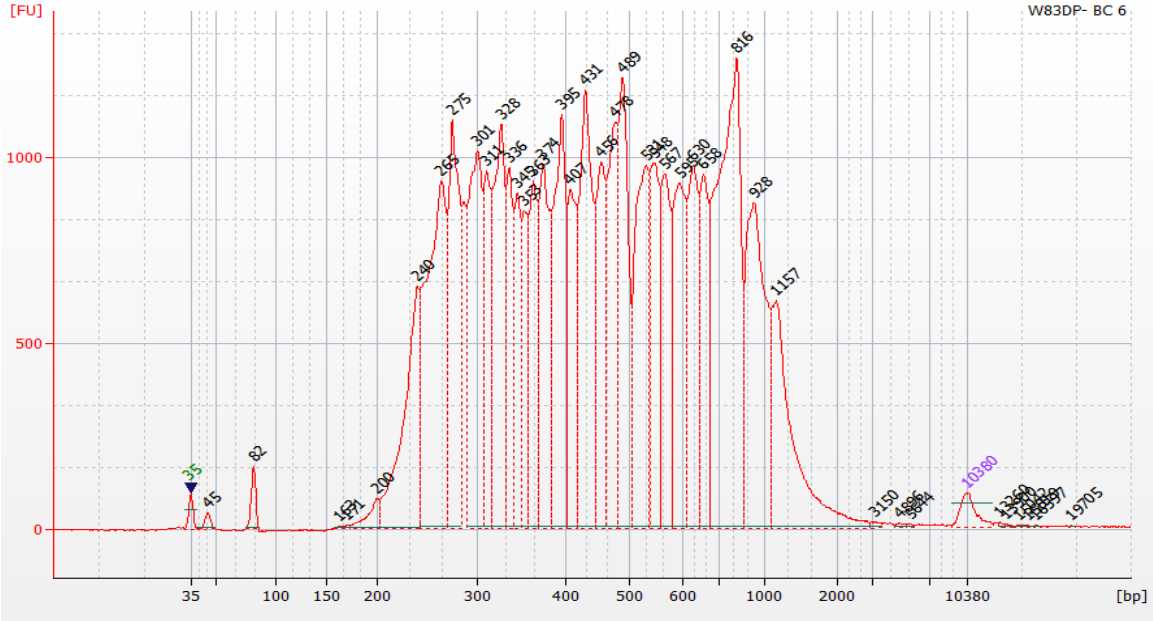

Figure 23. Electropherogram results from bioanalyzer of cDNA library from W83 RNA from 4.24.14. Y-axis is "FU" of fluorescence units; x-axis is "bp" or base pairs.

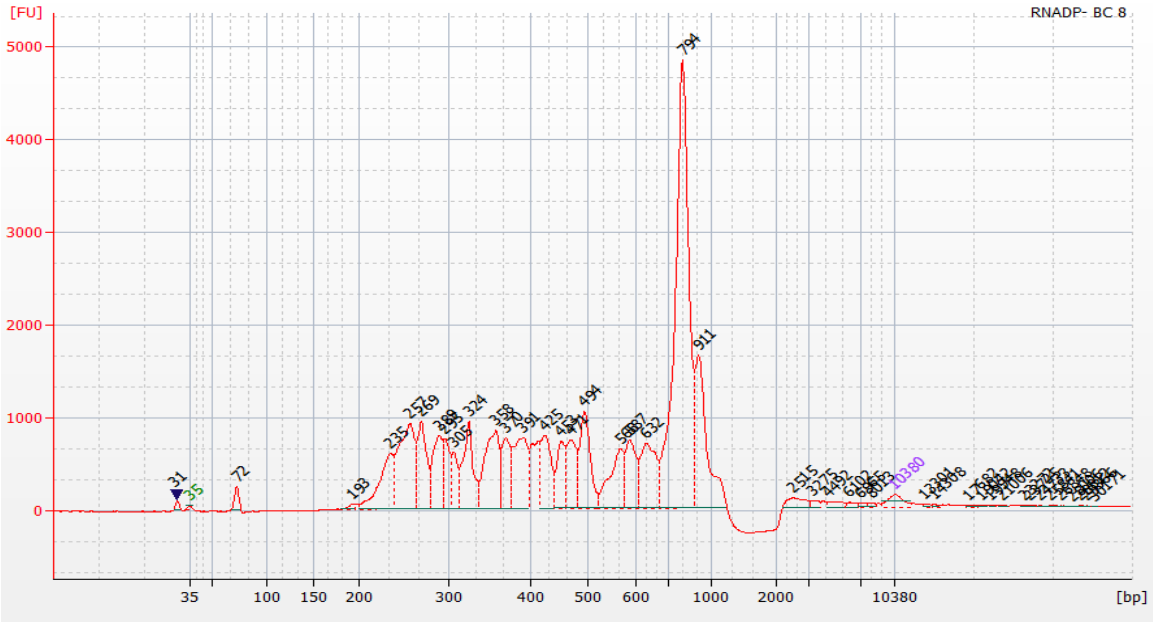

Figure 24. Electropherogram results from bioanalyzer of cDNA library from V3139 RNA from 4.24.14. Y-axis is "FU" of fluorescence units; x-axis is "bp" or base pairs.

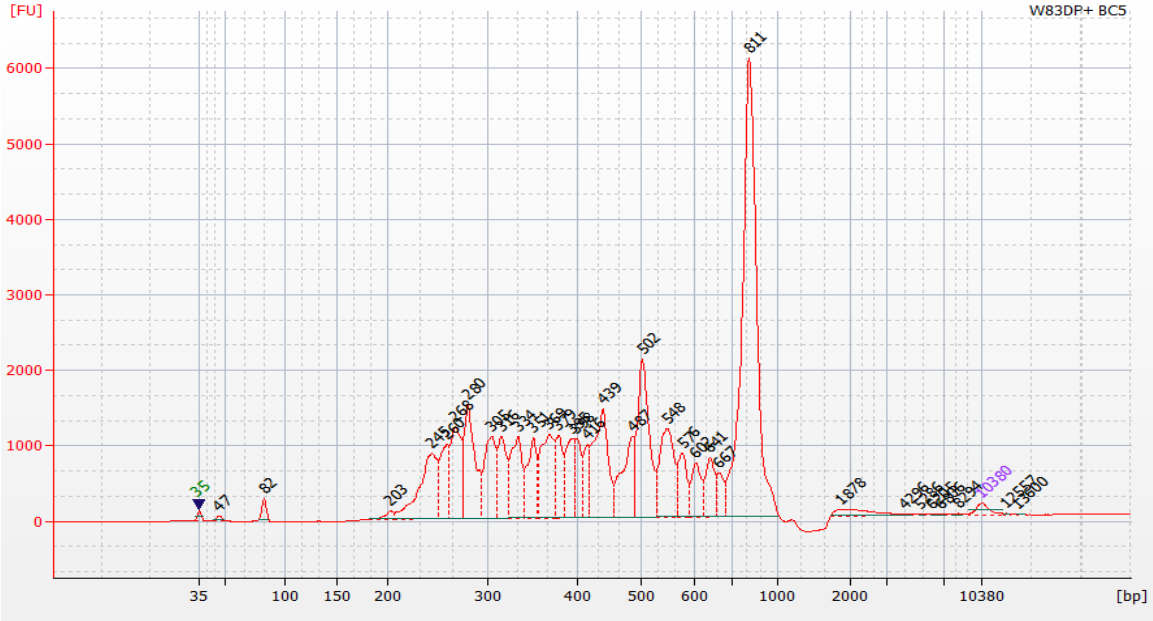

Figure 25. Electropherogram results from bioanalyzer of cDNA library from W83+DP RNA from 4.24.14. Y-axis is "FU" of fluorescence units; x-axis is "bp" or base pairs.

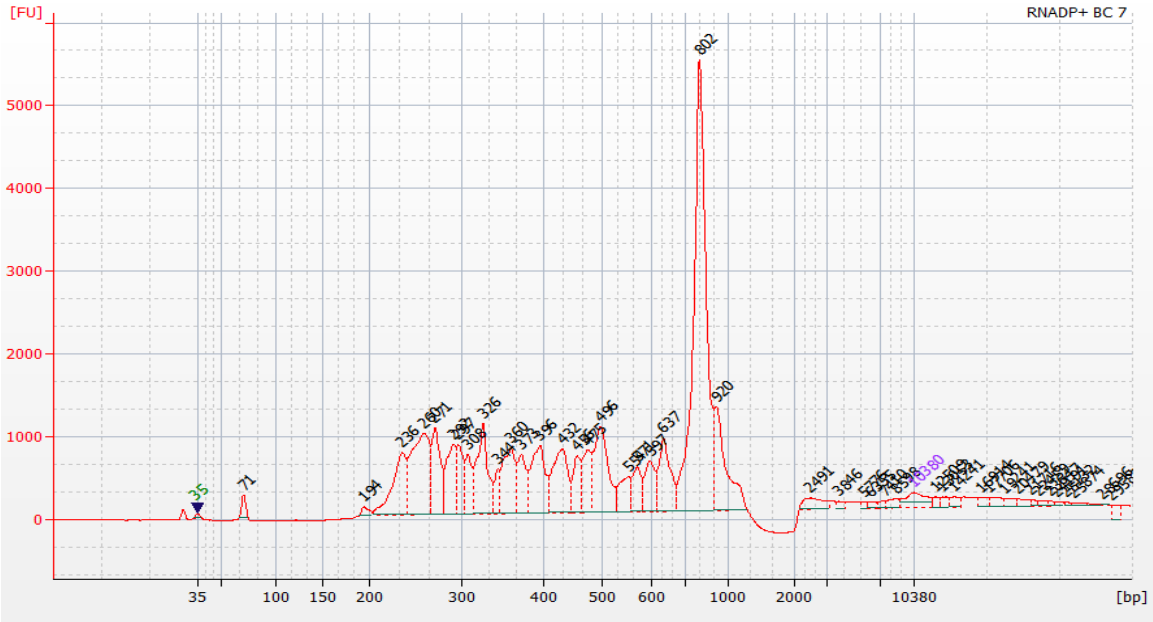

Figure 26. Electropherogram results from bioanalyzer of cDNA library from V3139+DP RNA from 4.24.14. Y-axis is "FU" of fluorescence units; x-axis is "bp" or base pairs.

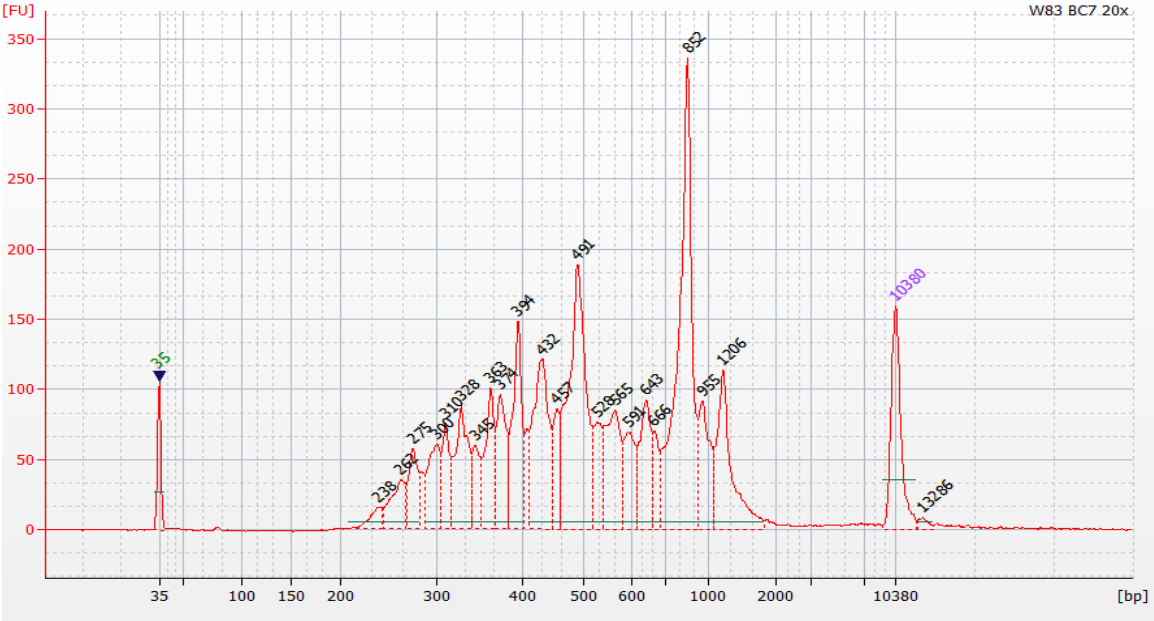

Figure 27. Electropherogram results from bioanalyzer of cDNA library from W83 RNA from 6.17.14. Y-axis is "FU" of fluorescence units; x-axis is "bp" or base pairs.

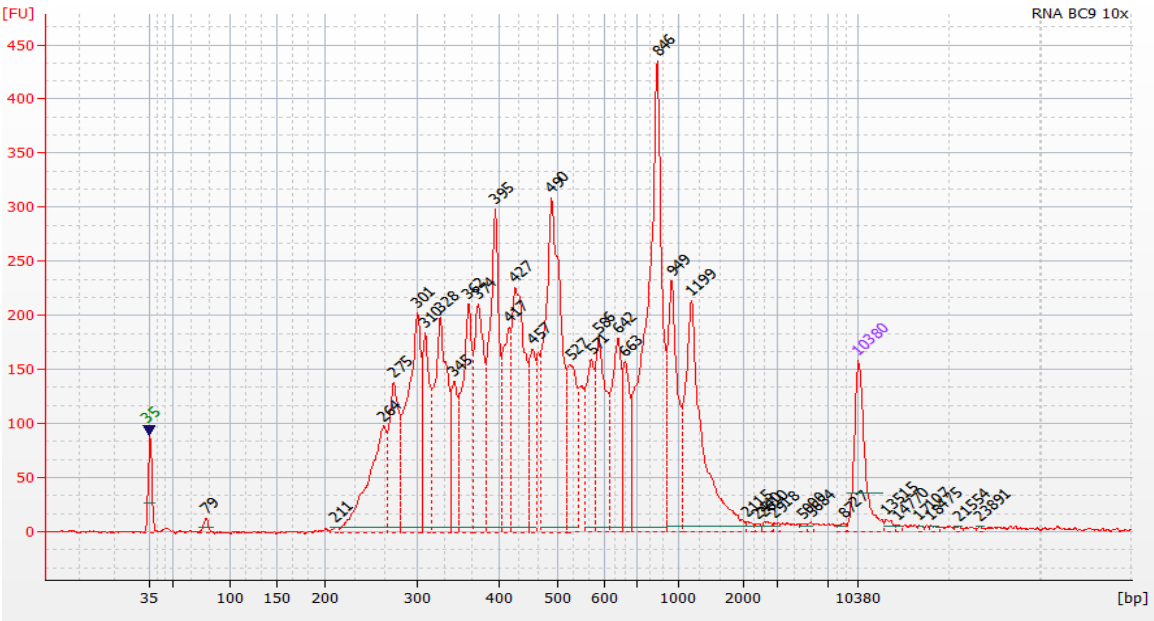

Figure 28. Electropherogram results from bioanalyzer of cDNA library from V3139 RNA from 6.17.14. Y-axis is "FU" of fluorescence units; x-axis is "bp" or base pairs.

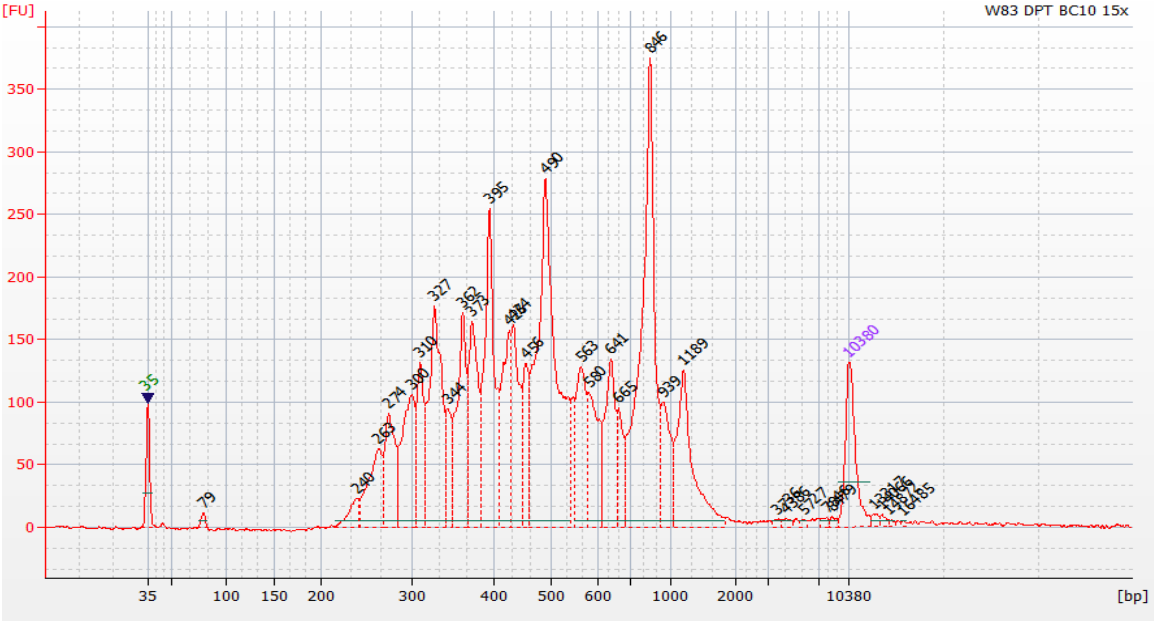

Figure 29. Electropherogram results from bioanalyzer of cDNA library from W83+DP RNA from 6.17.14. Y-axis is "FU" of fluorescence units; x-axis is "bp" or base pairs.

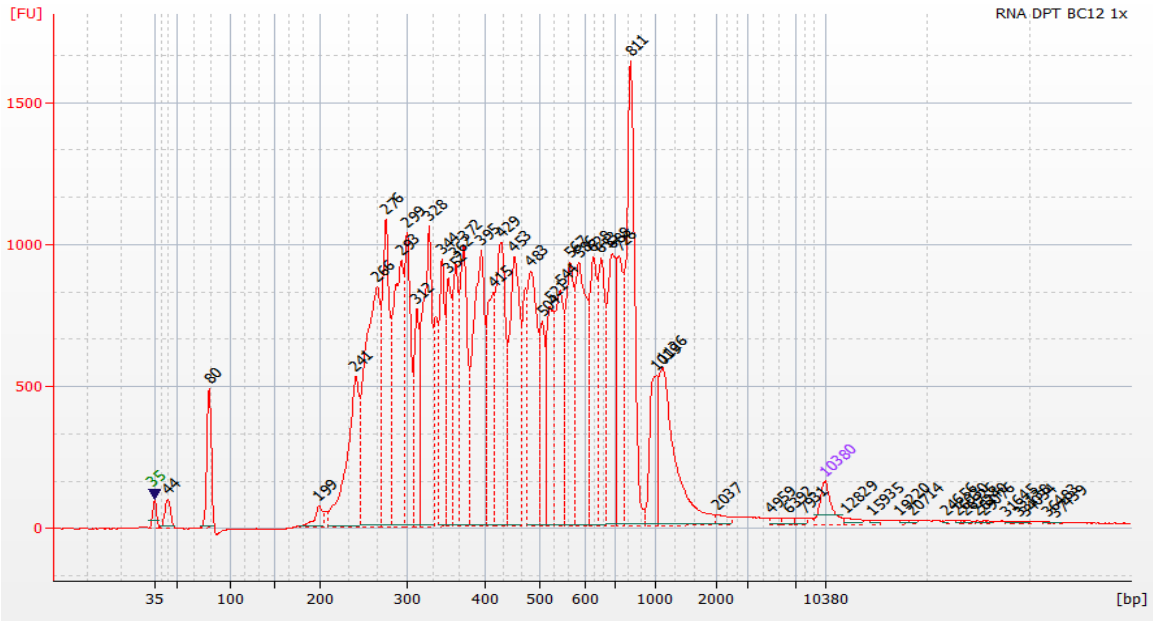

Figure 30. Electropherogram results from bioanalyzer of cDNA library from V3139+DP RNA from 6.17.14. Y-axis is "FU" of fluorescence units; x-axis is "bp" or base pairs.

3.7.3 RNA Sequencing of RNA libraries

After cDNA libraries were generated with the NuGEN sequencing kit for both W83 and V3139, next-generation sequencing of the whole transcriptome of both was performed in order to analyze whether RNA levels change between the two strains.

3.7.4 Statistical Analysis

Limited statistical analysis was conducted, as three biological replicates are needed for more decisive interpretation. Three separate libraries were generated, however, only two has thus far been sequenced with partial results reflected below. Of note, “library 1” was not DNase treated while “library 2” was and could account for some trend differences. One additional library is currently in the process of being sequenced with a fourth library that needs to be prepared.

Statistical analyses of the transcriptomes were performed by comparing the RPKM, or the reads by kilobase transcript per million reads, of V3139 to that of W83 for each sequencing data set, library one from 4.24.14 and library two from 6.17.14. From these RPKM values, fold changes were calculated to ascertain the differences in RNA levels between the two strains, and to view any differences. Both sets included samples with 2,2-dipyridyl and samples without it to see if there is differential expression in the presence of a high-affinity iron chelator.

Our target genes of interest are depicted in tables 6 and 7, which list the top 7 up- and down-regulated genes in RNA samples of V3139 relative to W83, for the dates of 4.24.14 and 6.17.14, both with and without 2,2-dipyridyl. Of note, there are two genes that occur more than once. PG0627, our putative RNA-binding protein, is the most down-

regulated gene in our second library of V3139 relative to W83, with a 128-fold and 225-fold decrease in preparations without and with the iron chelator, respectively. Our first library indicated that the gene did not have any copies in the V3139 strain (reflective in RPKM values). For comparison, in W83 samples without 2,2-dipyridyl, PG0627 had a relative RPKM of 788 reads, while in without 2,2-dipyridyl, PG0627 had a relative RPKM of 176 reads. Because fold changes take into account the comparison of two values and zero cannot be divided over, no fold changes are displayed for PG0627 for this first library and are indicated as "N/A." Conversely, PG0628, an ABC transporter ATP-binding protein, is the most up-regulated gene in RNA samples both with and without 2,2,-dipyridyl.

Additional target genes of interest are below.

For RNA samples without 2,2-dipyridyl added, down-regulation of genes in V3139 relative to W83 was seen in the following. Three CRISPR-associated proteins, PG1985, PG1986, and PG0215 were all down-regulated in the RNA samples without DP. These CRISPR-associated proteins have been known to be involved in adaptive immunity in bacteria and can serve gene editing purposes. PG0261, an ISPg3 transposase was the second most down-regulated gene in V3139 relative to W83, while PG0034, coding for a thioredoxin, was the sixth most down-regulated gene. Additionally, PG0539, a transmembrane transport protein, was also down-regulated.

For RNA samples without 2,2-dipyridyl added, up-regulation of genes in V3139 relative to W83 was seen in the following. PG1480, a conjugative transposon which has DNA helicase activity in E. coli was up-regulated in V3139, as was PG1551, which codes for the gene hmuY, a heme-binding protein. Additionally, PG1276, a histone-like

DNA-binding protein as well as PG0201, a ribonuclease with tRNA binding activity, were also up-regulated in V3139 relative to W83. Lastly, PG0900, a cytochrome d ubiquinol oxidase subunit, as well as PG0209, a formate/nitrite membrane transporter, were also up-regulated in V3139.

For RNA samples with 2,2-dipyridyl added, down-regulation of genes in V3139 relative to W83 was seen in the following. Five of the most down-regulated known genes in library two exhibited transposase activity, either ISPg3 or ISPg5. Namely, PG2129, PG0009, PG0194, PG2058, and PG1645. Additionally, PG2213, a nitrite reductase-related protein was also down-regulated. In librbary one, however, these transposases were mostly up-regulated. However, this was the preparation that was not DNase treated and could have skewed the result. Further sequencing data will need to be analyzed to conclusively state which trend is more accurate.

For RNA samples with 2,2-dipyridyl added, up-regulation of genes in V3139 relative to W83 was seen in the following. PG0223, an exonuclease with nucleic acid binding activity, as well as PG0589, a GMP synthase, were the second and third most up-regulated genes in V3139 relative to W83, respectively. A conjugative transposon protin TraF, PG1482, was also up-regulated, as was PG1256, which codes for a ribonuclease. Lastly, PG1505, which codes for a radical SAM domain protein and exhibits iron-sulfur cluster binding, as well as PG2034, an oxidoreductase, both are also up-regulated.

Table 6. Table depicting the top 7 up- and down-regulated known genes from RNA samples without 2,2,-dipyridyl, and serve as genes of interest.

A.

Gene ID (1)	Gene Description (2)	Cellular Location (3)	Function (4)	Fold change-Library 2 (5)	Fold change-Library 1 (6)
PG0627	RNA-binding protein, putative	Cytoplasm	Nucleotide binding; RRM domain	-128.56	N/A
PG0261	ISPg3	Cytoplasm	Insertion sequence element	-4.10	-1.21
PG2015	CRISPR-associated protein Cas4	Cytoplasm	CRISPR-associated protein Cas4	-1.99	-7.06
PG1985	CRISPR-associated protein, TM1792 family	Cytoplasm	CRISPR-associated Cmr4 family protein	-1.82	-1.66
PG1986	CRISPR-associated protein, TM1793 family	Cytoplasm	CRISPR-associated Cmr3 family protein	-1.76	-4.71
PG0034	thioredoxin	Cytoplasm	Electron carrier activity; oxidoreductase activity	-1.68	-3.15
PG0539	efflux transporter, MFP component, RND family	Cytoplasm	Transmembrane transport	-1.64	-1.32

B.

Gene ID (1)	Gene Description (2)	Cellular Location (3)	Function (4)	Fold change-Library 2 (5)	Fold change-Library 1 (6)
PG0628	ABC transporter, ATP-binding protein	Cytoplasm	Nucleotide binding; ATP binding; transporter activity	14.98	10.33
PG1480	conjugative transposon protein TraI	Unknown space	DNA relaxase, DNA helicase activity (*E. coli*)	7.21	14.44
PG1551	hmuY protein	Unknown space	Heme-binding protein	6.66	-1.18
PG1276	DNA-binding protein, histone-like family	Unknown space	Histone-like family DNA-binding protein	7.21	2.83
PG0201	ribonuclease P protein component	Unknown space	Enzyme; tRNA binding; nuclease activity	6.38	1.02
PG0900	cytochrome d ubiquinol oxidase, subunit I	Cytoplasm	Membrane oxidase	5.65	-1.02
PG0209	formate/nitrite transporter	Cytoplasm	Formate/nitrite membrane transport	5.31	2.00

* "A" depicts down-regulated genes while "B" depicts up-regulated genes. (1) Gene identification in *P. gingivalis*. (2) Description of the respective gene. (3) Cellular location of the respective gene. (4) Cellular function of the respective gene. (5) Fold change of library 2 compares the RPKM values of V3139 to that of W83, dated 6.17.14. (6) Fold change of library 2 compares the RPKM values of V3139 to that of W83, dated 4.24.14.

Table 7. Table depicting the top 7 up- and down-regulated known genes from RNA samples with 2,2,-dipyridyl, and serve as genes of interest.

A.

Gene ID (1)	Gene Description (2)	Cellular Location (3)	Function (4)	Fold change-Library 2 (5)	Fold change-Library 1 (6)
PG0627	RNA-binding protein	Cytoplasm	Nucleotide binding, RRM domain	-225.08	N/A
PG2129	ISPg5, transposase Orf1	Cytoplasm	Insertion sequence element	-11.63	5.60
PG0009	ISPg5 transposase Orf1	Cytoplasm	Insertion sequence element	-8.31	5.60
PG0194	ISPg3, transposase	Cytoplasm	Insertion sequence element	-7.87	1.36
PG2058	ISPg5, transposase Orf1	Cytoplasm	Insertion sequence element	-5.81	2.24
PG2213	nitrite reductase-related protein	Unknown space	Convert nitrite to NO	-5.68	1.00
PG1645	ISPg5, transposase Orf1	Cytoplasm	Insertion sequence element	-4.98	N/A

B.

Gene ID (1)	Gene Description (2)	Cellular Location (3)	Function (4)	Fold change-Library 2 (5)	Fold change-Library 1 (6)
PG0628	ABC transporter, ATP-binding protein	Cytoplasm	Nucleotide binding; ATP binding; transporter activity	8.64	14.46
PG0223	exonuclease	Cytoplasm	Nucleic acid binding; exonuclease activity	4.64	3.73
PG0589	GMP synthase	Cytoplasm	ATP --> GMP + AMP	4.18	1.65
PG1482	conjugative transposon protein TraF	Unknown space	N/A	3.73	4.48
PG1256	ribonuclease, Rne/Rng family	Cytoplasm	RNA binding and processing	3.18	1.28
PG1505	radical SAM domain protein	Cytoplasm	Iron-sulfur cluster binding	3.01	1.12
PG2034	oxidoreductase, FAD-binding, putative	Cytoplasm	ferredoxin-NADP(+) reductase subunit alpha	3.00	1.68

***** "A" depicts down-regulated genes while "B" depicts up-regulated genes. (1) Gene identification in *P. gingivalis*. (2) Description of the respective gene. (3) Cellular location of the respective gene. (4) Cellular function of the respective gene. (5) Fold change of library 2 compares the RPKM values of V3139 to that of W83, dated 6.17.14. (6) Fold change of library 2 compares the RPKM values of V3139 to that of W83, dated 4.24.14.

3.8 Proteomics

The image in figure 31 is that of a protein gel confirmation after proteomics preparation of W83 and V3139 samples. The purpose was to discern whether any proteins were up- or down-regulated when comparing W83 to V3139. As is evidenced in the gel image, there is no visual shift or change in protein band appearance between the two strains. Samples in lanes 2 (W83) and 3 (V3139) were both sent for proteomics analysis. Only one set of samples, without an iron chelator, were run and results displayed in table 10. However, as the exclusive unique peptide count for both samples was relatively low, these results as well as the relative fold changes of protein levels are not comprehensive and thus inconclusive.

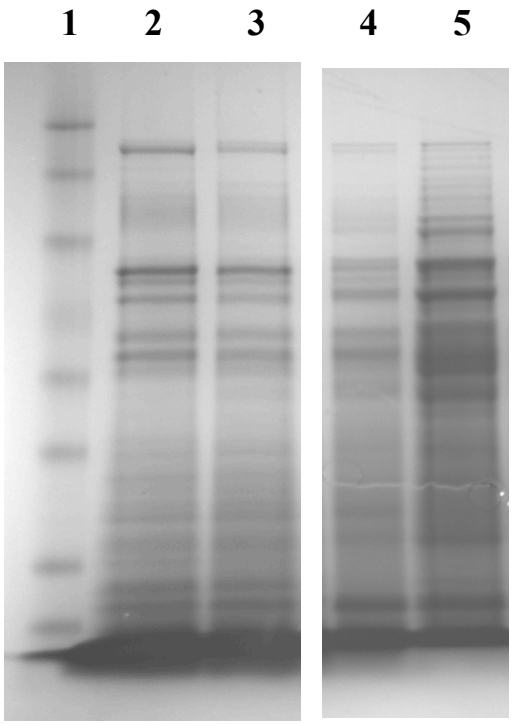

Figure 31. Protein gel. After proteomics preparation, samples were run on a protein gel for visual confirmation. Lane 1: protein ladder; lane 2: W83; lane 3: V3139; lane 4: W83 with 2,2-dipyridyl; lane 5: V3139 with 2,2-dipyridyl.

Table 8. Proteins and peptides identified via LC-MS.

Protein name (1)	Protein accession numbers (2)	Exclusive unique peptide count (3)		
		V3139	W83	Fold-change
electron transport complex, RnfABCDGE type, C subunit	PG0304	6	1	6.00
endopeptidase PepO (pepO)	PG0159	4	1	4.00
ribosomal protein S1 (rpsA)	PG1297	4	1	4.00
immunoreactive 42 kDa antigen PG33	PG0694	9	3	3.00
acyl-CoA dehydrogenase, short-chain specific (acdA)	PG1076	9	3	3.00
ribosomal protein L7-L12 (rplL)	PG0393	6	2	3.00
delta-1-pyrroline-5-carboxylate dehydrogenase (pruA)	PG1269	6	2	3.00
acyl carrier protein (acpP)	PG1765	3	1	3.00
succinate-semialdehyde dehydrogenase (sucD)	PG0687	11	4	2.75
superoxide dismutase, Fe-Mn (sodB)	PG1545	11	4	2.75
glutamate dehydrogenase, NAD-specific (gdh)	PG1232	32	12	2.67
peptidase, M24 family	PG1210	8	3	2.67
NAD-dependent 4-hydroxybutyrate dehydrogenase (4hbD)	PG0689	5	2	2.50
MotA-TolQ-ExbB proton channel family protein	PG0782	12	5	2.40
4-hydroxybutyryl-CoA dehydratase (abfD)	PG0692	33	14	2.36
immunoreactive 43 kDa antigen PG32	PG0695	7	3	2.33
phosphoenolpyruvate carboxykinase (ATP) (pckA)	PG1676	7	3	2.33
lipoprotein RagB (ragB)	PG0186	31	14	2.21
branched-chain amino acid aminotransferase (ilvE)	PG1290	13	6	2.17
ferritin (ftn)	PG1286	10	5	2.00
aminoacyl-histidine dipeptidase (pepD-2)	PG0537	6	3	2.00
thioredoxin reductase (trxB)	PG1134	4	2	2.00
hypothetical protein	PG1341	4	2	2.00
peptidase, M16 family	PG0196	2	1	2.00
internalin-related protein	PG0350	2	1	2.00
NAD(P)H dehydrogenase, quinone family, putative	PG1816	2	1	2.00
urocanate hydratase (hutU)	PG1872	2	1	2.00
lipoprotein PG3	PG2054	2	1	2.00
phosphoserine aminotransferase (serC)	PG1278	15	8	1.88
peptidylarginine deiminase	PG1424	12	7	1.71
ragA protein (ragA)	PG0185	39	23	1.70
triosephosphate isomerase (tpiA)	PG0623	5	3	1.67
peptidyl-dipeptidase Dcp (dcp-1)	PG0758	5	3	1.67
alkaline phosphatase, putative	PG0890	5	3	1.67
immunoreactive 53 kDa antigen PG123	PG2167	9	6	1.50
lipoprotein, putative	PG0611	3	2	1.50
Dps family protein	PG0090	7	5	1.40
heme-binding protein FetB (fetB)	PG0669	11	8	1.38
thioredoxin (trx)	PG0034	4	3	1.33
hemagglutinin protein HagE (hagE)	PG2024	8	7	1.14
rubrerythrin	PG0195	2	2	1.00
hemagglutinin protein HagA	PG1837	2	2	1.00
arginine-specific cysteine proteinase (prtRII)	PG0506	1	1	1.00
hypothetical protein	PG0706	1	1	1.00
extracellular protease, putative	PG0553	4	5	-1.25
purine nucleoside phosphorylase I, inosine and guanosine-specific	PG0558	1	2	-2.00

* (1) Name of *P. gingivalis* protein identified. (2) Respective gene identification number. (3) Exclusive unique peptide count is reflective of the number of peptides spectrally counted per sample. The LC-MS system consisted of a Thermo Electron LTQ-Orbitrap hybrid mass spectrometer system with a nanospray ion source interfaced to a Waters NanoAcquity C18 reversed-phase capillary column. The data were analyzed by database searching using the Sequest search algorithm against P. gingivalis database.

3.9 Hypothetical Model of the Role of *P. gingivalis* RBP

Based on the role of RBPs across various species as well as analyses conducted for this thesis, a hypothetical model of the role of RBP in *P. gingivalis* was created, and could potentially act in three ways as depicted in figure 32. First, RBP could complex with a small RNA to repress translation. Alternatively, the RBP-sRNA complex could assist in enhancing translation. Finally, RBP could itself cleave the target mRNA.

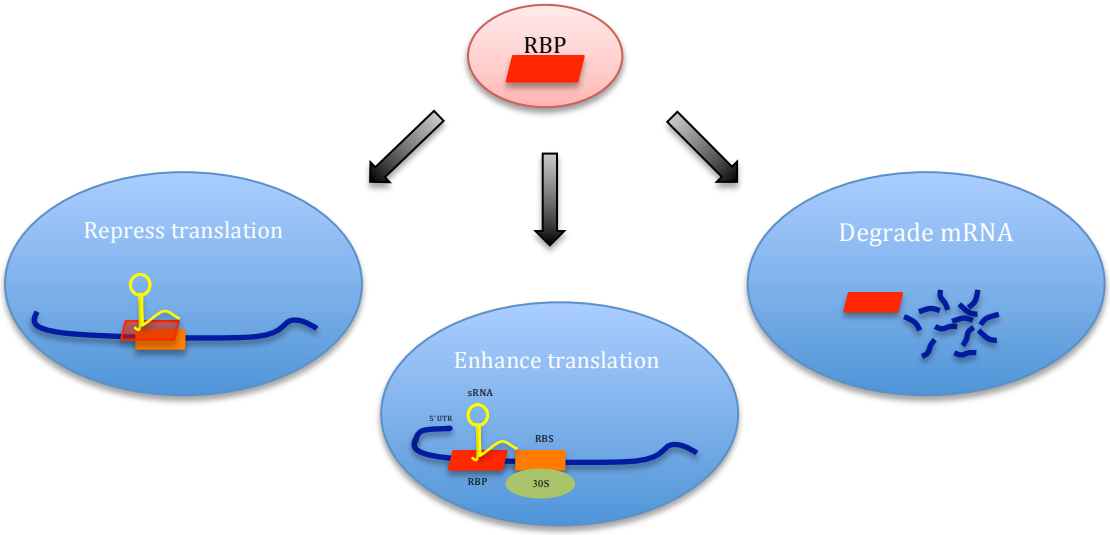

Figure 32. Hypothetical model of the role of *P. gingivalis* RBP. First, RBP in association with a small RNA (sRNA) may sequester the ribosomal binding site (RBS) of a target mRNA, thus blocking binding of the 30S and 50S ribosomal subunits and repressing translation. Second, a complex of RBP with a sRNA may prevent the formation of a secondary structure on the 5' untranslated region of the target mRNA, and thus enhance translation. Lastly, RBP may induce cleavage of the mRNA thereby degrading it. RBP is shown in red, the RBS in orange, the sRNA in yellow, the 30S ribosomal subunit in green and the target mRNA in dark blue.

3.10 Generation of Δ0893, Δ1421, Δ1820, and Δ1821 PCR Products

The Δ0893 mutant strain contains a knockout deletion of the PG0893 gene as well as a 1.1kb insert of the *ermF* cassette marker, an antibiotic resistance gene cassette marker for erythromycin and clindamycin (Fletcher and Macrina, 1991). Likewise, Δ1421, Δ1820, and Δ1821 all also contain a knockout deletion of their respective gene with an insert of the *ermF* cassette. Repeated cycles of targeted polymerase chain reaction (PCR) amplification of genomic *P. gingivalis* were conducted for each gene in order to acquire the desired knockout product. For each gene, three separate PCR reaction setups were conducted in order to amplify each flanking DNA fragment, and samples were run on a 1% agarose gel to confirm fragment length (Figure 33). Mut1 Δ0893 amplification shows a length of 337bp and Mut2 Δ0893 amplification has a length of 328bp. Likewise, the amplification lengths of the remaining three genes was as follows: Δ1421 (Mut1: 335bp; Mut2: 323bp), Δ1820 (Mut1: 349bp; Mut2: 300bp), and Δ1821 (Mut1: 300bp; Mut2: 337bp). Plasmid V2198, containing the *ermF*, was used as a template to amplify the *ermF* clindamycin resistance cassette, and when run on a 1% agarose gel, had a length of 1.1kb.

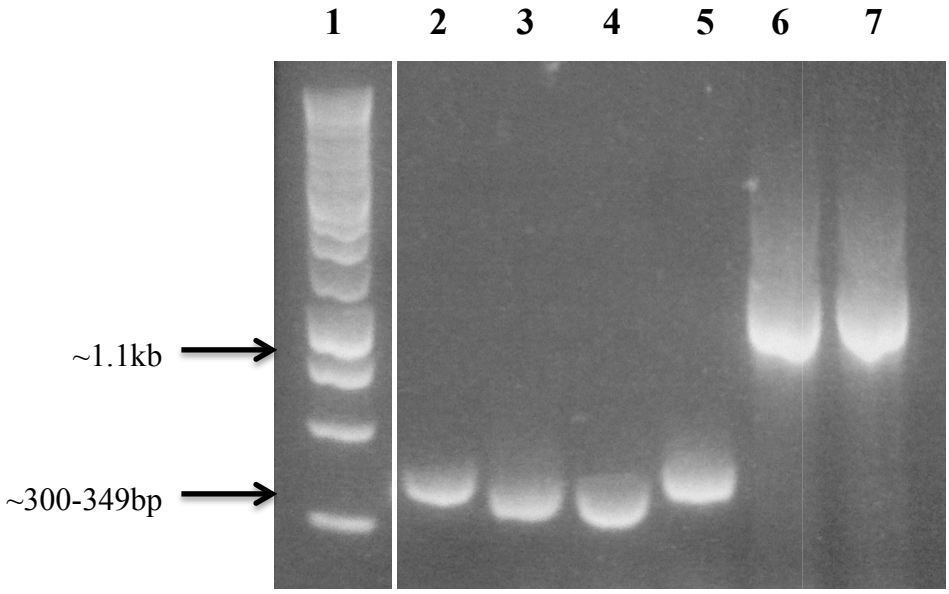

Figure 33. Agarose gel of initial PCR products, "Mut1" and Mut2" for respective genes. Gel was made by combining 50ml of TAE buffer (National Diagnostics, catalog No. EC-872) with 0.5mg of agarose, and heating. 2µl of GelRed Nucleic Acid Gel Stain dye (Biotium, catalog No. 41003) was added and mixed before pouring and solidifying the gel. Samples were combined with loading dye for visualization and image was taken via UV transilluminator. Lane 1, 1kb ladder; lane 2: Mut1 of PG1820; lane 3: Mut2 of PG1820; lane 4: Mut1 of PG1821; lane 5: Mut2 of PG1821; lanes 6 & 7: *ermF*. Bands 1-5 are between 300-349bp in size. Mut1 corresponds to upstream gene amplification while Mut2 corresponds to downstream gene amplification. The *ermF* cassette, 1.1kb, is shown in lanes 6 and 7.

Next, the flanking regions from this initial PCR were annealed together through a fusion PCR protocol using Mut1 Δ0893, *ermF* and Mut2 Δ0893 as templates (Figure 34). The same was done with the remaining three genes. The purified DNA construct was run on a 1% agarose gel and had a resulting length of 1690bb for Δ0893, 1683bb for Δ1421, 1674bb for Δ1820, and 1662bp for Δ1821 (Figure 35). These sizes indicated that the individual initial fragments, Mut1, *ermF*, and Mut2, annealed together and in the correct order in the fusion PCR.

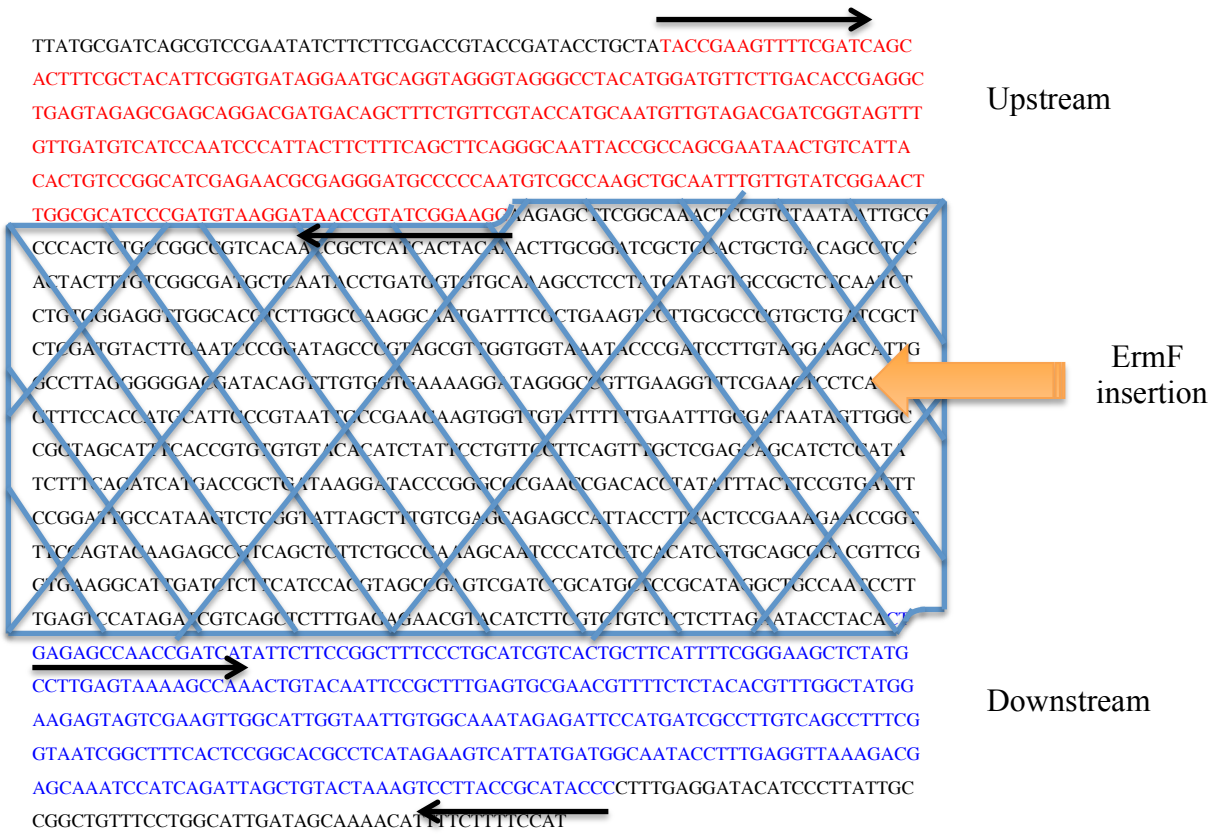

Figure 34. Disruption of the PG0893 gene via insertion of the *ermF* cassette between the upstream (red) and downstream (blue) PCR amplification products. The full gene is depicted in black. Two sets of primers were created for each up- and downstream region in order to introduce *ermF* in between the two. Black arrows indicate the two sets of primers for upstream and downstream regions.

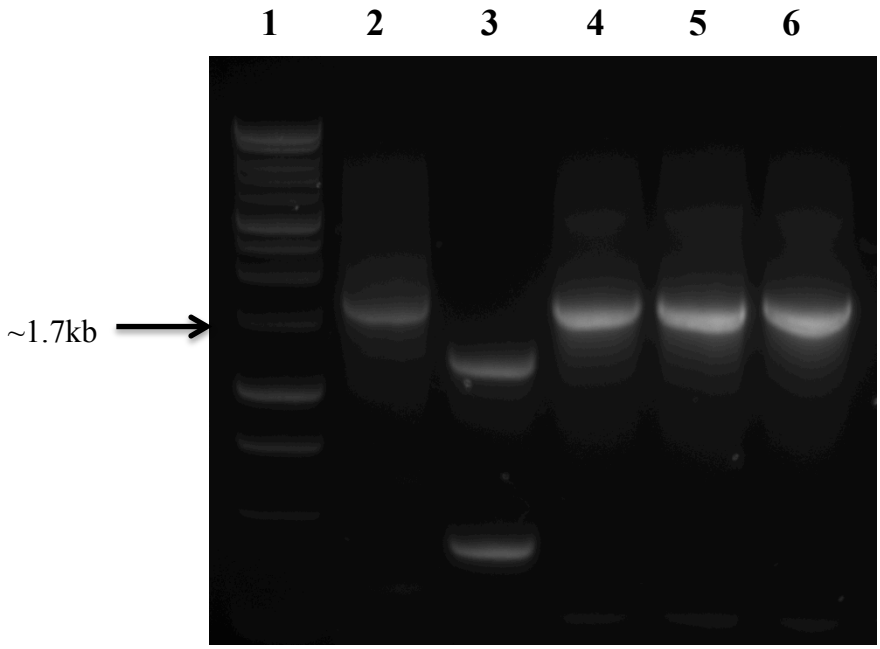

Figure 35. Agarose gel confirmation of PCR fusion products with *ermF* cassette inserted. Gel was made by combining 50ml of TAE buffer with 0.5mg of agarose, and heating. 2µl of GelRed Nucleic Acid Gel Stain dye was added and mixed before pouring and solidifying the gel. Samples were combined with loading dye for visualization and image was taken via UV transilluminator. Lane 1: 1kb ladder; lane 2: Δ1421; lane 3: PG1421 gDNA (control); lane 4: Δ1820: lane 5: Δ1821; lanes 6: Δ0893. Band size at around 1.7kb indicates a correctly fused product with Mut1, *ermF*, and Mut2 of each respective gene.

The desired fused PCR fragments were all cloned separately into the pCR 2.1 TA cloning vector that carries both an ampicillin (bases 2129-2989) and kanamycin (bases 1317-2111) antibiotic resistance-encoding gene. The desired PCR fusion product was inserted between the M13 forward primer (bases 389-404) and the reverse primer (bases 205-211). This 3.9kb vector also contains the *lacZ* gene for blue-white screening if needed. The candidate pCR 2.1 vector with the desired ligated PCR fusion product was then transformed into TOP10 *E. coli* chemically competent cells to check for gene insertion. This was done with each of the four knockout genes. After transformation, the mixture was spread on LB plates supplemented with X-gal and kanamycin to grow overnight. Transformed *E. coli* containing the plasmid with kanamycin resistance gene were able to grow on the LB plate, and both blue and white colonies appeared. Only white colonies were candidates for successful ligations. *E. coli* containing a functional β-galactosidase enzyme (encoded by the *lacZ* gene) metabolized the galactose sugar (X-gal) on the LB plate, forming a blue pigmented colony. *E. coli* containing the vector with the desired PCR fused product inserted within the *lacZ* gene would disrupt the β-galactosidase enzyme activity, turning the colonies white.

Plasmids were isolated from numerous white colonies for each gene knockout and digested with the *Eco*RI restriction enzyme. *Eco*RI restriction enzyme sites were located on both sides of the PCR fused product insertion and resulted in two DNA fragments at 6kb (vector with insert) and roughly 1680bp for each of Δ0893, Δ1421, Δ1820, and Δ1821, if insertion is correct. Digestions of all candidates for all four genes were run on 1% agarose gels for confirmation (Figure 36, only Δ1820 and Δ8093 shown). Plasmid digestion of colony in lane 2 shows one fragment of approximately 6kb in size and one

band less than 250bp. The colony in lane 5 shows a sole 6kb band, while the colony in lane 7 shows one band at 6kb and one band at 650bp. The colony in lane 11 shows one band at 6kb and one at 1.2kb. All four of these colonies show that the vector with insert was not successfully digested by the *Eco*RI restriction enzyme as no band at 1680bp is observable. One possible reason this could be the case is that not enough *Eco*RI was added to the sample. Colonies in lanes 3, 4, 6, 8, and 9 all contain one band at 6kb and one at approximately 1.7kb, indicating that the construct (PG1820 in this case) was not only ligated correctly into the plasmid, but also that enough restriction enzyme was used to digest out the construct. Likewise, colonies in lanes 10 and 12 contain one band at 6kb and one at approximately 1.7kb, indicating that the construct (PG0893 in this case) was ligated correctly into the plasmid like above. These 7 candidate plasmids were then transformed into chemically competent *E. coli* cells and stored at -80^{o}C for future use.

Meanwhile, the fused PCR products of these and additional colonies were used and amplified in large volumes for electroporation into *P. gingivalis* electrocompetent cells to obtain mutants of Δ0893, Δ1421, Δ1820, and Δ1821. Fresh purified PCR products were used for electroporation as opposed to the plasmids in order to preserve the plasmids after months of electroporation. No successful mutant candidates were elucidated.

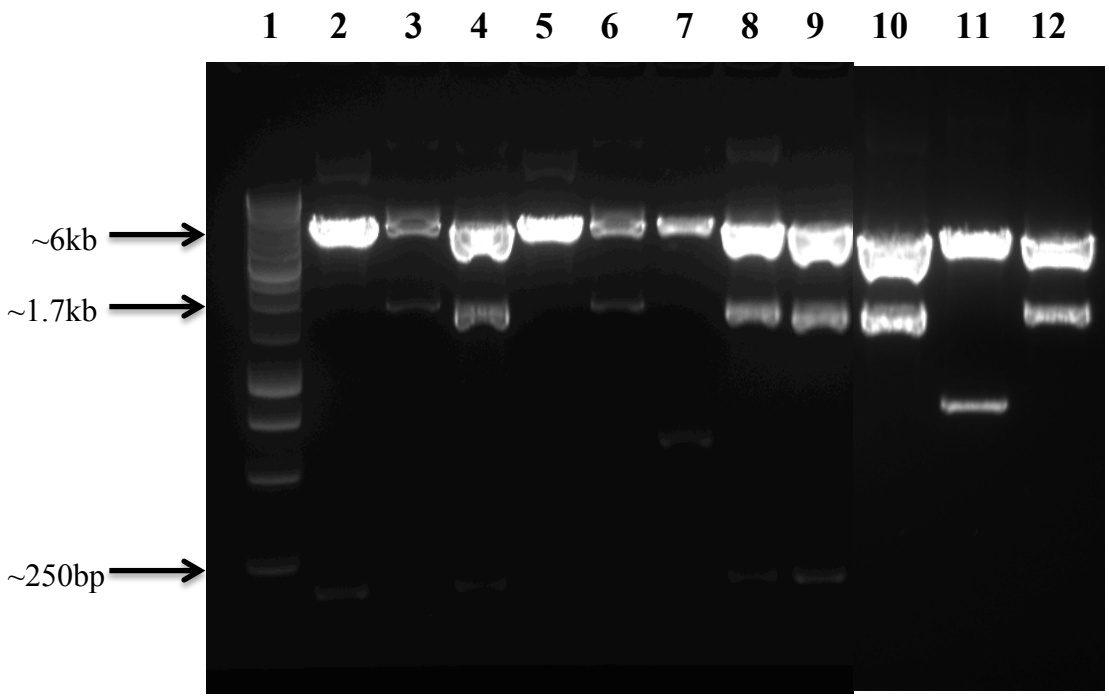

Figure 36. Gel confirmation of *Eco*RI digestion of plasmid DNA of Δ1820 and Δ0893. Gel was made by combining 100ml of TAE buffer with 1mg of agarose, and heating. 4µl of GelRed Nucleic Acid Gel Stain dye was added and mixed before pouring and solidifying the gel. Samples were combined with loading dye for visualization and image was taken via UV transilluminator. Lane 1: 1kb ladder; lanes 2-9: Δ1820; lanes 10-12: Δ0893. Lanes 3, 4, 6, 8 and 9 of Δ1820, as well as lanes 10 and 12 of Δ0893 all represent isolated pCR 2.1 vector + insert of interest. Lanes 2, 5, and 7 of Δ1820, as well as lane 11 of Δ0893 show either no vector+insert or else the incorrect band size. (Some positive bands at 1.7kb are very faint in image but existent.)

Chapter 4: DISCUSSION

In all organisms, RNA-binding proteins, or RBPs, play an important role in regulating gene expression by modulating RNA transcription, translation, processing and stability (Hajnsdorf and Boni, 2012)In bacteria, RBPs may be highly specific for one to a few RNA targets, or function as global regulators implicated in numerous regulatory networks without strict sequence specificity. Despite their evolutionary significance, there has yet to be an RBP resolved in the oral bacterium *P. gingivalis,* which is a major etiological agent in the initiation as well as progression of periodontal disease (Ray et al., 2013). In order to determine whether *P. gingivalis* in fact contains an RBP, the gene PG0627 was hypothesized to be a putative RBP and was thus characterized functionally to determine its biological role in response to several environmental cues.

Using bioinformatics and sequence homology across various species, our lab identified gene PG0627 as a putative RBP, and thus was further investigated. BLAST results showed that the nucleotide sequence of this gene had sequence similarities with three other organisms: 1) residues 1-76 of *Treponema pallidum* had 54% similarity, 2) residues 3-76 of *Synechocystis sp.* 53% similarity, and 3) residues 1-76 of *Brugia malayi* had 50% similarity (Table 1). Furthermore, the protein sequence of the N-terminal RRM domain of Cleavage stimulation factor 64KDa subunit (PDB:1P1T) had a 62% similarity to that of PG0627 (Table 2). From this information, a homology model for the RBP was generated using one-to-one threading by Phyre2. After using UCSF's Chimera software

to model the two monomers and alignment was done via MatchMaker, the overlay showed how well fit PG0627 was to the N-terminal RRM domain of CstF-64 (Figure 10). For confirmation, a second modeling database inquiry using SWISS-MODEL was done, and a QMEAN composite score measuring the model's quality was generated. The QMEAN was 0.814, indicating the model was of low energy as desired. The secondary structure agreement between the two models was also significant at 86.9% (Table 5).

As the N-terminal RRM of CsfF-64 in *H. sapiens* was the closest protein sequence hit to PG0627, research was done to deduce if function, in addition to structure, was also in parallel. CstF-64 binds a wide range of G/U-rich sequences on single-stranded RNA with comparable affinity, yet is not highly specific for any one target sequence (Canadillas and Varani, 2003). Thus, much like that of RBP, it displays slow kinetics and has the ability to bind tightly to a class of sequences without strong preference for any particular sequence, yet it can discriminate effectively against other RNAs. RBPs are known to bind to various motifs and ribosomal binding sites in order to instill their effect in degrading or stabilizing RNA, as well as inhibiting translation among other effects (Vogel and Luisi, 2011).

To further determine whether PG0627 was indeed a good candidate for a putative RBP, protein analysis of motifs was done via InterPro. Through GENE3D, it was determined that residues 4-92 of PG0627 represent a nucleotide-binding domain with an alpha-beta plait structures, such as that found in RBDs of various ribonucleoproteins. Pfam, SMART, and PROSITE databases also indicated that the PG0627 protein sequence indeed had an RNA recognition motif domain. These bioinformatics data gave us strong confidence that PG0627 could indeed be a good candidate for RBP, and led us to further

investigate its biological role in *P. gingivalis*. A previously-generated *P. gingivalis* W83 mutant deficient in the PG0627 gene was used in all ensuing studies.

In order to test our hypothesis, our first aim was to determine the intracellular content of various metals in V3139 compared to W83. Of particular interest was that of iron levels given its essential role as a nutrient in *P. gingivalis*. Comparative studies between W83 and V3139 strains were conducted and graphed in figures 12 and 13. The first is analysis via ICP-MS, and the second via a colorimetric ferrozine assay adapted for anaerobic conditions in order to minimize oxidation of iron. ICP-MS results only contain one biological replicate as the machinery went down for an extended amount of time, so the results are only preliminary. Given that we do not know the biological role yet of PG0627 and that is what is being investigated, we had no expected results regarding intracellular metal content differences between the wild-type and V3139, or even if there would be any. From figure 12, it is evident that V3139 shows a decrease in levels of magnesium, iron, cobalt, and nickel, and an increase in levels of copper and zinc. Of note is that the fold-change of intracellular iron between the wild-type and V3139 is a 1.23-fold decrease, indicating that the mutant is somehow a less efficient transporter of iron than W83.

Given the limited scope of a single biological replicate analyzed via ICP-MS, we decided to perform a colorimetric ferrozine assay adapted for anaerobic conditions to further analyze the intracellular iron content of our samples. Samples were prepared both with and without 2,2-dipyridyl, a high-affinity iron chelator. Its purpose is to limit available extracellular iron for transport into the cell, and thus mimics iron-limited conditions. From figure 13, it is evident that in iron-excess conditions, a 1.23-fold

decrease in intracellular Fe(II) was seen in V3139 compared to W83. Similarly, in iron-limited conditions, a 1.18-fold decrease was seen in V3139. Taken together, these results indicate that V3139 is a less efficient transporter of iron than the wild-type regardless of the iron availability. This is also consistent with the ICP-MS results above in fold-change, despite the ferrozine assay protocol not being fully optimized. Sample preparation was not indicated on the ferrozine assay protocol, so we prepared samples in the same manner as for the ICP-MS protocol. Furthermore, while the ferrozine assay protocol indicated that an evident color change would occur in 10 minutes, our experience was that it took five hours to see a full color change. For this reason, a more optimized ferrozine assay protocol may need to be generated and samples repeated. Alternatively, a radioactive hemin uptake assay may instead be conducted to further confirm intracellular iron levels, and it would serve as a better indicator of iron transport and related machinery.

Our next aim was to determine the protease activity on the extracellular surface of V3139 and the wild-type, and whether they differed. Three to four biological replicates of arginine-specific and lysine-specific assays were done in conditions with and without an iron chelator. Based on V3139 (above) exhibiting lower levels of intracellular iron content than W83, it can be expected that a difference in protease activity can also be seen as these gingipains are involved in hemin acquisition. From figure 14, a few inferences can be made about arginine-specific protease activity. First, in iron-excess conditions, V3139 displays a 1.79-fold decrease in arginine-specific protease activity compared to W83. Similarly, in iron-limited conditions, V3139 shows a 1.59-fold decrease in activity compared to the wild-type. Overall for both strains though, arginine-

protease activity was greater in iron-limited than in iron-excess conditions. Though this last observation is less common with *P. gingivalis*, it is not altogether surprising. A ChIP-seq study by Scott et al. showed that in the absence of hemin, there were more copies of the promoter for *rgpA,* the gene coding for the Arg-X protease (Scott et al., 2013). Lysine-specific protease activity was also analyzed and graphed in figure 15. First, in iron-excess conditions, V3139 exhibits only a slight decrease in activity, i.e. 1.10-fold, to that of W83. However, in iron-limited conditions, results are markedly different. In this environment, while the wild-type shows a similar fold-change increase to that of wild-type in iron-excess conditions, V3139 has a considerable decrease in lysine protease activity in the iron-limited versus the iron-excess state. Namely, V3139 had a 2.04-fold decrease in lysine protease activity compared to the wild-type in iron-limited conditions, and a 1.59-fold decrease to that of V3139 in iron-excess conditions. The same ChIP-seq study referenced above also saw that, in iron-limited conditions, there were more copies of the promoter for *kgp*, the gene coding for the Lys-X protease (Scott et al., 2013)While this can explain the activity of W83 increasing in iron-limited conditions, it doesn't support the same conclusion for V3139. With that, it's possible that the absence of iron in fact down-regulates *kgp* in the V3139 strain, but further sequencing studies would need to be performed.

Our next aim was to determine the virulence ability between our W83 and V3139 by performing total interactions and total invasion assays utilizing HUVEC eukaryotic cells. Both strains were labeled with the fluorophore FITC before incubation with eukaryotic HUVEC. FITC was used to determine extracellular interactions between each of our two strains and HUVEC, while trypan blue was later added to quench those

extracellular interactions and only allow for fluorescent measurement of invading bacteria. Our results as depicted in figure 16 show that V3139 was somewhat decreased in its virulence ability as compared to the wild-type. Specifically, there was a 1.15-fold decrease of total extracellular interactions with V3139 than with the wild-type. Similarly, a 1.13-fold decrease in total invasion of HUVEC with V3139 compared to the wild-type was seen. Taken together, these fold-changes are not vastly different, but could indicate differing levels of RNA or proteins specifically involved in virulence in V3139 compared to the wild-type. An early study by Van Steenbergen et al. showed that protease deficiency in *P. gingivalis* was correlated with lower virulence (Van Steenbergen et al., 1987)Given that V3139 exhibited a lower protease activity than our wild-type, that could be a potential reason why virulence was also decreased in V3139. Of note, paired student t-test p-values were rather high, 0.087 for total interactions and 0.159 for total invasions meaning that replication of the results was difficult, and that chance accounted for nearly 9% and 16%, respectively. This could be due to flow cytometry methods used or because the fluorophore used, FITC, may not be the optimal choice. Eight biological replicates were performed before five of these were consistent enough in their trends for use. However, interaction and invasion studies done on plates may give further information and should be attempted in the future.

Our next aim was to determine if growth changes were evident between V3139 and the wild-type in the limitation of available hemin. A decrease in growth was expected in the wild-type as hemin, the iron-containing protoporphyrin, is an essential nutrient for growth in *P. gingivalis*. A similar trend would be expected for V3139 unless it was somehow involved in iron transport. From figure 17, it is evident that V3139 grew

considerably better in the hemin-limited condition compared to the wild-type. This translated to a 33% decrease in growth of the wild-type versus an 11% decrease in growth of V3139. This suggests that the mutant is somehow more efficient in iron transport and scavenging for any available iron. Published data by Genco suggests that as the availability of hemin is decreased, the expression of virulence factors is decreased, and this in turn results in decreased virulence potential (Genco, 1995). However, given our previous results above that both protease activity and virulence are decreased in V3139 compared to the wild-type, there must be another explanation why, under hemin limitation, V3139 grows better than the wild-type. One possible reason as explained below in the sequencing results, is the up-regulation of PG0628, an ABC transporter whose function it is to carry heme across the periplasm and inner membrane (Nikaido and Hall, 1998). So, when hemin is limited, V3139 employs an alternative strategy to transport hemin intracellularly. An alternative method that could be done in the future to confirm the role of PG0627 in iron transport and/or related machinery is through a radioactive hemin uptake assay.

Our next aim was to determine if growth changes were evident between V3139 and the wild-type in the presence of various concentrations of nitrosative stress compounds. As *P. gingivalis* has a nitrosative stress protection network, it is important to ascertain whether PG0627 may play a role. If it does, we would expect to see less growth inhibition in V3139 than the wild-type when either nitrate and/or nitrite are added in various concentrations. Figures 18 and 19 outline our results and hint at the possibility that PG0627 may play role in the nitrosative stress protection mechanism, though it is somewhat inconclusive. Under growth with various concentrations of nitrate, V3139

grows better than W83 in both hemin-excess and hemin-limited conditions, with a marked further increase in growth differences in the hemin-limited conditions. In both strains, there wasn't a considerable difference in growth inhibition between 40mM $NaNO_3$ and 20mM $NaNO_3$. Under growth with various concentrations of nitrite, V3139 once again grows better than W83 in both hemin-excess and hemin-limited conditions, with a marked further increase in growth differences in the hemin-limited conditions. Markedly, V3139 has a small growth inhibition difference between 1mM $NaNO_2$ and 4mM $NaNO_2$, while the wild-type sees a slightly larger effect between the two in terms of growth inhibition. Also of note is the decrease in overall growth in the hemin-limited condition compared to hemin excess for both W83 and V3139 strains. Taken together, it can be said that PG0627 may potentially play a role in the nitrosative stress protection mechanism, but further sequencing and/or proteomics results may garner further information. Furthermore, the growth inhibition seen in the hemin depletion assay (above) was re-confirmed here with the controls, i.e. V3139 grew considerably better in hemin-limited conditions than W83. Of note, is that this nitrosative stress protocol was repeated several times with varying results. The first three replicates exhibited similar trends as expressed here, i.e. V3139 grew better than the wild-type in both hemin-excess and hemin-limited conditions, and in the presence of either nitrate or nitrite. The second set of triplicates showed the exact opposite data, i.e. W83 grew better than V3139 across all conditions and in the presence of all nitrosative stress-inducing compounds. This third set re-confirmed what the initial triplicate set of data exhibited so was utilized here.

Our next aim was to determine if V3139 grows differentially in response to oxidative stress when compared to W83. *P. gingivalis* also has a complex oxidative stress

protection network in which is combats reactive oxide species (ROS) and the particularly lethal hydroxyl radical. As nitrosative and oxidative stress have some overlap in their conversion products, it is significant to ascertain whether PG0627 also plays a role in protecting the bacterium in the presence of these harmful oxidative species. From figures 20 and 21, it is possible that PG0627 may play a small role in the oxidative stress protection mechanism, though the margins are rather small. The zone of inhibition of V3139 was just slightly bigger in the presence of both 1% and 5% H_2O_2 than for W83. This could be significant, though further testing would need to be done, including potentially a spectrophotometric growth assay similar to that conducted in the nitrosative stress approach.

As RBPs work co- or post-transcriptionally, our next aim was to determine whether there are differential RNA levels between V3139 and W83. Three libraries were generated, though only two have thus far been sequenced and are covered in this thesis. A third replicate is currently in the process of being sequenced. Given this, the data presented here is only preliminary and more replicates must be conducted for confirmation of results.

In iron-excess conditions (Table 6), when the RBP gene is missing, three CRISPR-associated proteins are down-regulated, PG1985, PG1986, and PG0215. These are involved in adaptive immunity and could be down-regulated if they are dependent on a functional RBP. Additionally, an ISPg3 transposase is also down-regulated, and could indicate potentially play role in quickly regulating other genes or proteins. Conversely, hmuY, a heme-binding protein (PG1551) as well as PG0628, an ABC transporter involved in transporting heme across the periplasm and inner membrane, have both been

up-regulated. This, along with the increase in growth of V3139 under hemin-depleted conditions, could indicate that V3139 is indeed involved in hemin transport. DNA machinery (PG PG1276) as well as translational machinery (PG0201) have also been up-regulated hinting that RBP may be involved in enhancing translation potentially. Likewise, the up-regulation of PG0209, a formate/nitrite transporter, indicates that RBP may help with nitrogen detoxification by transporting nitrite from the periplasm to the cytosol for conversion.

In iron-limited conditions (Table 7), when the RBP gene is missing, five of the most down-regulated genes were ISPg3 or ISPg5 transposases. These IS elements have been shown to activate cryptic genes by appropriate juxtaposition of promoter sequences, or conversely, to inactive gene expression by insertional mutagenesis and could play a role in enhancing or promoting translational or transcriptional machinery potentially (Califano et al., 2000). Additionally, PG2213, a nitrite reductase-related protein was also down-regulated, thus slowing conversion of nitrite to NO. Conversely, two of the most up-regulated genes deal with iron or hemin binding, PG1505 and PG2034, and could indicate RBP's direct role in hemin transport under iron-limited conditions. Additionally, translational machinery has also been up-regulated (PG1256), hinting once again that RBP could indeed enhance translation.

Our last aim for this part of the project was to compare proteomics data between V3139 and W83 to determine whether proteins are differentially translated between the two strains. As RBP may work at the RNA or protein level, there is a possibility that RNA levels and protein profiles may differ. That is why proteomics analysis was also performed. Proteomics replicates were initially prepared in February, but because the

analytical machinery was down, we didn't get results until months later. Unfortunately, the sample preparation protocol utilized used a detergent and gave poor results. Recently, another replicate was prepared and sent out for analysis but it has not yet been run. A protein gel, however, was run to visualize any protein band differences and is pictured in figure 31. Unfortunately, no obvious inferences can be made from just viewing the gel and proteomics results must be returned.

Finally, a hypothetical model of the role of RBP in P. gingivalis was created based on RBP function across species as well as data analyses from all the studies discussed here. This is depicted in figure 32 and shows that RBP may play a role in either repressing or enhancing translation, or alternatively degrading target mRNA directly. Taken together, RBP may potentially work to alter RNA and/or protein levels, but more studies would need to be conducted to confirm or deny this claim.

A second focus of this thesis is the characterization of four putative genes in response to environmental stress, PG0893, PG1421, PG1820, and PG1821. These four genes were chosen as sequences homologous to these in other species exhibited involvement in nitrosative and oxidative stress protection mechanisms. Mutants were attempted to be created as detailed in the "Material and Methods" and "Results" section, however, after months of electroporation, no viable mutants were discovered. First, up- and downstream regions of each gene were amplified via PCR, and a fusion PCR protocol was utilized to insert the *ermF* cassette into the gene, effectively knocking the gene out and instilling erythromycin resistance into the insert. Next, these PCR products were confirmed for size via restriction enzymes digestion (Figure 36) before they were utilized for electroporation. As I was unsuccessful to create a mutant deficient in any of

these genes, another lab member will need to continue the project going forward. It is possible that one or more of these genes is lethal to *P. gingivalis* when knocked out, but PG0893 was previously created though lost. Otherwise, non-optimal media broth or other various factors could account for why no mutant has thus yet been created.

In conclusion, we were able to demonstrate that PG0627 is a good candidate for an RNA-binding protein, and that it's biological characterization will help to further strengthen this hypothesis. We were able to show that PG0627 plays a role in the nitrosative stress protection mechanism in *P. gingivalis*, as well as in protease activity, virulence ability, hemin depletion, potential transport of iron and, somewhat, oxidative stress protection mechanisms. Further work must be done in order to confirm PG0627's role as an RNA-binding protein, specifically it's interactions with and affinity for RNA, and is a suitable project for another student to take over in our lab.

Literature Cited

1. Aas, J., Paster, B., Stokes, L., Olsen, I., and Dewhirst, F. (2005). Defining the normal bacterial flora of the oral cavity. J. Clin. Microbiol. *43,* 5721-5732.

2. Arnold, K., Bordoli, L., Kopp, J., and Schwede, T. (2006). The SWISS-MODEL Workspace: A web-based environment for protein structure homology modelling. Bioinformatics *22,* 195-201.

3. Bainbridge, B., Verma, R., Eastman, C., Yehia, B., Rivera, M., and Moffatt, C. (2010). Role of Porphyromonas gingivalis Phosphoserine Phosphatase Enzyme SerB in Inflammation, Immune Response, and Induction of Alveolar Bone Resorption in Rats. Infect. Immun. *78,* 4560-4569.

4. Belton, C., Izutsu, K., Godwin, P., Park, Y., and Lamont, R. (1999). Fluorescence image analysis of the association between Porphyromonas gingivalis and gingival epithelial cell. Cell. Microbiol. *1,* 215-223.

5. Benkert, P., Biasini, M., and Schwede, T. (2011). Toward the estimation of the absolute quality of individual protein structure models. Bioinformatics *27,* 343-350.

6. Benkert, P., Kunzli, M., and Schwede, T. (2009). QMEAN server for protein model quality estimation. Nucl. Acids Res. *37,* W510-W514.

7. Biasini, M., Bienert, S., Waterhouse, A., and Schwede, T. (2014). SWISS-MODEL: modelling protein tertiary and quaternary structure using evolutionary information. Nucl. Acids Res. http://nar.oxfordjournals.org/content/early/2014/04/29/nar.gku340.full?keytype=ref&ijkey=FrXy4oQwsZzEAsw.

8. Bochkarev, A., Barwell, J., Pfuetzner, R., Furey, W., Edwards, A., and Frappier, L. (1995). Crystal structure of the DNA-binding domain of the Epstein-Barr virus origin-binding protein EBNA 1. Cell *83,* 39-46.

9. Boston University Medical Center. (2011). Porphyromonas gingivalis accelerates inflammatory atherosclerosis in a mouse model. ScienceDaily *4,* www.sciencedaily.com/releases/2011/01/110104101344.htm.

10. Bramanti, T., and Holt, S. (1991). Roles of porphyrins and host iron transport proteins in regulation of growth of Porphyromonas gingivalis W50. J. Bacteriol. *173,* 7330-7339.

11. Brunner, J., Scheres, N., Idrissi, N., Deng, D., and Crielaard, W. (2010). The capsule of Porphyromonas gingivalis reduces the immune response of human gingival fibroblasts. BMC Microbiology *10,* 5.

12. Califano, J., Kitten, T., Lewis, J., Macrina, F., and Fleischmann, R. (2000). Characterization of Porphyromonas gingivalis Insertion Sequence-Like Element ISPg5. Infect Immun. *68,* 5247–5253.

13. Canadillas, J., and Varani, G. (2003). Recognition of GU-rich polyadenylation regulatory elements by human CstF-64 protein. EMBO *22,* 2821-2830.

14. Cha-aim, K., Hoshida, H., Fukunaga, T., and Akada, R. (2012). Fusion PCR via Novel Overlap Sequences.*852,*

15. Chan, S., Choi, E., and Shi, Y. (2011). Pre-mRNA 3'-end processing complex assembly and function. Wiley Interdiscip Rev RNA *2,* 321-335.

16. Chapple, C., Kumar, R., and Hunter, N. (2000). Vascular remodelling in chronic inflammatory periodontal disease. J. Oral Pathol. Med. *29,* 500-506.

17. Curtis, M., Aduse-Opoku, J., Slaney, J., Rangarajan, M., and Booth, V.C. (1996). Characterization of an adherence and antigenic determinant of the ArgI protease of Porphyromonas gingivalis which is present on multiple gene products. Infect. Immun. *64,* 2532-2539.

18. Dahlen, G., Manji, F., Baelum, V., and Fejerskov, O. (1992). Putative periodontopathogens in "diseased" and "non-diseased" persons exhibiting poor oral hygiene. J. Clin. Periodontol. *19,* 35-42.

19. Darveau, R. (2010). Periodontitis: a polymicrobial disruption of host homeostasis. Nature Reviews Microbiology *8,* 481-490.

20. Darveau, R., and Page, R. (2000). The microbial challenge in periodontitis. Periodontology *14,* 12–32.

21. Darveau, R., Pham, T., Lemley, K., Reife, R., Bainbridge, B., and Hajjar, A. (2004). Porphyromonas gingivalis Lipopolysaccharide Contains Multiple Lipid A Species That Functionally Interact with Both Toll-Like Receptors 2 and 4. Infect. Immun. *72,* 5041-5051.

22. Dashper, S., Cross, K., Slakeski, N., Lissel, P., and Reynolds, E. (2004). Hemoglobin hydrolysis and heme acquisition by Porphyromonas gingivalis. Oral Microbiol. Immunol. *19,* 50-56.

23. Diaz, P., and Rogers, A. (2004). The effect of oxygen on the growth and physiology of Porphyromonas gingivalis. Oral Microbiology and Immunology *19,* 88-94.

24. Diaz, P., Zilm, P., and Rogers, A. (2002). Fusobacterium nucleatum supports the growth of Porphyromonas gingivalis in oxygenated and carbon-dioxide-depleted environments. Microbiol *148,* 467-472.

25. Fang, F.C. (1997). Perspectives series: host/pathogen interactions. Mechanisms of nitric oxide-related antimicrobial activity. J. Clin. Invest. *99,* 2818-2825.

26. Fletcher, H., and Macrina, F. (1991). Molecular survey of clindamycin and tetracycline resistance determinants in Bacteroides specis. Antimicrob Agents Chemother *35,* 2415-2418.

27. Fletcher, H.M., Schenkein, H.A., Morgan, R.M., Bailey, K.A., Berry, C.R., and Macrina, F.L. (1995). Virulence of a Porphyromonas gingivalis W83 mutant defective in the prtH gene. Infect. Immun. *63,* 1521-1528.

28. Genco, C. (1995). Regulation of hemin and iron transport in Porphyromonas gingivalis. Adv. Dent. Res. *9,* 41-47.

29. Genco, C., and Dixon, D. (2001). Emerging strategies in microbial heme capture. Mol. Microbiol. *39,* 1-11.

30. Genco, C., Odusanya, B., and Brown, G. (1994). Binding and accumulation of hemin in Porphyromonas gingivalis are induced by hemin. Infect. Immun. *62,* 2885-2892.

31. Grenier, D., Bertrand, J., and Mayrand, D. (1995). Porphyromonas gingivalis outer membrane vesicles promote bacterial resistance to chlorhexidine. Oral Microbiol. Immunol. *19,* 319-320.

32. Grenier, D., and Mayrand, D. (1987). Selected characteristics of pathogenic and nonpathogenic strains of Bacteroides gingivalis. J Clin Microbiol *25,* 738-740.

33. Haffajee, A., Socransky, S., and Gunsolley, J. (2003). Systemic anti-infective periodontal therapy. A systematic review. Ann Periodontol *8,* 115-181.

34. Hajishengallis, G. (2009). Porphyromonas gingivalis–host interactions: open war or intelligent guerilla tactics? Microbes and Infection *11,* 637-645.

35. Hajnsdorf, E., and Boni, I. (2012). Multiple activities of RNA-binding proteins S1 and Hfq. Biochimie *94,* 1544-1553.

36. Han, N., Whitlock, J., and Progulske-Fox, A. (1996). The hemagglutinin gene A (hagA) of Porphyromonas gingivalis 381 contains four large, contiguous, direct repeats. Infect. Immun. *64,* 4000-4007.

37. Hanazawa, S., Murakami, Y., Hirose, K., Amano, S., Ohmori, Y., and Kitano, S. (1991). Bacteroides (Porphyromonas) gingivalis fimbriae activate mouse peritoneal macrophages and induce gene expression and production of interleukin-1. Infect. Immun. *59,* 1972-1977.

38. Hanes, P., and Purvis, J. (2003). Local anti-infective therapy: pharmacological agents. A systematic review. Ann Periodontol *8,* 79-98.

39. Hasegawa, Y., Mans, J., Mao, S., and Lopez, M. (2007). Gingival Epithelial Cell Transcriptional Responses to Commensal and Opportunistic Oral Microbial Species. Infect. Immun. *75,* 2540-2547.

40. Ho, S.N., Hunt, H.D., Horton, R.M., Pullen, J.K., and Pease, L.R. (1989). Site-directed mutagenesis by overlap extension using the polymerase chain reaction. Gene *77,* 51-59.

41. Hochgrafe, F.e.a. (2008). Nitric oxide stress induces different responses but mediates comparable protein thiol protection in Bacillus subtilis and Staphylococcus aureus. J. Bacteriol. *190,* 4997-5008.

42. Holt, S., and Ebersole, J. (2005). Porphyromonas gingivalis, Treponema denticola, and Tannerella forsythia: the "red complex", a prototype polybacterial pathogenic consortium in periodontitis. Periodontol. 2000 *38,* 72-122.

43. Holt, S., Kesavalu, L., Walker, S., and Genco, C. (1999). Virulence factors of Porphyrornonas gingivalis. Periodontol. 2000 *20,* 168-238.

44. Hung, H., and Douglass, C. (2002). Meta-analysis of the effect of scaling and root planing, surgical treatment and antibiotic therapies on periodontal probing depth and attachment loss. J. Clin. Periodontol. *29,* 975-986.

45. Ismail, A., and Hooper, L. (2005). Epithelial cells and their neighbors. IV. Bacterial contributions to intestinal epithelial barrier integrity. Am. J. Physiol. Gastrointest. Liver Physiol. *289,* G779-G784.

46. Jandik, K.e.a. (2008). Invasive differences among Porphyromonas gingivalis strains from healthy and diseased periodontal sites. J. Periodontal Res. *43,* 524-30.

47. Kelley, L., and Sternberg, M. (2009). Protein structure prediction on the web: a case study using the Phyre server. Nature Protocols *4,* 363-371.

48. Kielkopf, C., Lucke, S., and Green, M. (2004). U2AF homology motifs: protein recognition in the RRM world. Genes & Development *18,* 1513-1526.

49. Kolenbrander, P., Palmer, R., Rickard, A., and Diaz, P. (2000). Bacterial interactions and successions during plaque development. Periodontol. *42,* 47-79.

50. Kuramitsu, H., Yoneda, M., and Madden, T. (1995). Proteases and collagenases of Porphyromonas gingivalis. Adv. Dent. Res. *9,* 37-40.

51. Lamont, J., and Jenkinson, H. (1998). Life Below the Gum Line: Pathogenic Mechanisms of Porphyromons gingivalis. Microbiol. Mol. Biol. Rev. *62,* 1244-1263.

52. Lamont, R., and Jenkinson, H. (2010). Oral Microbiology at a Glance (Hoboken, NJ, USA: Wiley-Blackwell).

53. Lamont, R., and Jenkinson, H. (2000). Subgingival colonization by Porphyromonas gingivali. Oral Microbiol. Immunol. *15,* 341-349.

54. Lamont, R., and Yilmaz, O. (2000). In or out: the invasiveness of oral bacteria. Periodontol. *30,* 61-69.

55. LeResche, L., and Dworkin, S. (2002). The role of stress in inflammatory disease, including periodontal disease: review of concepts and current findings. Periodontol. 2000 *30,* 91-103.

56. Lewis, J., Dawson, J., Hannis, J., Muddiman, D., and Macrina, F. (1999). Hemoglobinase Activity of the Lysine Gingipain Protease (Kgp) of Porphyromonas gingivalis W83. J. Bacteriol. *181,* 4905-4913.

57. Lewis, J., Yanamandra, S., and Anaya-Bergman, C. (2012). HcpR of Porphyromonas gingivalis Is Required for Growth under Nitrosative Stress and Survival within Host Cells. Infect. Immun. *80,* 3319-3331.

58. Loe, H., Theilade, E., and Jensen, S. (1965). Experimental gingivitis in man. J. Periodontol 177-187.

59. Los Alamos National Security, LLC. (2010). ORALGEN: Human Oral Genomic and Metagenomic Resource. US Department of Energy http://www.oralgen.org/,

60. McCoy, S., Creamer, H., Kawanami, M., and Adams, D. (1987). The concentration of lipopolysaccharide on individual root surfaces at varying times following in vivo root planing. J. Periodontal *58,* 393-399.

61. Mombelli, A., and Samaranayake, L. (2004). Topical and systemic antibiotics in the management of periodontal diseases. Int Dent Journal *54,* 3-14.

62. Moore, J., Wilson, M., and Kieser, J. (1986). The distribution of bacterial lipopolysaccharide (endotoxin) in relation to periodontally involved root surfaces. J. Clin. Periodontol. *13,* 748-751.

63. Murakami, Y., Hanazawa, S., Watanabe, A., Naganuma, K., Iwasaka, H., and Kitano, S. (1994). Porphyromonas gingivalis fimbriae induce a 68-kilodalton phosphorylated protein in macrophages. Infect. Immun. *62,* 5242-5246.

64. Murakami, Y., Masuda, T., Imai, M., Iwami, J., and Nakamura, H. (2004). Analysis of major virulence factors in Porphyromonas gingivalis under various culture temperatures using specific antibodies. Microbiol Immunol. *48,* 561-9.

65. Nikaido, H., and Hall, J. (1998). Overview of bacterial ABC transporters. Methods Enzymol *292,* 3-20.

66. Ogawa, T., Uchida, H., and Hamada, S. (1994). Porphyromonas gingivalis fimbriae and their synthetic peptides induce proinflammatory cytokines in human peripheral blood monocyte cultures. FEMS Microbiol. Lett. *116,* 237-242.

67. Okamoto, K., Kadowaki, T., Nakayama, K., and Yamamoto, K. (1996). Cloning and sequencing of the gene encoding a novel lysine-specific cysteine proteinase (Lys-gingipain) in Porphyromonas gingivalis: structural relationship with the arginine-specific cysteine proteinase (Arg-gingipain). J. Biochem. *120,* 398-406.

68. Okamoto, K., Misumi, Y., Kadowaki, T., Yoneda, M., Yamamoto, K., and Ikehara, Y. (1995). Structural characterization of argingipain, a novel arginine-specific cysteine proteinase as a major periodontal pathogenic factor for Porphyromonas gingivalis. Arch. Biochem. Biophys. *316,* 917-925.

69. Palmerini, C.A., Palombari, R., Perito, S., and Arienti, G. (2003). NO synthesis in human saliva. Free Radic. Res. *37,* 29-31.

70. Pihlstrom, B., Carlson, J., and Smith, Q. (1980). Prevention of phenytoin associated gingival enlargement—a 15-month longitudinal study. J. Periodontal *51,* 311-317.

71. Pihlstrom, B., Michalowicz, B., and Johnson, N. (2005). Periodontal diseases. The Lancet *366,* 1809-20.

72. Pike, R., Potempa, J., McGraw, W., Coetzer, T., and Travis, J. (1996). Characterization of the binding activities of proteinase-adhesin complexes from Porphyromonas gingivalis. J. Bacteriol. *178,* 2876-2882.

73. Potempa, J., Pavloff, N., and Travis, J. (1995). Porphyronzonas gingivalis: a proteinase/gene accounting audit. Trends Microbiol *3,* 430-434.

74. Poulin, R., and Combes, C. (1999). The concept of virulence: interpretations and implications. Parasitol Today *15,* 474-5.

75. Preshaw, P., Hefti, A., and Novak, M. (2004). Subantimicrobial dose doxycycline enhances the efficacy of scaling and root planing in chronic periodontitis: a multicenter trial. J. Periodontal *75,* 1068-1076.

76. Ray, D., Kazan, H., Cook, K.B., Morris, Q.D., and Hughes, T.R. (2013). A compendium of RNA-binding motifs for decoding gene regulation. Nature *499,* 172-177.

77. Rosan, B., and Lamont, R. (2000). Dental plaque formation. Microbes Infect. *2,* 1599-1607.

78. Rylev, M., and Kilian, M. (2008). Prevalence and distribution of principal periodontal pathogens worldwide. J. Clin. Periodontol. *35,* 346-361.

79. Schifferle, R., Shostad, S., Bayers-Thering, M., Dyer, D., and Neiders, M. (1996). Effect of protoporphyrin IX limitation on Porphyromonas gingivalis. J Endod. *22,* 353-355.

80. Schwartz, J., Stinson, F., and Parker, R. (1972). The passage of tritiated bacterial endotoxin across intact gingival crevicular epithelium. J. Periodontol *43,* 270-276.

81. Scott, J., Klein, B., Duran-Pinedo, A., Hu, L., and Duncan, M. (2013). A Two-Component System Regulates Hemin Acquisition in Porphyromonas gingivalis. PLoS One *8,* e73351.

82. Seymour, G., Ford, P., Cullinan, M., Leishman, S., and Yamazaki, K. (2007). Relationship between periodontal infections and systemic disease. Clin. Microbiol. Infect. *13 (Suppl. 4),* 3-10.

83. Shah, H.N., and Gharbia, S.E. (1989). Ecological events in subgingival dental plaque with reference to Bacteroides and Fusobacterium species. Infection *17,* 264-268.

84. Shi, Y., Ratnayake, D., Okamoto, K., Abe, N., Yamamoto, K., and Nakayama, K. (1999). Genetic analyses of proteolysis, hemoglobin binding, and hemagglutination of Porphyromonas gingivalis. Construction of mutants with a combination of rgpA, rgpB, kgp, and hagA. J. Biol. Chem. *274,* 17955-17960.

85. Shizukuishi, S., Tazaki, K., Inoshita, E., Kataoka, K., Hanioka, T., and Amano, A. (1995). Effect of concentration of compounds containing iron on the growth of Porphyromonas gingivalis. FEMS Microbiol. Lett. *131,* 313-317.

86. Singh, A., Wyant, T., Anaya-Bergman, C., Aduse-Opoku, J., and Lewis, J. (2011). The Capsule of Porphyromonas gingivalis Leads to a Reduction in the Host Inflammatory Response, Evasion of Phagocytosis, and Increase in Virulence. Infect. Immun. *79,* 4533-4542.

87. Slots, J. (1999). Actinobacillus actinomycetemcomitans and Porphyromonas gingivalis in periodontal disease: introduction. Periodontol. 2000 *20,* 7-13.

88. Spiro, S. (2006). Nitric oxide-sensing mechanisms in Escherichia coli. Biochem. Soc. Trans. *34,* 200-202.

89. Sreenivasa, P., and Gaffar, A. (2002). Antiplaque biocides and bacterial resistance: a review. J. Clin. Periodontol. *29,* 965-974.

90. Sroka, A., Sztukowska, M., Potempa, J., Travis, J., and Genco, C. (2001). Degradation of Host Heme Proteins by Lysine- and Arginine-Specific Cysteine Proteinases (Gingipains) of Porphyromonas gingivalis. J. Bacteriol. *183,* 5609-5616.

91. Szewczyk, E., Nayak, T., Oakley, C.E., Edgerton, H., Xiong, Y., Taheri-Talesh, N., Osmani, S.A., and Oakley, B.R. (2006). Fusion PCR and gene targeting in Aspergillus nidulans. Nat. Protoc. *1,* 3111-3120.

92. Takagaki, Y., Seipelt, R., Peterson, M., and Manley, J. (1996). The polyadenylation factor CstF-63 regulates alternative processing of IgM heavy chain pre-mRNA during B cell differentiation. Cell *87,* 941-952.

93. Tanner, A., Kent, R., Maiden, M., and Taubman, M. (1996). Clinical, microbiological and immunological profile of healthy, gingivitis and putative active periodontal subject. J Periodontal Res *31,* 195-204.

94. Travis, J., Pike, R., Imamura, T., and Potempa, J. (1997). Porphyromonas gingivalis proteinases as virulence factors in the development of periodontitis. J Periodontal Res. *32,* 120-5.

95. Tribble, G., Mao, S., James, C., and Lamont, R. (2006). A Porphyromonas gingivalis haloacid dehalogenase family phosphatase interacts with human phosphoproteins and is important for invasion. Proc. Natl. Acad. Sci. USA *103,* 11027-11032.

96. University of Basel. (2014). QMEAN. Protein Structure Bioinformatics at Swiss Institute of Bioinformatics *http://swissmodel.expasy.org/qmean/cgi/index.cgi,*

97. Van Steenbergen, T., Delemarre, F., Namavar, F., and De Graaff, J. (1987). Differences in virulence within the species Bacteroides gingivalis. Antonie Van Leeuwenhoek *53,* 233-244.

98. Van Steenbergen, T., Petit, M., Scholte, L., Van Der Velden, U., and De Graaff, J. (1993). Transmission of Porphyromonas gingivalis between spouses. J. Clin. Periodontol. *20,* 340-345.

99. Vogel, J., and Luisi, F. (2011). Hfq and its constellation of RNA. Nature Reviews Microbiology *9,* 578-589.

100. Wayakanon, K., Thornhill, M., Douglas, C., Lewis, A., and Warren, N. (2013). Polymersome-mediated intracellular delivery of antibiotics to treat Porphyromonas gingivalis-infected oral epithelial cells. FASEB *27,* 1-11.

101. Wolf, R.E. (March 2005). What is ICP-MS? USGS 7-
http://crustal.usgs.gov/laboratories/icpms/What_is_ICPMS.pdf.

102. Yilmaz, O., Verbeke, P., Lamont, R., and Ojcius, D. (2006). Intercellular Spreading of Porphyromonas gingivalis Infection in Primary Gingival Epithelial Cells. Infect. Immun. *74,* 703-710.

103. Yilmaz, O., Watanabe, K., and Lamont, R. (2002). Involvement of integrins in fimbriae-mediated binding and invasion by Porphyromonas gingivalis. Cell. Microbiol. *4,* 305-314.

104. Yilmaz, O., Young, P., Lamont, R., and Kenny, G. (2003). Gingival epithelial cell signalling and cytoskeletal responses to Porphyromonas gingivalis invasion. Microbiology *149,* 2417-2426.

105. Zhang, D., Chen, L., Li, S., Gu, Z., and Yan, J. (2008). Lipopolysaccharide (LPS) of Porphyromonas gingivalis induces IL-1β, TNF-αand IL-6 production by THP-1 cells in a way different from that of Escherichia coliLPS. Innate Immunity *14,* 99-107.

VITA

Romana Cvitkovic holds a Bachelor of Science (B.S.) degree in Biology from Brigham Young University in Provo, UT. She obtained her Masters of Science (M.S.) degree in Physiology and Biophysics from Richmond, VA-based Virginia Commonwealth University in 2014. Following graduation, she will pursue admission into dental school.